université de BORDEAUX

THÈSE PRÉSENTÉE

POUR OBTENIR LE GRADE DE

DOCTEUR DE

L'UNIVERSITÉ DE BORDEAUX

ÉCOLE DOCTORALE : SCIENCES DE LA VIE ET DE LA SANTÉ

SPÉCIALITÉ : NEUROSCIENCES

Par Elena BAZ BADILLO

Rôle des protocadhérines gamma dans l'encodage des connections olivo-cérébelleuses

Role of gamma-protocadherins in the molecular encoding of olivo-cerebellar connections

Sous la direction de : Mathieu LETELLIER

Soutenue le 15/09/2025

Membres du jury :

Mme SELIMI Fekrije	Centre interdisciplinaire de recherche en biologie (CIRB), Collège de France	Rapporteur, Présidente du jury
M. SCHEIFFELE Peter	Biozentrum, University of Basel	Rapporteur
Mme PACARY Emilie	Neurocentre Magendie, Université de Bordeaux	Examinateur

Membres invités :

M. FAVEREAUX Alexandre	Institut Interdisciplinaire des Neurosciences, Université de Bordeaux	Invité

Résumés en français et en anglais

Rôle des protocadhérines gamma dans l'encodage des connections olivo-cérébelleuses

Résumé

Au cours du développement, des millions de neurones dans le cerveau doivent choisir leurs partenaires synaptiques et subir des changements fonctionnels et moléculaires profonds pour stabiliser des connexions specifiques. Le circuit olivo-cérébelleux présente un développement hautement stéréotypé, avec une sélection synaptique se produisant pendant des périodes critiques strictes, ce qui en fait un modèle parfait pour étudier ces phénomènes. Peu après la naissance, plusieurs fibres grimpantes (FG) émergeant du noyau olivaire inférieur innervent chaque cellule de Purkinje (CP) dans le cortex cérébelleux. Au cours des trois premières semaines postnatales, les FGs surnuméraires sont élaguées jusqu'à ce que chaque CP soit innervée par une seule FG (mono-innervation). Au-delà du rôle établi de l'activité dans ce rafinement synaptique, les mécanismes moléculaires sous-jacents aux interactions cellulaires et au processus de sélection synaptique dans ce circuit restent inconnus. La famille hautement diversifiée des gamma Protocadhérines (γPCDH) a été proposée à de multiples reprises comme pouvant contribuer à un « code moléculaire de connectivité » dans le cervelet, bien que les preuves expérimentales restent rares. Dans mon travail de thèse, la technique de PatchSeq m'a permis de montrer que la diversité des isoformes γPCDH exprimées par les CPs individuelles diminue progressivement et de manière corrélée avec le processus de sélection synaptique. De plus, la surexpression d'isoformes uniques pour mimer une diminution prématurée de la diversité γPCDH dans des CPs isolées accélère significativement la sélection des FGs dans un modèle d'explant de cerveau postérieur. En outre, nous avons détecté une similarité plus élevée dans le répertoire γPCDH exprimé par les CPs innervées par le même axone olivaire, suggérant que les isoformes de γPCDH exprimées dans les CPs sont déterminées par l'identité du neurone présynaptique. Dans l'ensemble, nos résultats soutiennent l'implication des γ-PCDH dans le code moléculaire de la connectivité olivo-cérébelleuse, avec un effet direct sur la spécificité synaptique des fibres grimpantes vers les cellules de Purkinje, ainsi qu'une expression d'isoformes γ-PCDH non aléatoire.

Mots clés: Cervelet – Protocadhérines – développement

Role of gamma-protocadherins in the molecular encoding of olivo-cerebellar connections

Abstract

During development, millions of neurons in the brain must choose their synaptic partners and undergo deep functional and molecular changes to stabilize specific connections. The olivo-cerebellar circuit presents a highly stereotyped development, with synapse selection happening during strict critical periods, making it a perfect model to study these phenomena. Early after birth, multiple climbing fibers (CF) emerging from the inferior olivary nucleus innervate each Purkinje cell (PC) in the cerebellum cortex. Over the three first postnatal weeks, supernumerary CF are pruned until each PC is mono-innervated by a single CF. Beyond the established role of activity in afferent selection, the molecular mechanisms underlying cell-cell interaction and recognition in this circuit remain unknown. The highly diverse family of gamma Protocadherins (γPCDH) has been recurrently proposed as part of a "molecular code of connectivity" in the cerebellum, although experimental evidence remains scarce. Here, using PatchSeq we show that during CF elimination, the diversity of γPCDH isoforms expressed by individual PC gradually decreases. In addition, overexpressing single isoforms to mimic a premature decrease in γPCDH diversity in single PCs significantly accelerates CF selection in a hindbrain explant model. Furthermore, we detected a higher similarity in γPCDH repertoire expressed by PCs connected by the same CF, suggesting that γPCDH expression in PCs is determined by the presynaptic neuron identity. Overall, our results support the role of γPCDH as part of the cerebellar molecular code of connectivity with a direct effect in CF-to-PC synapse specificity, and a not random γPCDH isoform expression.

Keywords: Cerebellum – Protocadherins – Development

Unité de recherche :

Interdisciplinary Institute for Neuroscience (IINS)

UMR 5297

Centre Broca Nouvelle-Aquitaine,

146 rue Léo Saignat

33076 Bordeaux (France)

A Geli y a Abu, que fueron valientes

y nos lo contagiaron a través del tiempo.

Gracias por abrirnos el camino a los demás.

Contents

Résumés en français et en anglais 1

Résumé 1

Abstract 2

List of figures 9

List of supplementary figures 11

List of tables 13

List of abbreviations 15

Introduction 23

Chapter I: Genetically encoded diversity and epigenetic landscape drive developmental brain wiring 25

Shaping brain wiring at different scales: probabilistic versus deterministic models 26

Genetically predetermined circuits as a first step towards selective connectivity: the CCD model 28

Environmental influence on the genetical envelope during developmental critical periods 29

Epigenetic changes promote long-term stability of connections 34

Chapter II: Nested cellular diversity in the mammalian brain and its implications in circuit wiring 37

Neuronal diversity: morphology, function and molecular identity 38

Hebb vs Sperry: two models to explain synaptic partner selection 43

Neurotransmission is not required for synapse formation or diversification 45

Chapter III: Clustered Protocadherins as candidates to encode single-neuron identity 47

CAM polymorphism: criteria for single-neuron identity encoding 48

Candidate CAMs for a molecular code of connectivity 50

Clustered Protocadherins fulfill the criteria for a molecular code of connectivity 52

Chapter IV: Cerebellum wiring during postnatal development 61
Anatomy and cellular organization of the cerebellar circuit 62
Development of the olivo-cerebellar circuit 64
A hindbrain explant model to study activity-gene interplay during development: CF-induced long-lasting changes in PCs 69
Questions, hypothesis and objectives 73
Materials and Methods 77
Wetlab materials and methods 78
Animals 78
Acute slices preparation 78
Olivo-cerebellar explants preparation and culture 78
Electrophysiological recordings and PatchSeq sample acquisition 79
Single-cell RNA sequencing 80
Single-cell electroporation (SCE) 81
Immunostaining and microscopy techniques 81
Analysis techniques 83
Electrophysiology analysis: eCF-EPSC 83
Image analysis 84
Single-cell RNA sequencing analysis 85
Materials and Methods Tables 87
Results 91
Chapter I: Regulation of γPCDH expression in Purkinje cells during Climbing Fiber competition 93
Context and aims 94
Functional classification of Purkinje cells 96
Expression changes of developmentally relevant genes 97
cPCDH regulation during the critical period 99

Conclusions 102

Supplementary figures Results Chapter I 103

Tables Results Chapter I 105

Chapter II: Olivo-cerebellar explants recapitulate circuit development *in vitro.* 109

Context and aims 110

Olivo-cerebellar explants preserve spatiotemporal development of cerebellar microcircuitry 110

CF-PC synaptic maturation follows ex vivo developmental dynamics 114

Conclusions 114

Chapter III: Brainstem innervation is required for γPCDH regulation in Purkinje cells. 117

Context and aims 118

Conserved PCs marker genes and sagittal bands genes profile in explants across developmental stages of PCs 120

Differential gene expression analysis reveals alteration in the expression of synaptic genes and CAMs in PCs that develop in absence of CF input 121

Naïve PCs retain an immature pattern of cPCDH expression 123

Conclusions 125

Supplementary figures Results Chapter III 127

Chapter IV: Single isoform overexpression to alter γPCDH diversity in Purkinje cells accelerates CF elimination 131

Context and aims 132

Single γPCDH isoform overexpression during development accelerates CF elimination in PC 134

Subcellular distribution of γPCDH-A11 protein in PCs 136

Conclusions 136

Chapter V: Influence of presynaptic partner identity in γPCDH isoform selection by PCs 139

Context and aims 140

γPCDH signature of PCs innervated by the same CF 140

Conclusions 143

Supplementary figures Results Chapter V 144

Discussion 147

Recapitulation of results 148

Bridging connectivity refinement to single cell molecular identity with PatchSeq 150

C-type *versus* alternate γPCDHs: divergent regulation and function during development 153

Translating γPCDH homophilic interaction into CF selection 156

Adhesive *versus* repulsive signals 156

Downstream signaling associated with γPCDHs' role in CF selection 157

Possible contribution of γPCDH interaction with synaptogenic molecules 158

Stochastic *versus* deterministic expression of cPCDH isoforms in Purkinje cells 160

Working model: how γPCDH alternative isoforms diversity regulates CF selection 163

Overview of unresolved questions and proposed approaches 166

General conclusions 168

References 171

Acknowledgments ..... Error! Bookmark not defined.

List of figures

Figure 1: Schematic model of the selective stabilization of synapses during developmental critical periods. 31

Figure 2: Schematic representation of cells nested diversity in the brain, from cell types to single-cell identity. 41

Figure 3: Polymorphic CAMs functions in connectivity. 49

Figure 4: cPCDH genomic organization, protein expression and intracellular signaling. 55

Figure 5: Cerebellar cortex circuitry. 63

Figure 6: Sequential events of CF and PF to PC circuit formation. 66

Figure 7: Hindbrain explants system. 70

Figure 8: Electrophysiology and imaging of sequenced cells. 95

Figure 9: Differential expression analysis Differential expression analysis of electrophysiologically defined groups. 99

Figure 10: cPCDH expression in PC during CF elimination. 101

Figure 11: Immunostaining of Calb1, Igsf9-GFP (CF), vGLUT2 and vGLUT1 in explants over development. 112

Figure 12: Immunostaining of Calb1, Igsf9-GFP (CF), vGLUT2 and vGAT in explants over development. 113

Figure 13: Electrophysiological characterization of CF to PC synapses in explants. 114

Figure 14**:** Comparison of sagittal bands-gene expression across developmental stages of PCs in explants and acute slices. 119

Figure 15: Differential expression analysis in full and naïve explants. 122

Figure 16: Genes regulated in both conditions and exclusively regulated in full explants. 124

Figure 17: cPCDH expression in PC from full and naïve explants during and after developmental critical period. 126

Figure 18: γPCDH-C3 and γPCDH-A11 expression in the cerebellum and brainstem.....133

Figure 19: CF-EPSCs from control and single isoforms-overexpressing PCs..135

Figure 20: Subcellular localization of γPCDH-A11 and vGLUT2 in PCs. 137

Figure 21: Experimental and analysis design of γPCDH repertoire in PCs depending on CF identity.....141

Figure 22: cPCDH isoforms expression comparisons in PCs attending to CF identity. 142

List of supplementary figures

Supplementary Figure 1: Quality controls and GOIs expression. 103

Supplementary Figure 2: Quantification of cPCDH expression per cluster. 104

Supplementary Figure 3: Quality controls of explants single-cell RNA sequencing. 127

Supplementary Figure 4: Scaled (0-10) expression of sagittal bands-genes in PCs from explants (left panels, golden) and acute slices (right panels, blue-yellow). 128

Supplementary Figure 5: Expression in full and naïve explants of genes related to CF elimination. 129

Supplementary Figure 6: PatchSeq quality controls (Chapter V). 144

Supplementary Figure 7: Normalized cPCDH expression per CF nest and pairwise comparisons. 145

List of tables

Table 1: Slicing solution composition. 87

Table 2: Aritificial cerebrospinal fluid (aCSF). 87

Table 3: Dissection medium composition. 88

Table 4: Culture medium composition. 88

Table 5: Whole-cell patch-clamp internal solution for voltage-clamp recordings. 88

Table 6: Sterile aCSF 89

Table 7: Primary-Secondary antibodies combinations used. 89

Table 8: Genes included in cluster 1 from LRT – DGE analysis in Figure 2, left panels 105

Table 9: Genes included in cluster 2 from LRT – DGE analysis in Figure 2, middle-left panels. 106

Table 10: Genes included in cluster 1 from LRT – DGE analysis in Figure 2, middle-right panels. 107

Table 11: Genes included in cluster 1 from LRT – DGE analysis in Figure 2, left panels 107

List of abbreviations

aCSF	Artificial cerebrospinal fluid
ADAM10-22	Desintegrin and Metalloproteinase domain-containing protein 10/22
Aldoc	Aldolase C
Alkbh5	Alpha-Ketoglutarate-dependent dioxygenase AlkB Homolog 5
AMPA	Alpha-amino-3-hydroxy-5-methyl-4-isooxazole-propionic acid
AS	Alternative splice segment
Atxn1	Ataxin 1
B3gat1	β-1,3-glucuronyltransferase 1
Bai3	Brain-specific angiogenesis inhibitor 3
BDNF	Brain-derived neurotrophic factor
BSA	Bovine serum albumin
C1ql1	Complement component 1q-related factor
CA1-3	Hippocampal cornu ammonis region 1-3
Calb1	Calbindin 1
CAM	Cell adhesion molecule
Camk2b	Calcium/calmodulin dependent protein kinase II β
CBLN1-2	Cerebellin 1-2
CCD	Changeux-Courrège-Danchin model

Cdh7	Cadherin 7
Cdh-II	Classic cadherins type II
cDNA	Complementary DNA
CF	Climbing fiber
Cntns	Contactins
cPCDHs	Clustered protocadherins
CRTAC1	Cartilage Acidic Protein 1
CSE	Conserved sequence element
CTCF	CCCTC-binding factor
DI	Disparity index
DIV	Days *in vitro*
Dnmt	*De novo* methyltransferase
Dscam	Down syndrome cell adhesion molecule
E14	Embryonic day 14
Ebf2	Early B cell factor 2
EC	Extracellular domain
eCF-EPSC	Evoked climbing fiber excitatory postsynaptic current
EDR	Exponential distance rule
eGFP	Enhanced green fluorescent protein
EPSC	Excitatory postsynaptic current

ET	Extratelencephalic
FACS	Fluorescence-activated cell sorting
FAK	Focal adhesion kinase
Foxp1	Forkhead box protein P1
FRET	Fluorescence resonance energy transfer
Fto	FTO Alpha-Ketoglutarate Dependent Dioxygenase
GABA	Gamma-aminobutyric acid
Gabbr1-2	GABA-B receptor 1-2
Gad1	Glutamate decarboxylase 1
GAD65	Glutamic acid decarboxylase 65
GLUD1-2	Glutamate receptor δ 1-2
GO	Gene ontology
Gria3	Glutamate ionotropic receptor AMPA-type subunit 3
Grik4	Glutamate ionotropic receptor kainate-type subunit 3
Grin1	Glutamate ionotropic receptor NMDA-type subunit 1
Grm1	Glutamate metabotropic receptor type 1
Gsk3b	Glycogen synthase kinase-3β
HEK293	Human embryonic kidney 293 cell line
H-index	Shannon's *H* diversity index
Hspb1	Heat-shock protein family B member 1

ICD	Intracellular domain
IgSF	Immunoglobulin superfamily
Igsf9	Immunoglobulin superfamily member 9
IHC	Immunohistochemistry
Il1rapl2	Interleukin 1 receptor accessory protein like 2
IntDen	Integrated density
IO	Inferior olive
ION	Inferior olivary neuron
IQR	Interquartile range
IT	Intratelencephalic
Itpr1	Inositol 1,4,5-triphosphate receptor type 1
KO	Knock-out
LGI2	Leucine rich glioma inactivated 1
Lhx2	LIM homeobox 2
Lrrc4b	Leucine-rich repeat-containing protein 4B
LRRTMs	Leucine-rich repeat transmembrane proteins
LRT	Likelihood ratio test
mGluR1	Metabotropic glutamate receptor 1
MIP	Maximum intensity projection
Munc18-1	Mammalian uncoordinated-18 protein

NA	Numerical aperture
NCAM	Neural cell adhesion molecule
Nlgn	Neuroligin
NMDA	N-methyl-D-aspartate
Notch1	Neurogenic locus notch homolog protein 1
Nova2	NOVA Alternative Splicing Regulator 2
Nptn	Neuroplastin
NRCAM	Neuronal cell adhesion molecule
Nrxn	Neurexin
Oligo-dT	Deoxy-thymidine oligonucleotides
ORN	Olfactory receptor neurons
P3-30	Postnatal day 3-30
PBS	Phosphate-buffered saline
Pbx1	Pre-B leukemia transcription factor 1
PC	Purkinje cell
Pcp2/4	Purkinje cell protein 2/4
PCR	Polymerase chain reaction
PFs	Parallel fibers
PKC	Protein kinase C
PLC	Phospholipase C

Plcb3	Phospholipase C β3
Ppp1r17	Protein phosphatase 1 regulatory subunit 17
PPR	Paired-pulse ratio
Prkcg	Protein kinase C-γ
PSD95	Postsynaptic density protein 95
PTPδ	Protein tyrosine phosphatase δ
Pyk2	Proline-rich tyrosine kinase 2
RNA-ISH	RNA *in situ* hybridization
ROI	Region of interest
RT	Room temperature
RT-qPCR	Real time quantitative PCR
SCA14	Spino-cerebellar ataxia subtype 14
SCE	Single-cell electroporation
sc-RNAseq	Single cell RNA sequencing
Sdk	Sidekick cell adhesion molecule
SE	Super-enhancer
SEM	Standard error of the mean
Sema7A	Semaphorin 7A
Slc1a2	Solute carrier family 1 member 2 (glutamate transporter 1)

Slc1a6	Solute carrier family 1 member 6 (excitatory amino acid transporter 4)
Slc32a1	Solute carrier family 32 member 1 (vGAT)
Slitrk2	Slit- and Trk-like family member 2
sn-RNAseq	Single-nucleus RNA sequencing
Sphk1	Sphingosine kinase 1
TE	Tris-EDTA
TrkB	Tropomyosin receptor kinase B
U5 snRNP	20S U5 small nuclear ribonucleoprotein particle
vGAT	Vesicular inhibitory amino acid transporter
vGLUT1-2	Vesicular glutamate transporter 1-2
VST	Variace stabilizing transformation
WAVE	WASP family Verprolin homolog
WIRS	WAVE interacting receptor sequence
Z+PC, Z-PC	Zebrin-positive PC, zebrin-negative PC

Introduction

Introduction

Chapter I: Genetically encoded diversity and epigenetic landscape drive developmental brain wiring

Shaping brain wiring at different scales: probabilistic versus deterministic models

Adaptative behaviors require highly specific neuronal connections, ranging from motor control and coordination, spatial navigation, and sensory information integration to emotional processing, decision-making, and social behavior. Across Animalia phyla, we can observe that the complexity of behavior correlates not only with brain size (and in turn the number of neurons) (Williams & Herrup, 1988), but also with the density and level of specialization of brain connections. For instance, small mammals, with a reduced repertoire of behaviors, possess a lower number of cortical neurons compared to cetaceans and primates (4 million in mice *versus* 10500 million in whales) (Herculano-Houzel, 2009; Marino, 2002; Roth & Dicke, 2005). In addition, these neurons are spatially organized across the cortex. In macaques, the cortex is conventionally divided into 100 specialized areas forming an extremely dense but highly organized network of synaptic connections (Markov et al., 2013; Van Essen et al., 2012).

Historically, one of the most debated questions in Neuroscience has been how neurons connect to each other during development to form such functional and adaptative circuits. At the cellular level, this process can be decomposed into the following steps: (1) formation of neuronal processes, (2) development of growth cones, (3) axonal pathfinding, (4) target field recognition, (5) postsynaptic cell selection, (6) subcellular targeting, (7) synaptogenesis, (8) synapse elimination and synapse pruning, and finally, (10) structural and functional reconfiguration of synapses (synaptic plasticity) (Juttner & Rathjen, 2005). Therefore, newborn neurons need to recognize their possible partners, connect and stabilize some of them while selectively discarding inappropriate ones. But how are the final synaptic partners chosen and stabilized in the long term?

At the cellular scale, Peter's rule was introduced as a probabilistic mechanism to explain the formation of connections between cortical neurons following axonal pathfinding (Braitenberg & Schüz, 1991; Peters & Feldman, 1976). It posits that the probability of connection between two neurons is primarily

determined by the spatial proximity of their axonal and dendritic arbors (Rees et al., 2017).

At the meso/macroscale, analyses of brain connectivity across phylogenetically distant species point to two additional probabilistic wiring rules. First, the Exponential Distance Rule (EDR), based on large-scale retrograde tracing studies in the macaque cortex (Markov et al., 2013), describes how the probability and strength of connections decrease exponentially with physical distances between cortical areas. Second, the "connectional homophily" principle, based on social networks observations (Granovetter, 1973), proposes that brain regions with similar connectivity profiles are more likely connected with each other (Goulas et al., 2015). Interestingly, modelling connectomes of several species (*Drosophila*, mouse*,* macaque and humans) integrating both EDR and connectional homophily rules can explain on average 83% of the variance in connection probability and strength, as well as ~80% of the overall topology of brain wiring (Goulas et al., 2019). Such models of neuronal wiring at large scale complement Peter's rule at the microscale. These models propose that specific neuronal wiring can be explained, at least in part, through probabilistic processes.

However, there is strong evidence that neuronal connectivity is biased by deterministic. First, synthetic connectomes models built on EDR and homophily principles fail to capture an important percentage of connections diversity *in vivo* (~20-30% of unexplained variance) (Goulas et al., 2019; Goulas et al., 2015; Markov et al., 2013). This may reflect the contribution of axon guidance cues, and activity-dependent plasticity that are expected to refine circuits in a more deterministic manner. In line with this idea, the connectional homophily model introduced by Goulas indicates that local efficiency of connections improves as weak links are pruned, since neighboring connections redundancy is reduced. In fact, the connectional homophily principle represents a non-spatial factor that bias connectivity. This further supports the contribution of selective synaptic pruning mechanisms that depend on local activity-dependent mechanisms (see Introduction Chapter II). Most importantly, recent connectomics studies refute Peter's rule, i.e. the idea that physical proximity is sufficient to predict synaptic

connectivity. For instance, the saturated reconstruction of a mouse neocortex sub-volume using electron microscopy revealed that each cell is surrounded by a high number of possible partners (193 dendrites and 1407 axons in 1,500 μm^3), but the connectivity observed between them does not fit a random distribution that would simply result from axon-dendrite adjacency (Kasthuri et al., 2015).

Altogether, the non-random arrangement of connections support the idea that possible synaptic partners, even belonging to the same region and cell type, are not equivalent and that cellular cues must be used to discriminate them and guide the selection process in support of adaptation (Juttner & Rathjen, 2005; Sanes & Zipursky, 2020; Shen & Scheiffele, 2010). Modern single-cell profiling techniques (single-cell RNA sequencing and patch-clamp, among others) have shown that, indeed, neurons display different activity patterns and molecular features at the population and single-cell level, differentiating cells at both the genetic and functional levels. The origin of these differences, as well as the consequences in circuit wiring, are discussed in the following paragraphs.

Genetically predetermined circuits as a first step towards selective connectivity: the CCD model

What are the cues that shape and determine connectivity? The species-specific intrinsic constrains to brain development have been referred to as the "genetic envelope" according to the Changeux-Courrège-Danchin model (CCD model) from 1973 (Changeux, 2022; Changeux et al., 1973). Such genetically encoded instructions dictate the fundamental scaffolding of connectivity – the "proto-organization" of the brain. The genetic envelope provides the limits of circuit wiring because it phenotypically defines a discrete number of possibilities regarding brain cell types, possible neurotransmitters, receptors, cell-recognition molecules, as well as higher-order features such as those shaping the macroscopic morphology of the brain. At the same time, the genetic envelope is diverse enough as to provide a pool of possibilities on which "variation-selection-amplification" processes operate to fine-tune connectivity (Changeux, 2022).

Each individual, starting with predetermined phenotypic features, inevitably assembles, selects and stabilizes synaptic connections that will provide an adequate adaptation to its environment. In other words, neurons connect spontaneously, in a predetermined manner, and selected connections are later stabilized depending on neuronal activity (see Introduction Chapter II).

The activity-dependent stabilization of specific connections from the initial genetically-defined pool can be seen as a micro-level form of natural, Darwinian selection occurring over the course of an individual's lifetime. "Variation – selection – amplification" Darwinian processes operate at the ecosystems level driving the evolution of species – from the initial genetical variability pool within a defined species, the features that provide a better adaptation to the environment are selected and stabilized in the population. Applying this logic to the vertebrate nervous system, certain environmental adaptations are determined by an optimal interaction with the organism surroundings. This includes an adequate stimuli perception, integration of sensory information, and the generation of a suitable response. For example, a predator's hunting success relies on exact timing between visual processing neurons that detect prey movement and motor neurons that coordinate the strike. Therefore, the selection of specific connections able to synchronize both sensory processing and motor coordination. Success of such behaviors is achieved through trial and error, as proposed by the CCD model. This way, the neuronal connections able to better encode this synchronicity are strengthened while inappropriate ones are eliminated. Hence, the environment is able to modulate the genetic envelope to stabilize connections that evoke the most adapted behaviors.

Environmental influence on the genetical envelope during developmental critical periods

During perinatal development, neurons will thus connect as encoded by the genetic envelope. A peak of connectivity around the second postnatal week in mice can be observed in different brain regions, after which selective synaptic

pruning will fine-tune the final wiring based on the environmental effect (Holtmaat & Svoboda, 2009; Lendvai et al., 2000). The ability of environmental inputs on shaping neuronal circuits varies dynamically throughout an individual's lifespan. Critical periods have been defined as developmental time windows during which nervous cells display high plasticity that enables them to form and refine synaptic contacts depending on environmental stimuli (Cisneros-Franco et al., 2020; Hensch, 2004; Hensch & Bilimoria, 2012; Takesian & Hensch, 2013). During development, hyper-plastic neurons might form as many different connections, or accept as many different afferents, as it is genetically possible. Then, environmental stimuli – translated as synaptic activity at the cellular level – applies a selective pressure on the available functional and molecular diversity of connections (**Figure 1**).

Environmental stimulation is crucial for the functioning and development of the brain. If a given circuit remains unstimulated during the time window of a critical period, its function may be compromised in the long term (Hensch & Bilimoria, 2012). Although environmental stimuli influence brain circuits during the entire individual's life (through synaptic plasticity), the profound structural changes in connectivity that sensory inputs can induce during development are restricted to critical periods. This means that certain adaptations can only be acquired during limited time periods of development (Hensch, 2004). Hubel and Wiesel's pioneering experiments on the development of the cat visual system provided the first experimental evidence for the existence of critical periods in brain circuit development (Hubel & Wiesel, 1963; Hubel & Wiesel, 1972, 1977). They demonstrated that when visual input from one eye was blocked shortly after birth, neurons in the primary visual cortex lost their ability to respond to stimuli

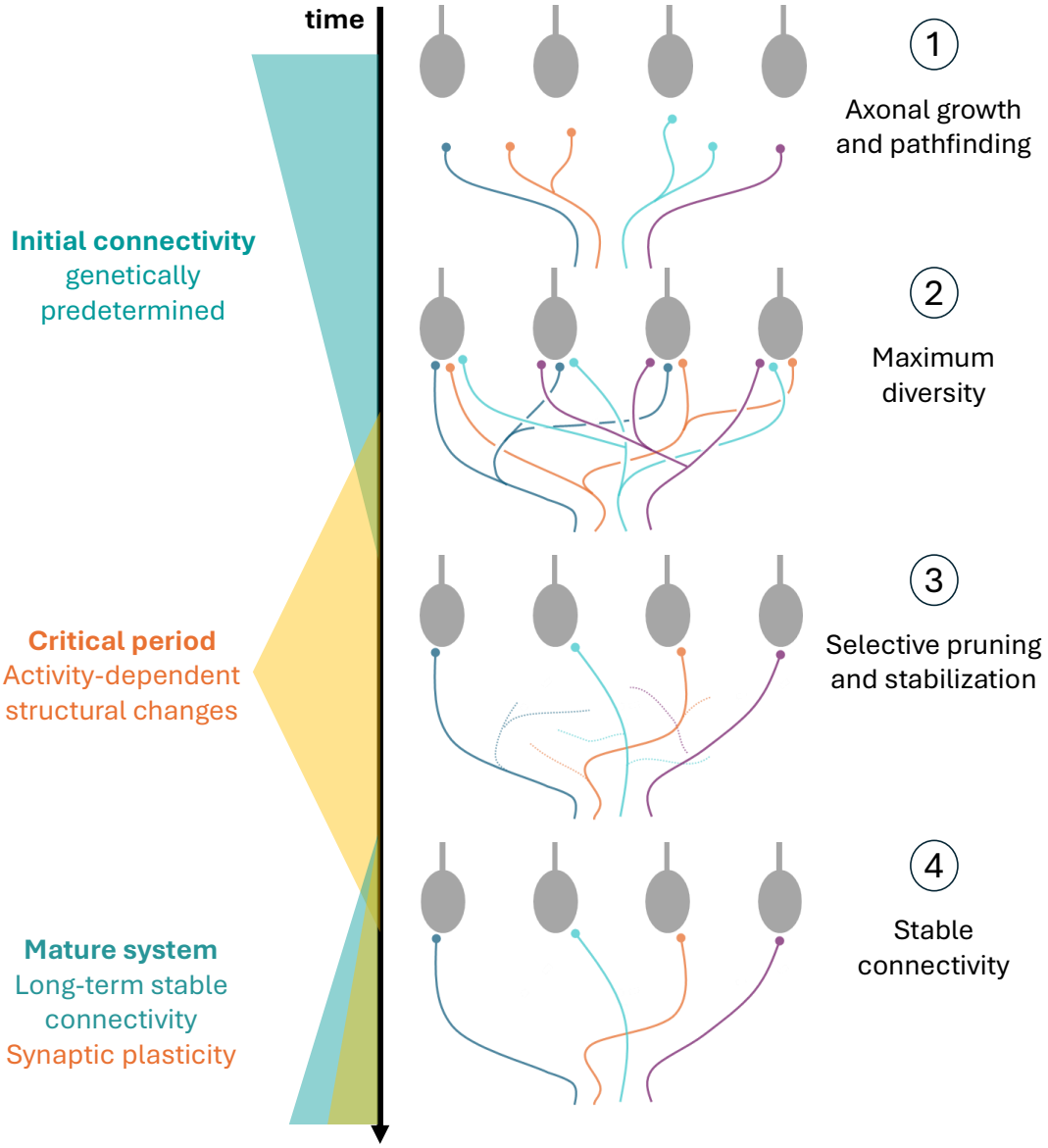

Figure 1: Schematic model of the selective stabilization of synapses during developmental critical periods. On the left, the main factors biasing circuits wiring across time are represented as "genetically encoded" in blue and activity or environmental-dependent in yellow. Each triangle represents approximately one postnatal week starting at P0, although it is variable across brain regions and environmental conditions. On the right, the phenomena happen over time. (1) Axonal growth and pathfinding happen perinatally in a genetically predetermined manner. (2) All genetically possible synaptic partners connect. Maximum connectivity diversity is achieved. (3) Environmental stimulation Adapted from Changeux (2022) and Juttner and Rathjen (2005).

from the deprived eye. This functional loss is accompanied by anatomical changes: axonal projections within the retino-geniculo-cortical pathway from the deprived eye retract, while those from the non-deprived (contralateral) eye expand into the now vacant target territory. When such monocular deprivation is maintained throughout the entire critical period, these structural and functional alterations become irreversible (Antonini & Stryker, 1996; Hubel & Wiesel, 1963; Le Vay et al., 1980).

At the behavioral level, neural structural remodeling likely supports the acquisition of important cognitive skills known to be restricted to critical periods. A well-known critical period in humans is the acquisition of language, that requires language exposure during the first year of postnatal development. The required plasticity to acquire maternal language is limited in time but highly effective. In fact, the learnt maternal language is not forgotten even under deprivation. On the other hand, the ability to acquire a second language is highly reduced during adolescence (Johnson & Newport, 1989; Lenneberg, 1967). These phenomena highlight the importance of environmental sensory stimulation for circuit wiring early in life, as well as the unique plastic properties of circuits during critical periods.

However, critical periods are not well-delimited time windows and age is not the sole factor driving their opening and closing. Instead, they are regulated by experience and by the activity of a given neuronal circuit. In fact, high plasticity can last longer with exposure to an enriched environment (Francis et al., 2002). At the cellular level, it has been shown that the excitatory-inhibitory balance plays a crucial role in the regulation of critical periods. Inhibitory GABAergic signaling maturation is thought to “open” critical periods. In fact, loss of GABAergic functions through deletion of glutamate decarboxylase 65 (GAD65) blocks the onset of critical periods: GAD65 knock-out (KO) mice do not display the electrophysiological and structural changes described by Hubel and Wiesel (1963) upon monocular deprivation. Conversely, pharmacological enhancement of GABAergic signaling with benzodiazepines restored critical period plasticity and thus monocular deprivation-derived changes happened normally (Hensch et

al., 1998). Enhanced excitatory activity through NMDA receptors similarly reduced the effects of monocular deprivation (Fagiolini et al., 2003). These results highlight the role of excitatory/inhibitory balance as a trigger for critical periods plasticity (Hensch & Bilimoria, 2012; Takesian & Hensch, 2013).

Similarly, the maturation of the brain induces the expression of certain "break-like" factors that close critical periods by limiting adult plasticity and hence prevent excessive rewiring. For this reason, certain connectivity modifications achieved perinatally are irreversible in the mature system. For example, the formation of myelin around axons improves signals transmission but simultaneously prevents axonal growth, which restricts plasticity and excessive rewiring (McGee et al., 2005). In addition, the closure of critical periods has been correlated with a decrease in histones acetylation (Putignano et al., 2007). Gene expression changes of a variety of factors, such as brain-derived neurotrophic factor (BDNF) and others, further promote critical periods closure (Takesian & Hensch, 2013).

Within critical periods, specific connections are strengthened and stabilized in an activity-dependent manner while others are selectively pruned. In neural circuits where postnatal selective elimination of synapses was reported, it has been shown that artificial modifications of neuronal activity during the critical period prevents synapse stabilization and pruning (Kano & Hashimoto, 2012; Luo et al., 2005). This is the case at the neuromuscular junction (Redfern, 1970; Turney & Lichtman, 2012; Walsh & Lichtman, 2003) and the olivo-cerebellar circuit (Hashimoto, Ichikawa, et al., 2009; Hashimoto & Kano, 2003, 2013). In both cases, several presynaptic afferents (motor neurons or olivary neurons) innervate simultaneously each postsynaptic element (muscular plate or Purkinje cell, respectively) during the first postnatal week. Rapidly after, axons engage in an activity-dependent competition to get stabilized on the postsynaptic cell. One afferent is selected and strengthened and by the third postnatal week, all postsynaptic targets are mono-innervated. The "winning" afferent occupies progressively a larger space in the postsynaptic element and the connection is

stabilized in the long term. In parallel, “loosing” axonal branches progressively retract and get pruned.

Epigenetic changes promote long-term stability of connections

The environment's influence on the "genetic envelope", in the form of neuronal activity, can be considered an epigenetic modification following Waddington’s original definition of the term: "how external events, some random, combined with inherited information coded in the genes to produce acquired variability between individuals of the same species." (Waddington, 1942). Although Waddington postulated that such epigenetic changes might be heritable, in a Lamarckian way, experimental observations of brain development points otherwise, since each individual undergoes “variation-selection” phenomena during postnatal development, as exemplified above. This means that circuitry is genetically biased, but not entirely predetermined. Such flexibility may, in fact, confer an evolutionary advantage: only major connectivity features are genetically encoded (hence heritable), but each individual can adapt brain wiring to the features of a changing environment.

Besides the structural remodeling that occurs during developmental critical periods, the maintenance of synaptic circuits organization beyond the critical period likely requires long-term, “epigenetic”, regulation of gene expression. For instance, experimental evidence suggests that olivo-cerebellar circuit development imprints molecular changes in cerebellar Purkinje cells (PCs), changing its function and integration in the circuit ((Letellier et al. (2007); (Letellier et al., 2009; discussed in Introduction Chapter IV). Therefore, one could infer that, during critical periods, environmental stimuli may induce gene expression modifications in the selected synaptic partners to ensure long-term stability. Consequently, it implies the existence of a genetic system variable enough to encode all possible connections, yet flexible enough to be regulated by environmental cues.

In this thesis work, we focus on the study of the genetically encoded variability of putative synaptic partners and the effect of stimuli on such diversity. In other words, our interest is on the variation-selection mechanisms at the cellular level regulated through the epigenetic landscape.

Introduction

Chapter II: Nested cellular diversity in the mammalian brain and its implications in circuit wiring

Neuronal diversity: morphology, function and molecular identity

Terminal selectors: master keys defining cell populations

The mammalian genome remarkably encodes multiple layers of nested diversity in brain cells, encompassing cell types, populations, subpopulations, and the unique molecular identities of individual cells. During embryonic development, neural stem cells must progressively engage into nested specific genetic programs that will progressively define their identity. Cell fate engagement is mediated at early developmental stages by “terminal selectors”: a reduced series of transcription factors able to orchestrate the co-expression of cell type specific genes, defining and maintaining cell identity in the long term. This is a highly evolutionarily preserved regulatory mechanism across multicellular organisms (Arendt et al., 2016; Hobert & Kratsios, 2019). Terminal selectors govern key and basic morphological, functional, and molecular characteristics of a neuron type, including the size and complexity of its dendritic arbor, its firing properties, and the molecular components underlying excitatory or inhibitory synaptic signaling. Together, these features critically shape the neuron's fundamental role within the neural circuit it belongs to.

Several terminal selectors have been discovered in mice. Knocking out these transcription factors prevents the proper development of their corresponding neuron types. For instance, the Lhx2 LIM homeobox gene is required for olfactory receptor neurons (ORN) differentiation. Lhx2-KO mice embryos are unable to form an olfactory bulb structure, and no olfactory receptors are expressed. Although progenitor cells differentiate into neurons, these are not able to acquire the specific features of ORNs (Hirota & Mombaerts, 2004; Kolterud et al., 2004). Similarly, the transcription factor Pbx1 regulates the differentiation of dopaminergic neurons in the olfactory bulb. While it binds and activate the expression of dopamine machinery (dopamine synthesis and transporters), it prevents alternative interneuron cell fates (Remesal et al., 2020). In the cerebellum, early B cell factor 2 (Ebf2) is expressed by all cerebellar PCs progenitors, but its expression is later restricted to zebrin-negative PCs. Therefore, the dynamic regulation of Ebf2 expression defines PC subtypes

(Badaloni et al., 2019). Terminal selectors can be understood thus as master regulators of cell type differential gene expression, necessary and sufficient for specific cell fate definition.

Morphological and functional differences across neuronal subpopulations

The existence of neuronal subpopulations was first noticed at the morphological level through the groundbreaking observations made by Santiago Ramón y Cajal at the end of the nineteenth century. Using Golgi's staining method, he could identify numerous neuron types based on their shape, size, dendritic and axonal architecture (Cajal, 1893, 1894, 1899, 1904; DeFelipe, 2002; Garcia-Lopez et al., 2010). These major morphological differences between neuronal cells populations are expected to strongly bias the connections that can possibly be established. For example, pyramidal neurons in the layer 5 of the neocortex can be classified into two distinct subtypes: intratelencephalic (IT) and extratelencephalic (ET) neurons. While ITs present a small soma and little distal dendritic branching, ETs have a larger cell body and a higher diameter apical dendrite with extensive branching in layer 1. In the primary somatosensory cortex, several inputs from other cortical regions and thalamic nuclei are densely found in layer 1, where they find a connect ETs. On the other hand, cortico-cortical projections arrive preferentially to layer 5a, finding preferentially the cell bodies IT pyramidal neurons. Thus, their dendritic morphology may strongly bias the type of inputs they receive (Groh et al., 2010; Hattox & Nelson, 2007; Kasper et al., 1994; Moberg & Takahashi, 2022).

The first intracellular recordings were achieved during the 1950s (Brock et al., 1951, 1952a, 1952b; Woodbury & Patton, 1952a, 1952b). Sharp glass electrodes were used to penetrate single cells and record action potentials *in vivo*. The first giga-seal patch-clamp recordings were achieved during 1970s, which considerably increased the sensibility and range of recordings that could be performed (low leak and low noise; whole-cell, single-channel, voltage-clamp…). Importantly, patch-clamp electrodes allow the addition of drugs and

dyes in the intracellular solution. In 1988, Horikawa and Armstrong set today's gold-standard by filling recorded cells with biocytin and reconstructing single neurons dendritic trees (Horikawa & Armstrong, 1988). Intracellular and patch-clamp recordings allowed to further classify neurons according to both their electrophysiological properties (e.g., firing pattern) and morphologies (biocytin or dye filling) (Stuart & Brownstone, 2011). In the case of layer 5 pyramidal neurons, morphological subtypes additionally display different electrophysiological properties. ETs, due to the higher diameter of their apical shaft, display lower axial resistance, meaning that distal depolarizations reach the soma with less attenuation. Such depolarizations trigger voltage-dependent Ca^{2+} plateaus, leading to burst firing. On the contrary, the smaller IT pyramidal neurons have higher input resistance, higher firing thresholds and higher rheobase. ITs display a strong adaptation during sustained inputs, which favors single-spike (non-bursting), adapting trains (Hattox & Nelson, 2007; Kasper et al., 1994; Mason & Larkman, 1990; Moberg & Takahashi, 2022).

Molecular heterogeneity of cell populations, subpopulations and single neurons

Besides morphological and functional heterogeneity across neuron types, molecular characterization has revealed additional layers of diversity. Neuronal subtypes express discrete sets of genes (marker genes) that differentiate them from other cell populations and possibly reflect different functional contributions to synaptic circuits. Such differences in gene expression confer a population-level identity to discrete groups of neurons. In the cerebellum, for example, most cerebellar PCs express calbindin 1 (Calb1) and inositol 1,4,5-trisphosphate receptor type 1 (Itpr1). The expression of these genes in PCs was first described using immunochemical assays (Celio, 1990; Suburo et al., 1993). In addition, only subsets of PCs express subpopulation markers, creating the so-called cerebellar sagittal bands. Similarly, these antigens were first discovered through immunolabelling and include Zebrin I, Zebrin II (identified later as aldolase C),

Q113 antigen, 9-O-acetylGD3 or the P-path antigen (Apps & Hawkes, 2009; Hawkes et al., 1985; Leclerc et al., 1990; Plioplys & Hawkes, 1987) (**Figure 2**). These molecular patterns are closely aligned with the topographical organization of PC afferents (Sugihara, 2005; Sugihara & Shinoda, 2004) and parallel functional diversity. Zebrin-negative (Z-) PCs, for instance, exhibit higher firing rates than Zebrin-positive (Z+) PCs (Nguyen-Minh et al., 2019; Zhou et al., 2014). This functional distinction extends to their targets in the deep cerebellar nuclei, where Z-PC targets also fire at higher frequencies (Beekhof et al., 2021), highlighting the relevance of subpopulation identity in the information processing by neuronal circuits.

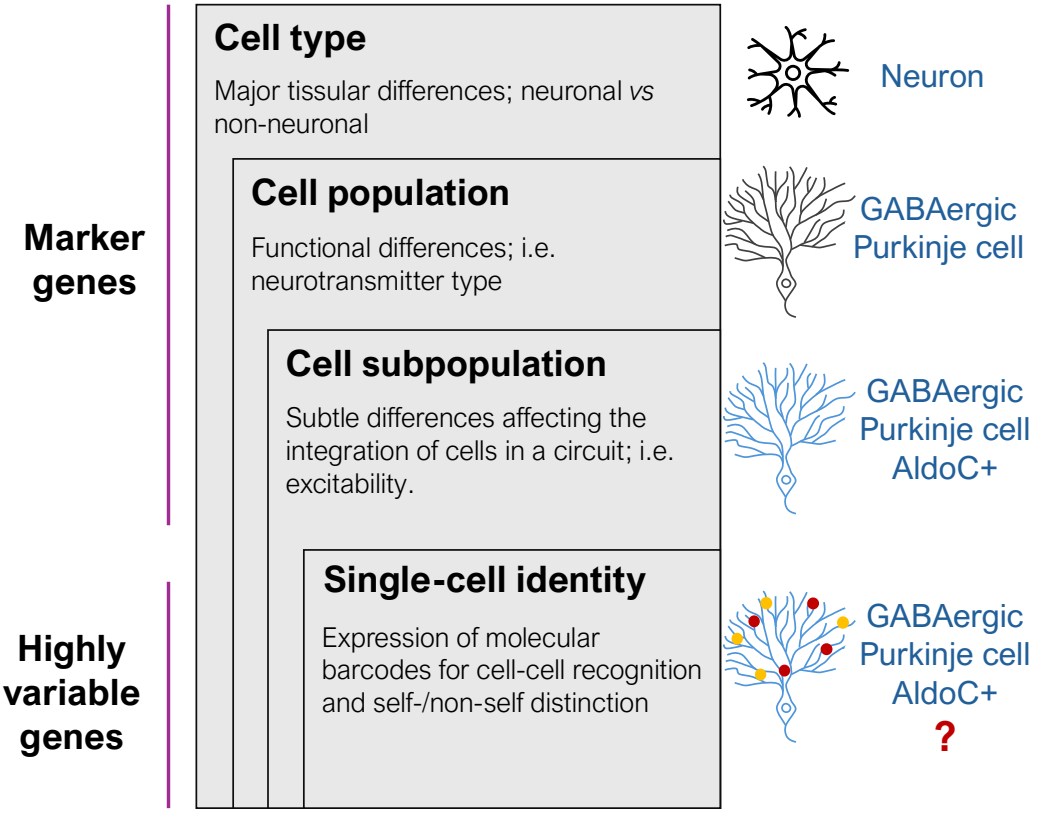

Figure 2: Schematic representation of cells nested diversity in the brain, from cell types to single-cell identity. Cell types, populations and subpopulations can be identified molecularly by the expression of common marker genes. Single-cell identity is encoded by highly variable genes that display different expression patterns in each cell. On the right, cell identity at each level is exemplified with cerebellar PCs.

Recent advances in gene expression analysis techniques, such as single-cell RNA sequencing (sc-RNAseq) have allowed the identification of new PC marker genes, such as Ppp1r17 (Kozareva et al., 2021; Peng et al., 2019). Similarly to other *omics* approaches, sc-RNAseq presents a major benefit when compared to other RNA profiling techniques. It allows the simultaneous and unbiased quantification of up to 60% of the genes expressed by individual cells (Hagemann-Jensen et al., 2022), which enables the identification of novel molecular signatures. Taking advantage of this technique, Özel et al. (2020) studied the molecular identity of *Drosophila* spp. optic lobes, which are composed by 200 morphologically differentiated cell populations (Nern et al., 2015). 275000 individual cells were analyzed, and each previously described subpopulation was correlated with a discrete gene expression signature. These results exemplify the potential of sc-RNAseq for exploratory experimental designs.

Molecular profiling experiments do not only find correlated gene expression to the phenotypical properties described for the neurons of interest but also discover new subpopulations. Kozareva et al. (2021) employed single-nuclei RNAseq to study mouse cerebellar cell populations. They found several new subpopulations belonging to each cell type; specifically, they found 46 molecular clusters that could be attributed to18 major cell types. PCs were divided into 9 transcriptional subtypes, seven of which are Z+PCs and many of them were previously unknown. Moreover, they discovered two distinct types of molecular layer interneurons. The two clusters also differ in firing properties and developmental trajectories. These results highlight the importance of in-depth multimodal profiling techniques in order to fully understand cell diversity in the brain, and how such different identities might contribute to circuits functioning.

Patch-clamp allows, as explained above, the introduction of a variety of reagents in the recorded cell, facilitating single-cell morphological reconstruction, as well as single-cell manipulations. It is also possible to recover intracellular material from the recorded cell. PatchSeq combines electrophysiological recordings with sc-RNAseq and morphological analyses, allowing to directly correlate these three parameters (Cadwell et al., 2016). Using this approach, it

was shown that firing properties of hippocampal neurons are tightly correlated with ion channels expression. In addition, a common signature of 10 cell-adhesion molecules (CAM) was found expressed in every cell type, while discrete differential CAMs were enriched in specific electrophysiologically-defined cell populations (Földy et al., 2016). Hence, PatchSeq is able to obtain a single-cell multimodal passport by correlating cells functional features with the expression of genes that might not have direct implications in their electrical activity, such as CAMs, but that may play important roles in synaptic specificity (Sanes & Zipursky, 2020). The dual readout of PatchSeq makes it thus ideal for mapping neuronal diversity and predicting connectivity.

Altogether, nested layers of cellular identity at the morphological, functional and molecular levels may bias neurons' activity and therefore their integration in synaptic circuits. Yet, as explained in Chapter I, synaptic partners need to recognize each other to selectively stabilize and eliminate connections. Therefore, a final layer of differentiation to encode single-neuron identity might contribute to the process of synaptic partners selection (Yagi, 2012). Single-cell identity has been proposed to be encoded by the combinatorial expression of CAMs, due to their variability and to their role mediating cell-cell interactions (see Chapter III). In addition, highly variable CAMs, able to encode a broad diversity of isoforms within a limited amount of genes, may be important actors of such a "molecular code of connectivity" (Sanes & Yamagata, 2009; Sanes & Zipursky, 2020). Certain CAMs display a differential pattern of expression at single-cell resolution rather that cell populations; this is, each cell expresses a specific combination of CAMs that distinguish them from other neighboring partners. Specific protein families able to encode single-cell identity are discussed in Chapter III.

Hebb vs Sperry: two models to explain synaptic partner selection

In the context of synaptic circuit assembly, to what extent is morphological, functional and molecular heterogeneity used by individual neurons to

discriminate and choose their potential partners, i.e., achieving and maintaining synaptic specificity? During the twentieth century, two models rose as possible criteria underlying synaptic specificity: Hebb's postulate (Hebb, 1949) and Sperry's chemoaffinity hypothesis (Sperry, 1963). Donald Hebb proposed the famous statement "cells that fire together, wire together". In the context of developmental plasticity, neurons with highly synchronized activity tend to reinforce their mutual synaptic connections while those that are out of synchrony lose them. Correlated firing drives larger and more sustained pre- and postsynaptic signaling events (Ca^{2+} transients, increased neurotransmitter release or enhanced receptor insertion), which in turn stabilizes and strengthens those particular afferents over the others. On the other hand, Roger Sperry proposed, based on his experiments in *Xenopus* spp. retino-tectal system, that brain connectivity might be molecularly encoded and refined according to chemical gradients. Sperry surgically removed the frog's eye, rotated it 180 degrees and reimplanted it. After optic nerve regeneration, the frog's visual behavior was inverted, meaning that in response to a stimulus appearing above, the animal would response with a strike downward. This showed that the regenerating optic fibers reconnected to their original locations in the tectum, not to new ones corresponding to the rotated eye's orientation. These experiments led to the hypothesis that optic nerve and tectum cells displayed specific "cytochemical labels" that guided synaptic partners during wiring. Thus, Sperry proposed that connectivity might be guided by predetermined chemical (genetic) cues (Sperry, 1963).

Although both models may seem contradictory (activity-dependent *versus* predetermined connectivity), modern experimental evidence supports both, suggesting that it is the interplay between molecular identity and environmental stimuli which defines the final circuitry. Hubel and Wiesel (1977) studies on the primary visual cortex demonstrated that ocular-dominance stripes are immature at birth and sharpen with visual experience (see Chapter I). Their results show that environmental stimuli during critical periods bias brain connectivity. Later, similar experiments were performed with other species and cortical areas,

reaching similar conclusions. For example, the pathway from the central nucleus to the external nucleus of the inferior colliculus encodes a map of the auditory space, allowing birds to detect the source of a sound and move to include it within their visual field (Knudsen, 2002). In juvenile owls, auditory and visual stimuli were altered using ear plugs and prisms, respectively. Juveniles thus learnt to localize sound sources according to the altered auditory input and visual field (Brainard & Knudsen, 1998; Knudsen et al., 1984). When connectivity changes were assessed in this circuit, axonal sprouting and new boutons were detected, as well as abnormal projections from the central to the external nucleus. These results indicate stimuli-dependent reorganization of connectivity. Yet, normal, predetermined projections coexist with new learnt ones (DeBello et al., 2001; Feldman & Knudsen, 1997; Knudsen, 2002). These results highlight thus the ability of environmental stimulation in shaping neuronal circuits. Yet, it does not discard the influence of genetically-encoded information shaping circuits in coordination with neuronal activity.

Neurotransmission is not required for synapse formation or diversification

Intriguingly, studies from different research groups have shown that the formation and diversification of glutamatergic synapses in the hippocampus can be achieved in the total absence of neurotransmitter release. Spontaneous and evoked synaptic transmission was silenced in mouse embryos through the deletion of the vesicle fusion protein Munc18-1. Despite the lack of chemical synapse activity, synapses assembled during development with normal morphology and ultrastructure (Verhage et al., 2000). Later, Sando et al. (2017) selectively silenced synaptic glutamate release using tetanus toxin selective expression in cortical and hippocampal neurons and analyzed synapse formation. Hippocampal circuits assembled correctly, and axonal projections reached the expected target areas, indicating that stereotyped connectivity can be achieved in the absence of stimuli and is likely genetically-encoded. In addition, dendritic arborization and spine density and morphology showed minimal alterations,

indicating that these may rely on cell-autonomous mechanisms. At the synaptic level, both pre- and postsynaptic membranes showed morphological specialization, meaning that neurotransmitter release is dispensable for the scaffolding of synapses (Sando et al., 2017; Zhu et al., 2021). It was then questioned whether these morphologically correct synapses were functional even if they assembled in the absence of neurotransmitter release. To address this question, Sigler et al. (2017) silenced CA3 pyramidal neurons in organotypic slices, and subsequently assessed the functionality of dendritic spines on their CA1 targets. Through two-photon glutamate uncaging, they could evoke robust synaptic currents mediated by alpha-amino-3-hydroxy-5-methyl-4-isooxazole-propionic acid (AMPA) and NMDA receptors (AMPAR, NMDAR), similar to those elicited in control neurons. These results importantly showed that synapses assembled in the absence of neurotransmitter release display mature functional properties (Sigler et al., 2017). Altogether, these studies demonstrate that synapse architecture is specified by intrinsic molecular programs, not by activity-dependent feedback, although neuronal activity is later needed to achieve adaptative refinement of circuits.

The fact that neurons can recognize each other to form synapses in the absence of activity implies the existence of molecular codes that would enable cell-cell recognition and interaction. However, an interesting paradox emerges from this idea: how can the limited number of genes in the genome encode the diversity of an almost infinite number of possible synaptic connections?

Introduction

Chapter III: Clustered Protocadherins as candidates to encode single-neuron identity

CAM polymorphism: criteria for single-neuron identity encoding

The search for a molecular connectivity code capable of individually labeling every neuron has long focused on CAM families, whose diversity rivals the complexity of neural circuits (Sanes & Yamagata, 2009; Sanes & Zipursky, 2020; Yagi, 2012). To be viable candidates, such CAM families must exhibit specific characteristics at both the gene and protein levels. First, they must be able to mediate transmembrane interactions between cells. Second, the candidate gene family must provide a repertoire large enough to generate unique surface profiles. However, it is estimated that the mouse brain is formed by about 10^8 neurons and 10^{11} synapses (Koch et al., 2022), but the mouse genome contains ~ 20000 protein-coding genes (Mudge et al., 2025). Therefore, candidate genes must be the object of transcriptional and post-transcriptional mechanisms able to increase genetic product diversity; for example, the use of alternative promoters and alternative splicing mechanisms. At the protein level, the interactome diversity can increase depending on how CAMs arrange and interact in the membrane. If the interacting unit is a monomer, the diversity of possible interacting units will equal the gene products obtained after post-transcriptional processing. However, if the interacting units of a given CAM family are arranged in the membrane as heteromultimers, the final product diversity can be calculated as:

$$\binom{n}{m} = \frac{n!}{m!\,(n-m)!}$$

, where *n* indicates the number of post-transcriptional products, and *m* stands for the number of monomers composing each heteromultimer.

Third, the transmembrane interactions mediated by these proteins must involve highly specific binding to ensure unambiguous, selective recognition. If a given CAM variant could promiscuously interact with several binding partners in *trans*, the recognition code would become noisy and confusing. Fourth, each variant should not be uniformly expressed across cells but rather follow a scattered pattern within the cell population. That is, protein variants should show

differential expression at single-cell resolution. This way, a recognition code could be expressed by each cell in the form of stochastic combinations of isoforms. Fifth, we could expect a regulated pattern of expression during perinatal development, since it is during this period when neurons form and select specific synaptic connections, shaping in turn their molecular identity for long-term maintenance of the selected circuits. Consequently, candidate genes might be the object of activity-dependent transcriptional regulation. Attending to these criteria, vertebrate CAM families can be inspected in search of candidates (**Figure 3**).

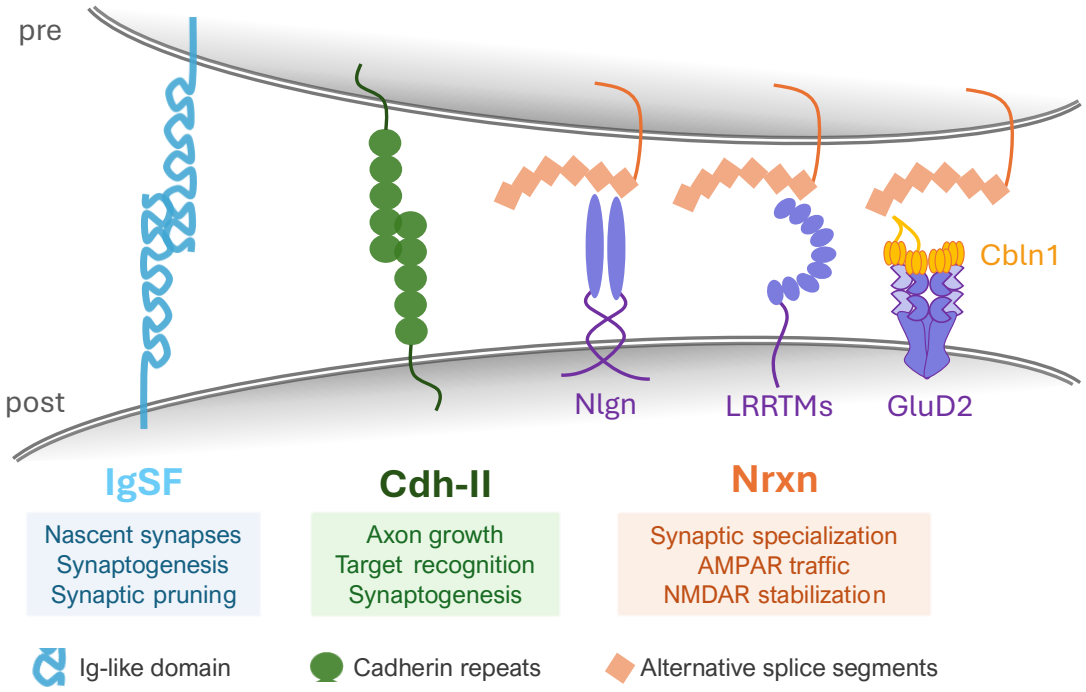

Figure 3: Polymorphic CAMs functions in connectivity. Immunoglobulin superfamily proteins (IgSF), such as NCAM, are located at nascent synapses and are involved in synapse formation and maturation, as well as synaptic pruning. Classic cadherins type-II (Cdh-II) guide axon growth and are involved in target recognition and synaptogenis. Neurexins (Nrxns) interact heterophilically with different synaptic postsynaptic molecules, including Nlgn, LRRTMs and the GLUD2/CBLN1 complex. They induce pre- and postsynaptic specialization, promote AMPAR trafficking and NMDAR stabilization.

Candidate CAMs for a molecular code of connectivity

Among those involved in target recognition, we can then focus on the families providing the wider protein repertoires (reviewed by Sanes & Zipursky, 2020). The immunoglobulin superfamily (IgSF) is formed by more than 500 genes and some of its members have been studied for their implication in synapse formation, maturation, maintenance and plasticity. It has been shown that neural cell adhesion molecules (NCAM), IgSF members, regulate the number and maturation of excitatory and inhibitory synapses. Several NCAM isoforms can be generated through alternative splicing, although their extracellular, interacting domains are equal across isoforms. They mediate homophilic adhesion in *trans*, but they also interact with different molecules through *cis*- and *trans*-heterophilic binding (Sytnyk et al., 2017). NCAM accumulates at emerging synapses in the hippocampus and promotes preferential synaptogenesis *in vitro*. It may act as a molecular tag indicating the location of new synapses (Dityatev et al., 2004). Interestingly, NCAM undergoes post-translational polysialylation, which modifies its binding properties and plays a relevant role in developmental synaptic pruning. Blocking NCAM polysialylation affects NMDA receptor dynamics in CA3 synapses and hence deeply affects hippocampal wiring (Guirado et al., 2014; McCall et al., 2013).

In the retina, the IgSF members Sidekick CAMs (Sdks), vertebrate Down syndrome CAMs (Dscams) and contactins (Cntns) are expressed in subsets of interneurons and retinal ganglion cells (Yan et al., 2020). Loss-of-function approaches showed that these proteins coordinately form a surface code that bias connectivity between neuronal subpopulations (Fuerst et al., 2008; Krishnaswamy et al., 2015; Yamagata & Sanes, 2012). Precisely, their role as marker genes differentiates subsets of possibly matching neurons but homogenizes intercellular identity. IgSF proteins are essential for synapse development, plasticity and function. Yet, their promiscuous interactions and relatively low isoform diversity prevent them from encoding connectivity at the single-neuron level.

Classical cadherins type II are implicated in connectivity in several brain regions. The 18 genes of this family are expressed in combinatorial patterns in neurons thanks to the use of alternative promoters and alternative splicing mechanisms. Classical cadherins regulate circuit assembly through homophilic binding (Basu et al., 2015). Therefore, they accomplish two of our criteria: high diversity (due to the number of encoded isoforms, plus combinatorial expression) and highly specific interactions through homophilic binding. Mossy fibers, axons emerging from pontine neurons, form synapses with cerebellar granule cells during the second postnatal week. Kuwako et al. (2014) showed that cadherin 7 (Cdh7) is expressed in both mossy fibers and granule cells during the time window for synapse formation. Using a shRNA silencing strategy, they showed that Cdh7 homophilic interaction mediates axon growth of mossy fibers to the granule cell layer and is required for synaptogenesis between these cell types. Modified expression of this protein in pontine neurons induced mossy fiber contacts to PCs. This is why it is considered that Cdh7 mediates target recognition for synapse formation during development. Yet, as in the case of IgSFs, classic cadherins are able to encode cell-type specific connectivity patterns but lack the ability to signal single-neurons target recognition.

Among vertebrates' CAMs, neurexins have been extensively studied as possible actors of a molecular connectivity code due to their vast isoform diversity and synaptogenic properties. Three neurexin genes can be found in mammals (Nrxn1-3). Each of them can be transcribed using multiple promoters (α, β and γ), giving rise to different lengths pre-mRNAs. In addition, six different segments can be alternatively spliced (AS1-6), with the potential to produce more than 12000 different transcripts. Hundreds of these transcripts have been detected in both mouse and human brain tissue. Importantly, different neuronal types express unique combinations of Nrxns splice variants, correlating with their differential physiological properties (Gomez et al., 2021; Reissner et al., 2013; Schreiner et al., 2014; Treutlein et al., 2014). In addition, neuronal activity can shift splicing, modifying Nrxn repertoires (Ding et al., 2017). Nrxns mediate transsynaptic binding through heterophilic interaction with a variety of possible partners,

including cerebellin 1 / glutamate receptor δ2 (CBLN1/GLUD2), CBLN1/GLUD1, leucine-rich repeat transmembrane proteins (LRRTMs) and neuroligins (Nlgns) (Chih et al., 2006; de Wit et al., 2009; Graf et al., 2004; Uemura et al., 2010). Different affinities are achieved through protein structural modifications, dependent on promoter choice and splicing, as well as heparan-sulfate glycosylation (Zhang et al., 2018). The interaction of Nrxns with their different partners induces pre- and postsynaptic specialization (Dean et al., 2003; Ko et al., 2009; Linhoff et al., 2009; Scheiffele et al., 2000). In the presynapse, Nrxns promote Ca^{2+} influx, an essential process for neurotransmitter release (Luo et al., 2020; Missler et al., 2003). In the postsynapse, specific features are achieved depending on the interacting partners. For instance, Nrxn1/3 AS4- can recruit LRRTM2 to the postsynapse, which mediates AMPA receptor trafficking, while AS4+ isoforms preferentially bind Nlngs, favoring NMDA receptors stabilization in the postsynaptic membrane (Ko et al., 2009; Uemura et al., 2010). Therefore, Nrxnx, through their great diversity of isoforms and interactions, are able to specify different synapse types. However, Nrxns repertoires cluster at the level of neuronal subclasses rather than uniquely labeling individual neurons. Consequently, they likely require additional combinatorial partners to achieve true single-cell specificity during neuronal wiring.

Clustered Protocadherins fulfill the criteria for a molecular code of connectivity

Although central synapses likely rely on a complex combination of multiple signaling systems, one CAM family accomplishes the previously explained criteria for molecular identity at single-cell resolution. Since their discovery, Clustered Protocadherins (cPCDHs), belonging to the cadherin superfamily, were targeted as possible connectivity encoders (Wu & Maniatis, 1999). cPCDH locus in mouse encodes 58 isoforms distributed in three gene clusters: α, β and γPCDHs. Each cluster contains 14, 22 and 22 exons variable exons, respectively. In addition, α and γ clusters contain three constant exons that encode an intracellular domain

common to all the isoforms in each cluster. βPCDHs lack such intracellular domain. α and γPCDH isoforms are further classified into subtypes according to their sequencing similarity. Specifically, α cluster contains 12 alternate exons plus two C-type isoforms. γPCDH alternate isoforms are divided into 12 γA-type exons, plus 7 γB-type. Similar to α cluster, there are 3 γC-type isoforms. Downstream α constant exons, HS7 and HS5-1 sequences form a super-enhancer (SE) that controls αPCDH transcription. Similarly, another super-enhancer element (HS7L, HS5-1L, HS18-22) can be found downstream γ constant exons and controls, in this case, both β and γPCDHs (**Figure 4a**) (Wu & Jia, 2021).

Each variable exon has its own dedicated promoter preceded by a forward-oriented CTCF binding site. Conveniently, downstream SEs harbors several CTCF sites in the reverse orientation. When cohesin and CTCF bind an isoform promoter, a chromatin loop is formed, allowing the interaction between SE elements and promoters (Guo et al., 2012; Kiefer et al., 2023; Monahan et al., 2012; Tasic et al., 2002; Xiaozhong Wang et al., 2002). Starting early during development, the *de novo* methyltransferase DNMT3b stochastically methylates certain promoters in each cluster, preventing CTCF binding and thus blocking its expression (Tarusawa et al., 2016; Toyoda et al., 2014). As a result, each neuron activates few alternate variable exons per cluster in a monoallelic fashion, achieving a sparse, combinatorial expression pattern at single-cell resolution (Esumi et al., 2005; Frank et al., 2005). By contrast, the C-type genes (αC1/C2 and γC3–C5) are not subject to this stochastic silencing: they are expressed biallelically in cortical pyramidal cells, dorsal root ganglion sensory neurons, cerebellar PCs, and most other neuron types, but are absent in olfactory sensory neurons, where only monoallelic alternate exons appear (Esumi et al., 2005; Frank et al., 2005; Kaneko et al., 2006). Serotonergic neurons are a further exception, expressing only αPCDH-C2 (Chen et al., 2017). Until recently, isoform selection was assumed to be purely random, but it has been shown that sister neocortical neurons inherit a partially shared pattern of alternate cPCDH isoforms (Lv et al., 2022). If cPCDH truly encode and adjust to connectivity, it would be expected that

their expression would adapt depending on synaptic partners' pruning and stabilization.

After transcription of a given alternate exon, pre-mRNA is *cis*-spliced to bind variable extracellular domains sequences and intracellular constant exons. The intronic sequence between the end of the variable exon and the start of the first constant exon is removed, producing a continuous open reading frame that encodes the full ectodomain fused to the constant intracellular domain (Tasic et al., 2002; Xiaozhong Wang et al., 2002). The final mRNA product thus encodes a signal peptide, the extracellular domains EC1 to EC6, a transmembrane domain, a variable cytoplasmic membrane – unique to each variable exon – and the constant intracellular domain (ICD), common to all isoforms. βPCDH isoforms transcription is simpler: because they lack the common, downstream ICD, their expression does not require *cis* splicing (Wu & Maniatis, 1999, 2000).

cPCDHs arrange as dimers in the membrane. β and γ isoforms, as well as αPCDHC2, are able to form homodimers through the interaction of membrane-proximal EC5 and EC6 domains (Brasch et al., 2019; Rubinstein et al., 2015; Wiseglass et al., 2024). Homodimers are then delivered to the membrane via the secretory pathway. In contrast, most αPCDHs and γC4 isoform can only be arranged as heterodimers (**Figure 4b**). To be transported to the membrane, they need heterophilic *cis* binding to a β or γ isoform, that will act as a carrier. Endoplasmic reticulum – Golgi – membrane trafficking has been studied in depth for γPCDHs, showing that their ICD plays an important role in their cycling in the secretory pathway. Plus, clusters of γPCDH-containing specialized vesicles were detected near synaptic compartments during postnatal development, suggesting that controlled delivery of γPCDHs to maturing synapses may play a role in synaptic assembly, remodeling, or signaling at critical developmental windows (Fernández-Monreal et al., 2009; Fernández-Monreal et al., 2010).

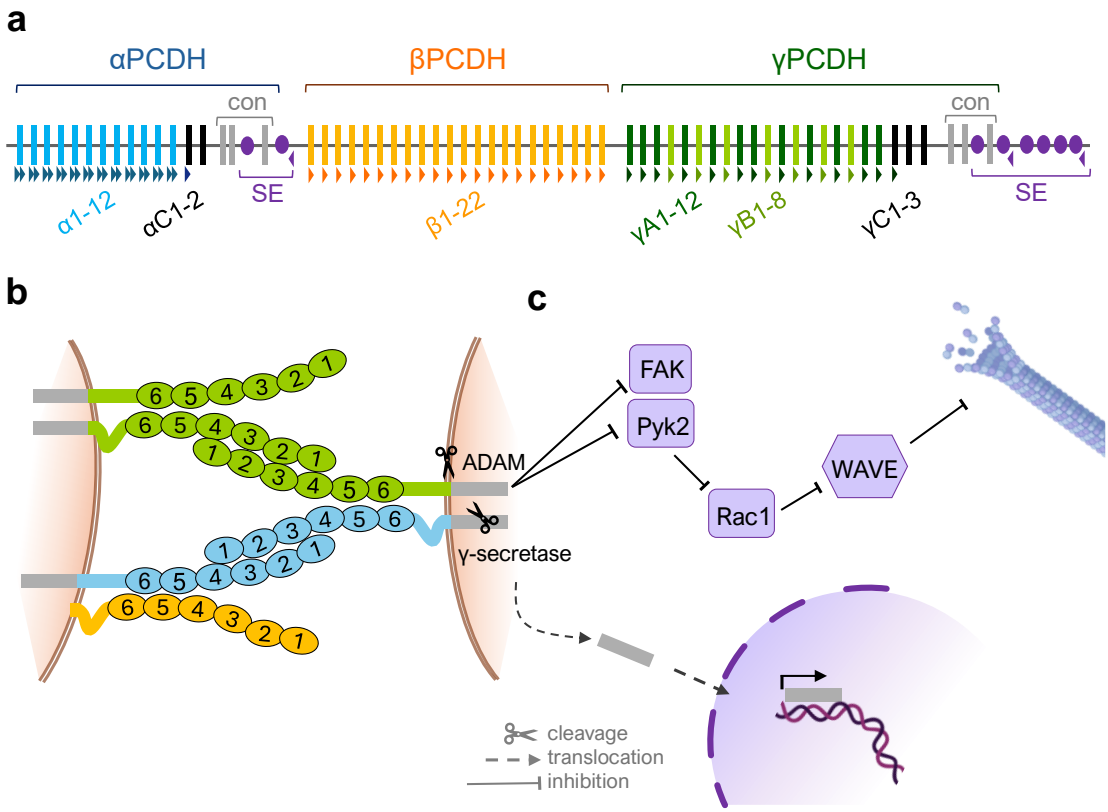

Figure 4: cPCDH genomic organization, protein expression and intracellular signaling. (a) cPCDH locus organization. Colorful and black represent alternate and C-type exons, respectively. Grey represents intracellular constant segment in α and γ clusters ("con"). Purple circles represent super-enhancer elements (SE); from left to right: HS7, HS5-1, HS7L, HS5-1L, and HS18 to 22. Triangles represent CTCF promoters sites and their orientation. (b) cPCDH proteins expression and arrangement in the membrane. Interaction of extracellular domains 5 and 6 may form homodimers (up) and heterodimers (bottom). Transmembrane interaction happens through strict homophilic interaction of extracellular domains 1 to 4. (c) cPCDH intracellular signaling pathways.

While EC5 and EC6 underly promiscuous *cis* dimerization, cPCDHs interact in *trans* through strictly homophilic binding of EC1 to EC4 domains in a Ca^{2+}-dependent manner (Hoshino et al., 2023; Kanadome et al., 2021). Matching isoforms on apposed cell surfaces bind in an antiparallel, head-to-tail orientation to form elongated oligomeric "zippers" (Rubinstein et al., 2015). *Cis* interactions are essential for the stabilization of transmembrane zipper structures (Wiseglass et al., 2024). Strict homophilic binding ensures that a putative recognition code mediated by cPCDH is highly specific and stable. In addition, the high exon

diversity, stochastic expression and dimer configuration contributes to the neuron-specific combinatorial expression of isoforms. Yagi (2012) calculated all the possible cPCDH a PC may express, considering (1) the number of isoforms in each cluster, (2) the number of isoforms expressed per PC through monoallelic regulation (Esumi et al., 2005; Kaneko et al., 2006) and (3) the multimers organization in the membrane. However, Yagi considered that cPCDHs are expressed biallelically and form heterotetramers, but now it has been proven that they form *cis* homo and heterodimers (Rubinstein et al., 2015; Wiseglass et al., 2024) and that their expression is monoallelic. Therefore, following Yagi's calculations, the possible combinations of cPCDHs expressed by a single PC could be expressed as follows.

Single cell real time quantitative PCR (RT-qPCR) and RNA-ISH experiments showed that each mature PC expresses on average 2 out of 12 αPCDH variable isoform, 2 out of 22 βPCDHs and 2 out of 19 γPCDH variable exons from each allele, plus the five C-type isoforms (αC1-2 and γC3-5), which are expressed constitutively and biallelically (Esumi et al., 2005; Hirano et al., 2012; Kaneko et al., 2006). Hence, for each PC there are

$$\underbrace{\binom{12}{2}}_{\alpha PCDH} \times \underbrace{\binom{22}{2}}_{\beta PCDH} \times \underbrace{\binom{19}{2}}_{\gamma PCDH} = 66 \times 231 \times 171 = 2607066$$

possible combinations of cPCDH variable exons expressed at the single-cell resolution. In addition, considering 11 expressed isoforms (6 variable ones, plus 5 C-type) and that they arrange as homo- and heterodimers, except for αPCDHs that can only form heterodimers, each PC can virtually express

$$\underbrace{\binom{n+2-1}{2}}_{All\ possible\ dimers} - \underbrace{\binom{n+2-1}{2}}_{\substack{\alpha PCDH\ forbidden \\ homodimers}} = \binom{11+2-1}{2} - \binom{4+2-1}{2} = 56$$

different dimers from its unique cPCDH repertoire. Nevertheless, there might be unknown factors biasing the preferential *cis* binding between certain isoforms. Altogether, the probability that two PCs randomly express the same cPCDH

subset is ~ $3.84 \cdot 10^{-7}$. Therefore, these numbers support the hypothesis that cPCDHs may mediate single-cell identity in PCs and other neurons showing combinatorial cPCDHs expression.

As discussed above, single-cell identity may play an important role in circuit wiring during development, since a given postsynaptic cell must be able to recognize each possible partner in order to form and stabilize synaptic contacts. Molecularly, this process requires that highly diverse, yet specific cell-cell recognition codes translate into stable and uniform intracellular signaling. cPCDHs achieve this through their common ICD. α- and γPCDHs contain an ICD encoded by the constant exons in each cluster and shared among all isoforms (**Figure 4b**). When α- and/or γPCDHs find an identical partner transmembrane, its ICD is cleaved by the metalloprotease ADAM10 and phosphorylated by protein kinase C (PKC). The phosphorylated ICD can then inhibit focal adhesion kinase (FAK) and proline-rich tyrosine kinase 2 (Pyk2) (Garrett et al., 2012; Keeler et al., 2015). Ultimately, this pathway leads to the inhibition of actin cytoskeleton remodeling. α-ICD, but not γ, contains a WAVE interacting receptor sequence (WIRS) motif that allow direct regulation of cytoskeleton dynamics through the WAVE regulatory complex (**Figure 4c**, top) (Chen et al., 2014; Fan et al., 2018). In addition, ICD can be cleaved by γ-secretase and translocated to the nucleus (**Figure 4c**, bottom). There, it can induce the expression of its own cPCDH cluster (Haas et al., 2005; Hambsch et al., 2005; Reiss et al., 2006). Additionally, nuclear ICD was shown to downregulate Notch1-mediated translation in vascular endothelial cells (Joshi et al., 2024). However, beyond the two known targets described above, the roles of the cPCDH ICD as a gene-expression regulator remain largely unexplored.

The role of cPCDHs in cell-cell recognition underlies a range of physiological functions that vary depending on the studied region. In the spinal cord, γPCDHs are essential for neuronal survival as well as excitatory synapse formation (X. Wang et al., 2002; Weiner et al., 2005). In the retina, γPCDHs are required for survival but they were not found to be involved in circuit formation (Lefebvre et al., 2008). On the contrary, synaptogenesis is prevented by γPCDHs

in the brain cortex. γPCDHs are able to interact in *cis* with Nlgn molecules, inhibiting their synaptogenic effect as well as spine formation (Molumby et al., 2017; Steffen et al., 2021). These general functions of γPCDHs were studied mainly with KO models of the entire γ-cluster, including all variable isoforms and constant exons. Coherently with their ubiquitous pattern of expression, γC3 isoform was found later to mediate synaptogenesis and postsynaptic specialization on its own (Meltzer et al., 2023). Other studies that considered alternate isoforms diversity in depth found, in addition, highly interesting features of γPCDHs in circuit formation and selective synaptic partner selection.

In 2012, Lefebvre *et al*. demonstrated that γPCDHs are essential for controlling cerebellar PCs dendritic arborization, as γPCDH knockout cells exhibited increased self-crossing branches. The authors hypothesized that γPCDHs act as a molecular barcode, interacting homophobically only when two dendritic branches from the same cell make contact. This is supported by the extremely low probability of two PCs expressing the same repertoire of γPCDHs (calculated above). Later, Toyoda et al. (2014) showed that high γPCDH diversity, achieved through the prevention of promoters methylation (Dnmt3b KO), causes the same phenotype in PCs dendrites. High isoform diversity or the total absence of it leads to the same outcome because in both cases, the zipper-like structure between membranes is presumably destabilized, allowing membrane interaction between dendrites of the same cell. Following Toyoda's experiments, Tarusawa et al. (2016) studied the role of cPCDHs promoters methylation in the connectivity between excitatory cortical neurons derived from the same progenitor ("clones"). They found a peak in connectivity during the second postnatal week. Only one week later, selective pruning leads to 80% of clonal pairs reciprocally connected, while non-clones reach 40%. Loss of Dnmt3b allowed the peak in connectivity, but synapse pruning failed during the third postnatal week, turning the probability of clone pairs connection similar to the non-clone pairs. Indeed, cPCDH diversity was increased after Dnmt3bKO. KO of the three cPCDH clusters, in contrast, prevented both establishment and pruning of supernumerary connections. These

experiments highlight the importance of cPCDH homophilic interaction in cell-cell recognition, underling circuit wiring during postnatal development.

Recent studies have adressed this phenomenon in depth in the mouse cortex. It is now known that among the three clusters, γPCDH is specifically mediating cortex connectivity. While γPCDH conditional KO allows a higher percentage of reciprocal connections, single-isoforms overexpression significantly decreases connectivity during postnatal development (Lv et al., 2022; Zhu et al., 2024). However, certain discrepancies appear between both articles. On the one hand, Lv *et al*. analyses showed that clonal pairs shared similar γPCDHs repertoire, correlated with their higher probability of reciprocal connections. In addition, overexpression of γC3 lead to a decrease in connectivity. Contrarily, Zhu *et al*. showed that neurons electroporated with similar γPCDHs combinations were less likely to connect, and that connectivity is regulated by alternate isoforms, but not C-type exons. Although Zhu *et al* provided arguably more robust γPCDH detection techniques, the differences between both investigations remain under debate.

The role of γPCDH in connectivity has also been studied in other type of synapses in the cortex, such as parvalbumin-expressing neurons and pyramidal cells (Kawamura et al., 2023), as well as several brain regions. Their specific roles seem to vary depending on the area and cell type. Olfactory sensory neurons require cPCDHs-mediated self/non-self recognition for glomeruli formation; yet, functional redundancy among clusters was found through KO of each set, showing that, in this case, all cPCDHs are part of the recognition code and downstream signaling (Mountoufaris et al., 2017). Altogether, despite region-specific differences, cPCDHs seem to have an essential role regulating synaptic partner choice acting as a cellular recognition code.

Although several important advances on the knowledge of cPCDHs were achieved studying cerebellar PCs (Esumi et al., 2005; Frank et al., 2005; Hirano et al., 2012; Kaneko et al., 2006; Lefebvre et al., 2012; Toyoda et al., 2014), the involvement of these molecules in circuit wiring in the cerebellum remains largely

unexplored. In this project, we aimed to investigate the role of cPCDHs in the specification of synaptic partner choice between cerebellar PCs and olivary climbing fibers (CF).

Introduction

Chapter IV: Cerebellum wiring during postnatal development

Anatomy and cellular organization of the cerebellar circuit

The cerebellum, located posterior to the cerebral hemispheres, derives its etymology from the Latin meaning "little brain," likely due to its macroscopic similarities with the cerebrum. The cerebellar cortex is anatomically organized into ten lobules (anterior: I-V; central: VIa, VIb, and VII; posterior: VIII and IX; and nodular: X), creating its characteristic foliated morphology. By contrast, the cerebellum differs from the forebrain both functionally and histologically. Regardless of this name, the cerebellum itself contains more neurons than the rest of the brain. About 23 billion neurons are estimated to form the human cerebral cortex, while the cerebellum alone counts with 101 billion neurons (Andersen et al., 1992; Pelvig et al., 2008). The cerebellar cortex is organized in a simple, repeated three-layered architecture: the molecular layer, the Purkinje cell layer, and the internal granule cell layer. PC bodies, which convey the sole output of the cerebellar cortex, are arranged in a monolayer. Their extensive dendritic trees project into the molecular layer, the outermost part of the cortex. The molecular layer contains inhibitory interneurons — basket cells and outer stellate cells — that synapse onto PC dendrites. Parallel fibers (PFs), which are granule cell axons, bifurcate and run transversely through the molecular layer, forming hundreds of thousands of synaptic contacts with each PC they encounter (Napper & Harvey, 1988). The granule cell bodies lie beneath the Purkinje cell layer, forming the internal granule cell layer, which also contains inhibitory Golgi interneurons (**Figure 5**).

Cerebellar cortex inputs arrive through the white matter under the granular layer. Two excitatory afferents reach the cerebellum: climbing fibers (CF) and mossy fibers. CFs, the axons of the inferior olivary neurons (ION) in the brainstem, contact PCs in their proximal dendrites. Most PCs in the mature system receive one single CF afferent, which is referred to as “CF mono-innervation”. Mossy fibers emerge from several distal brain regions, including different spinal cord tracts, vestibular nuclei, the reticular formation and others (**Figure 5**). In the

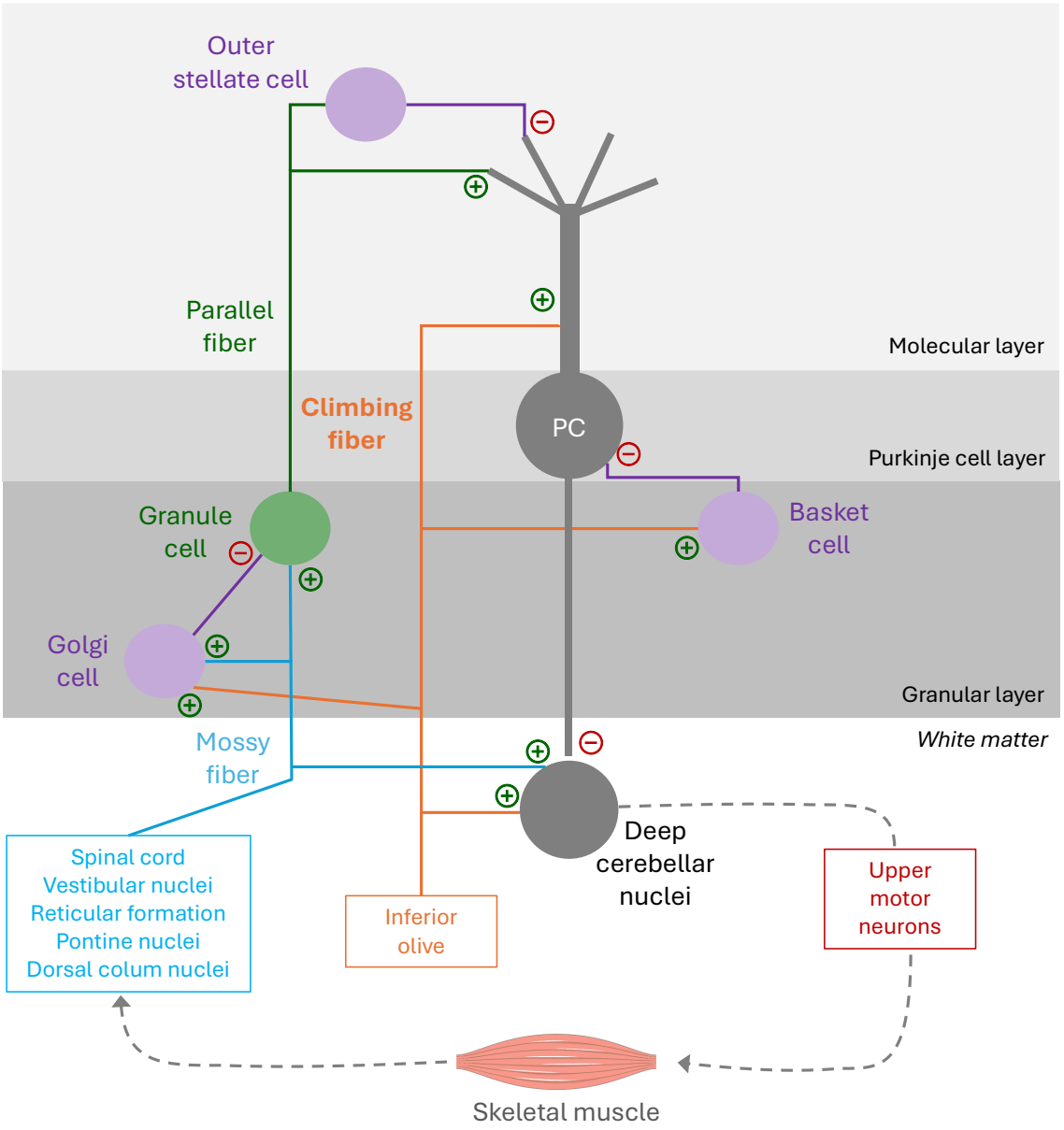

Figure 5: Cerebellar cortex circuitry. Mossy fibers (blue) emerging from different brain areas converge in the cerebellum white matter and form excitatory connections with granule cells and Golgi interneurons. A mossy fiber collateral contacts deep cerebellar nuclei. In the granule cell layer, granule cells receive excitatory inputs from mossy fibers and inhibition from Golgi interneurons. Golgi interneurons receive excitatory inputs from both mossy fibers and a CF collateral. Inhibitory basket cells in the granule cell layer project to the PCs in the Purkinje cell layer. In the molecular layer, parallel fibers (granule cell axons) form excitatory connections with outer stellate cells and PCs distal dendrites. CFs connect strongly with PCs at their proximal dendrites. Information is integrated in PCs, that project their axons beyond the cortex to the deep cerebellar nuclei. Deep cerebellar nuclei receive connections from PCs, but also from cerebellar input collaterals (mossy fibers and CFs). The cerebellum output will eventually

reach upper motor neurons and skeletal muscle. Information from this motor systems, as well as proprioceptive and sensory ones, goes back then to the cerebellum, forming a loop of motor coordination control. Dashed lines indicates the presence of intermediate connections absent in the scheme.

granular layer, mossy fibers and granule cell dendrites form glomeruli where a single mossy fiber and 8-20 granule cell dendrites connect (Billings et al., 2014; Quy et al., 2011; Wu et al., 1999). Both CF and mossy fibers contact cerebellar areas selectively, following a patterned topographical organization (Apps & Hawkes, 2009; Cerminara et al., 2015; Reeber et al., 2012). In addition, noradrenergic afferents from the locus coeruleus reach the three layers of the cerebellar cortex, as well as deep cerebellar nuclei, and modulate synaptic transmission (Hökfelt & Fuxe, 1969; Nelson et al., 1997). Information from all cerebellar inputs, regulated by the activity of cerebellar inhibitory interneurons, is integrated by PCs. In turn, PCs project to the vestibular nuclei and the deep cerebellar nuclei located at the roof of the fourth ventricle (Eccles, 1967; Itō, 1984). Deep cerebellar nuclei form topographically organized connections with reticular, vestibular and red nuclei, as well as the thalamus, creating thus a loop for fine motor coordination. In fact, the cerebellum is able, thanks to its afferents from several brain regions, to anticipate the outcome of motor commands, contrast such outcome with the feedback received from spinal tracts, and finely adjust future movements (Hull, 2020; Ito, 1972). Beyond motor control, the cerebellum has been more recently linked to emotional and sensory processing, including a role in autism spectrum disorder symptomatology (Stoodley et al., 2017).

Development of the olivo-cerebellar circuit

Cerebellar cortex circuitry emerges during postnatal development in a well-known, highly stereotyped fashion. The two excitatory inputs that PCs receive, CFs and PFs, appear at different postnatal times and follow distinct functional and molecular mechanisms for synaptogenesis and partner selection.

While PFs form more than 100000 synapses into PCs distal dendrites, a single CF is selected during the three first postnatal weeks. At birth, each PC is innervated by 5-7 CF, which are then selectively pruned during the first three postnatal weeks (Hashimoto & Kano, 2013; Kano et al., 2018). This indicates that a highly restrictive selection process occurs postnatally, which might include the cell-cell recognition of each given PC and its possible synaptic partners, the selective strengthening of one of them and the progressive pruning of the others.

CF synapse formation happens around birth in mice. By postnatal day 3 (P3), PCs are contacted by 5-7 different CFs at the cell body, considered as the "multi-innervation peak" (Hashimoto, Yoshida, et al., 2009). These CFs elicit responses of similar amplitude in PCs; i.e., they have equivalent synaptic strength. Morphologically, CF during this "multi-innervation stage" have been described as "creeper type" (Sugihara, 2005). From P3 to P7, approximately, one CF is progressively strengthened, a phenomenon known as "functional differentiation" (Hashimoto & Kano, 2003). The strengthened CF, considered the winning one, elicits then a much larger response in its target PC than the rest of the connected CF inputs. The winer CF shows then a "nest-type" morphology (Sugihara, 2005). Supernumerary CFs are progressively eliminated until the third postnatal week, when CF to PC connectivity is stabilized (**Figure 6**). Although the canonical model indicates that each PC retains a single ION afferent, it was recently showed about 15% of murine PCs retain multiple CFs in the mature system. This was strongly correlated with the dendritic morphology of PCs, which also develops during the same time window. They found that PCs with multiple primary dendrites were more likely to retain several ION axons, and that each branch would respond independently to sensory stimulation, creating differentiated PC receptive fields limited by each CF territory (Busch & Hansel, 2023). Their results highlight the diversity and complexity of CF selection in each individual PC.

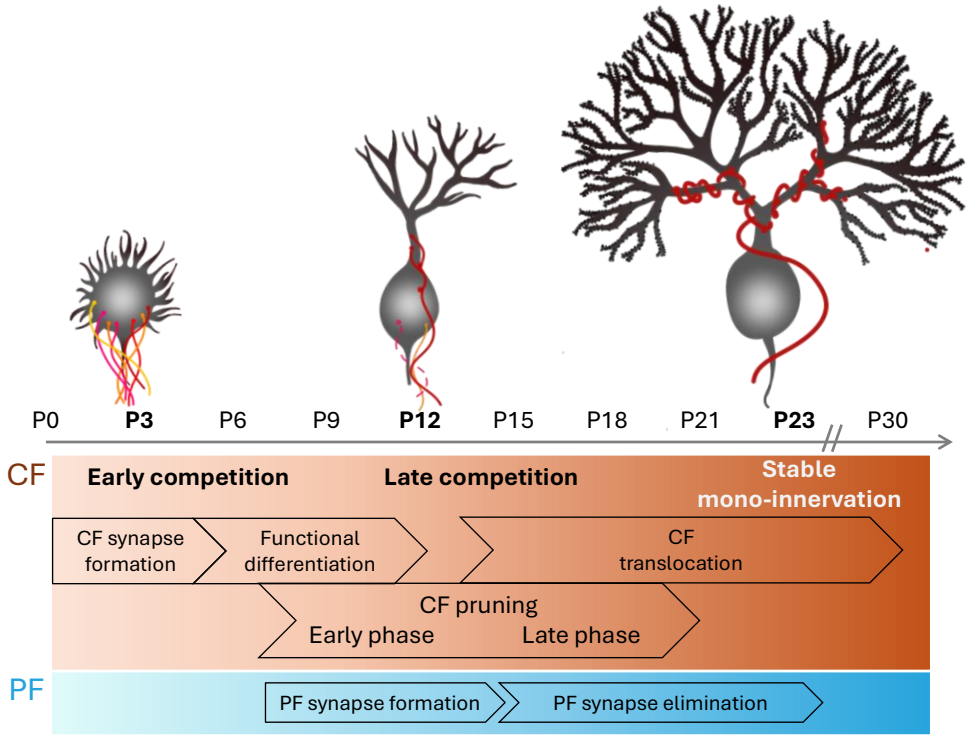

Figure 6: Sequential events of CF and PF to PC circuit formation. Drawings show P3, P10 and >P21 PCs (in grey) connected to sequentially less CF (red). These timepoints correspond to the three main stages of CF selective stabilization: early competition (multi-innervation peak), late competition (CF pruning) and the mature system (CF mono-innervation). In the orange box, the detailed steps of CF development are represented across the timeline. Similarly, steps towards PssF development are specified in the blue box. Adapted from Watanabe and Kano (2024).

Therefore, during the early phase of CF elimination (P7-P12), several phenomena occur simultaneously, including CF selection and strengthening, CF elimination and the translocation of the selected CF from the PC soma to the proximal dendrites. This is known as the "dendritic translocation phase" and starts around P9. During this time window, it has been shown that specific firing patterns from both synaptic partners are needed to conduct selection and elimination (Andjus et al., 2003). In PCs, P/Q type voltage-dependent Ca^{2+} channel is closely linked to the generation of such activity patterns, and its loss prevents both CF selection and dendritic translocation (Hashimoto et al., 2011; Miyazaki et al., 2004). In addition, PCs P/Q channels currents are needed for AMPA receptors organization, which is essential for proper CF signaling (Kawata

et al., 2014). Therefore, Ca^{2+} influx to PCs acts as master intracellular signal that bridges the early and late phases of CF elimination.

During this early phase of development, transient connections of mossy fibers from the pontine nucleus to PCs have been described. These synapses, however, are heavily pruned and completely disappear by P21 (Kalinovsky et al., 2011; Mason & Gregory, 1984). On the contrary, CFs do not contact granule cells. In fact, granule cells *in vitro* preferentially form synapses with mossy fibers *versus* CFs (Ito & Takeichi, 2009). This phenomenon of afferents and targets distribution highlights the diversity of cerebellar synaptic connections, as well as the presence of biasing mechanisms that operate during development to reach final wiring architecture.

The late phase of CF elimination is framed between P12 and P17 and it is heavily influenced by PF to PC synapses (Hashimoto, Yoshida, et al., 2009). Among the molecular actors involved, including phospholipase C and PKCγ in PCs (Chen et al., 1995; Kano et al., 1998; Rai et al., 2021), the metabotropic glutamate receptor type 1 (mGluR1) expressed at PF-PC synapses is known to promote CF elimination (Nakayama et al., 2024). mGluR1 activation leads to the activation of intracellular signaling in PCs involving BDNF and the CAM Sema7A in PCs (Choo et al., 2017; Uesaka et al., 2014). Both of these molecules bind their presynaptic partners in the surplus CFs (tropomyosin receptor kinase B (TrkB), and integrin β1 and plexin C1, respectively), promoting their elimination. In addition, mGluR1 can also trigger the activation of PKC and PLC signaling cascades (Kano et al., 1998; Rai et al., 2021), both related to CF elimination, as discussed above. Hence, PCs are able to integrate synaptic signaling from various inputs to generate retrograde transsynaptic signals for the selective pruning of certain afferents.

Simultaneously, PCs need to produce stabilizing signaling guided towards the winer CF. The famous cell-adhesion pair Nrxn/Nlgn is known to be required to increase CF synaptic strength, but dispensable for supernumerary CFs pruning (Zhang et al., 2015). In addition, protein tyrosine phosphatase δ (PTPδ) is thought

to act presynaptically mediating CF strengthening (Okuno et al., 2023). Notably, the cell adhesion G-protein–coupled receptor Bai3 (brain-specific angiogenesis inhibitor 3) selectively consolidates the most active CF connection, with its ligand C1ql1 (complement component 1q-related factor) being expressed and released from CF terminals in an activity-dependent fashion. C1ql1 binds kainte-type glutamate receptors in the PC membrane. This complex then recruits Bai3, which leads to the stabilization of the synaptic contact. This synaptic complex is also involved in synaptic plasticity processes in the CF to PC synapse (Kakegawa et al., 2015; Kakegawa et al., 2024). By analyzing genes co-expressed with C1ql1 in IONs at different developmental stages, Paul et al. (2024) described the molecular actors involved in each phase of CF-PC wiring. During early postnatal development (P4-P7), synaptic contacts are stabilized through CBLN1/GLUD2 complex, which is also present in PF-PC synapses. Since this molecular mechanism is shared among all excitatory PC afferents, it is believed that it may have a permissive synaptogenic effect. Later, especially after P14, researchers found a peak of expression of the CF secreted molecules C1QL1, CRTAC1, NRCAM and CRTAC1. The expression of these molecules is activity-dependent and thus it was proposed that the co-expression of these genes may be a maturation tag for CF-PC synapses.

Neuronal activity patterns and synchronicity between CFs and PCs is known to play a fundamental role in CF selection (Bravin et al., 1999; Tyssowski et al., 2018). Among all the possible initial afferents, the most active CF seems to be retained through Hebbian-like plasticity. In addition, many authors have pointed to the importance of activity-regulated genes, which may modify the identity of a given CF upon selection. This would imply that all selected CFs across cerebellar cortex would express a similar set of surface proteins, differentiating them from the ones to be pruned. However, previous research points to the existence of single-cell resolution molecular codes signaling each partner's identity during cerebellum development.

A hindbrain explant model to study activity-gene interplay during development: CF-induced long-lasting changes in PCs

Hindbrain explants are “open-book” organotypic cultures, prepared from E14 mouse embryos, that allow the co-culture of the full cerebellum connected to the brainstem (**Figure 7a**). Explants can be cultured for up to 40 days *in vitro*, which includes the critical period of CF selection, elimination and stabilization. Other advantages, such as the easier access and manipulation of IONs and PCs, make them an interesting model for the study of CF synapse selectivity. Using these cultures, Letellier et al. (2009) performed postlesional reinnervation experiments. Specifically, they prepared full explants (cerebellum and brainstem connected) and “naïve” explants (isolated cerebellar plates from which the brainstem is dissected out at the moment of culture preparation) (**Figure 7b**). After the closure of the critical period, “naïve” explants were connected to brainstems of the same age that had developed normally in a “full” explant. Similarly, PCs from full explants that had completed CF selection were disconnected from their original brainstem and presented to a new set of mature CFs (**Figure 7c, d**). Reinnervated PCs were not able to select a single CF input and therefore they retained multi-innervation. On the contrary, PCs that had been previously exposed to CF innervation were directly mono-innervated, skipping the competitive selection process (**Figure 7d**). Their results indicate, first, that CF selective stabilization can only happen during the developmental critical window. Secondly, “experienced” PCs getting directly mono-innervated suggests that CF innervation induces long-term chances in the surface molecular environment of PCs, providing, putatively, a recognition code that “pre-selects” their optimal partner. Altogether, it is possible that a molecular code of connectivity emerges in PCs during the developmental critical period induced or regulated by CF activity.

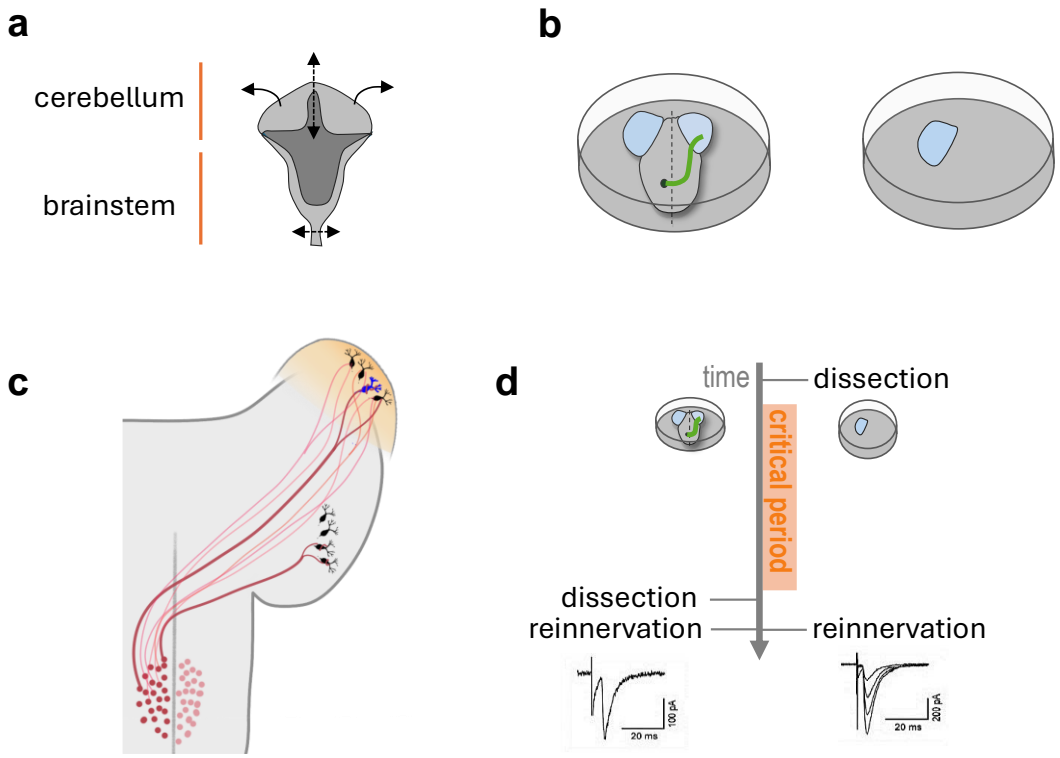

Figure 7: Hindbrain explants system. (a) Schematic of "open-book" culture preparation from E14 hindbrain. (b) Schematic image of culture plates containing a “full” (left) and a “naïve” explant. (c) Schematic image of postlesional reinnervation experiment. In orange, a cerebellum plate derived either from a dissected full explant or a naïve one is reinnervated by the host CFs. (d) Outcome of reinnervation experiments when brainstem is dissected out before or after the developmental critical period. Electrophysiology traces represent a mono-innervated PC (left) and a multi-innervated one (right). From Letellier et al. (2009).

However, which molecules might be able to regulate to encode individual CF-PC connections? Due to the known physiology of this circuit, together with the growing body of evidence about cPCDHs expression in PCs and their role in regulating connectivity in other brain areas, in this thesis work we focus on the investigation of cPCDHs as possible molecular encoders of CF to PC synapse selection.

Questions, hypothesis and objectives

Previous research has established that PCs express cPCDH isoforms in a combinatorial fashion, with their cPCDH repertoire undergoing regulation during perinatal development—a timeframe that coincides with olivo-cerebellar circuit refinement. Furthermore, cPCDHs have been shown to mediate synaptic wiring in multiple brain regions, including the spinal cord, olfactory bulb, and neocortex. Despite this evidence and the identification of several molecules in both PCs and CFs that can select and stabilize specific synaptic partners, the potential role of cPCDHs in cerebellar connectivity remains unexplored. Such convergence of evidence led us to hypothesize that cPCDHs may act as a molecular barcode in PCs, allowing CF multi-innervation at early postnatal development, and being regulated to retain a single CF afferent while preventing adult multi-innervation. To test this idea, we pursued the following objectives:

1. **Explore the expression of cPCDHs in single PCs at defined stages of CF connectivity**. During development, PCs may differ slightly in the timing of CF selection. In addition, no commercial antibodies are available for cPCDHs detection, requiring the use of RNA detection techniques. To bypass biological variability while detecting cPCDH transcripts, we implemented PatchSeq on acute cerebellar slices. This technique allows the electrophysiological characterization of CF to PC connectivity (estimation of the number of inputs and their functional differentiation stage), while retrieving cell content for single-cell RNA sequencing. This way, we aimed to correlate the functional development of olivo-cerebellar inputs to the cPCDHs.

2. **Investigate the effect of CF input on PCs cPCDH expression.** Given that CF activity has been proven to modulate gene expression in PCs during postnatal development, we aimed to address the influence of CF connectivity in cPCDH expression during development. In order to easily manipulate CF innervation, we implemented the use of hindbrain explants and characterized the morphological and electrophysiological development of CF and other PC

afferents *in vitro*. Using this system, we aimed to prevent CF innervation to PCs and test possible changes in cPCDH expression using PatchSeq.

3. **Assess the role of cPCDH diversity on CF selection during the developmental critical period.** We then focused on influence of cPCDH combinatorial expression on CF selection postnatally. In the explant system, we aimed to induce a mature pattern of cPCDH expression in PCs during CF competition and to study possible changes in CF connectivity.

4. **Test whether presynaptic CF identity may modulate cPCDH isoform selection in PCs.** Our last objective was to test whether the identity of the selected CF has an influence on the final repertoire of cPCDHs expressed by its target PC. Because CF emit branches at their arrival to the cerebellum, and each CF can innervate multiple PC targets in the adult circuit, we used PatchSeq to determine the similarity of cPCDH isoforms between PCs innervated by the same ION.

Materials and Methods

Wetlab materials and methods

Animals

P4 to P25 C57B6/J mice were used to obtain acute slices for electrophysiology, PatchSeq and imaging. RjOrl:SWISS (Janvier labs) were crossed with Igsf9-eGFP (Tg(Igsf9-EGFP)JR10Gsat/Mmucd; REF PMID: 14586460) (Pätz et al., 2018), kindly donated by Prof. Fekrije Selimi (Collège de France, Paris, France; MMRC n°030804-UCD), to obtain E14 embryos for olivo-cerebellar explants preparation.

Acute slices preparation

Wild-type C57B6/J mice between P4 and P25 were used for the preparation of acute slices. Animals were anesthetized using 5% isoflurane chamber during 3 minutes, after which were euthanized by decapitation. The brain was quickly extracted and submerged in ice-cold, high sucrose slicing solution bubbled with carbogen (95% O_2 / 5% CO_2) (Table 1). After this, 350 µm parasagittal cerebellar slices were obtained as described previously (Llano et al., 1991) using a vibratome (VT1000S; Leica, Vienna, Austria) and placed in carbogen-bubbled artificial cerebrospinal fluid (aCSF, Table 2) at 30ºC, were they stayed for at least 30 minutes before use.

Olivo-cerebellar explants preparation and culture

Explants were prepared from 14 days embryos (E14) SWISS(x)Igsf-eGFP mice as previously explained (Chedotal et al., 1997; Letellier et al., 2009). A pregnant female was anesthetized through isoflurane inhalation and euthanized through cervical dislocation to quickly extract the uterus. Embryos were then placed in 4ºC dissection medium (Table 3) in sterile conditions. Brains were extracted and meninges were carefully removed. The region between tecto-cerebellar and medullo-spinal junctions was isolated, and the two cerebellar

plates were separated. Explants were placed on Millicell culture inserts with the dorsal side facing culture medium (Table 4). To prepare “naïve” explants, the cerebellar plates were dissociated from the brainstem right after placing them in the culture insert. Explants were cultured at 35ºC, 5% CO_2 for up to 35 days *in vitro* (DIV).

Electrophysiological recordings and PatchSeq sample acquisition

Whole-cell patch-clamp recordings were performed at room temperature (RT) using an upright Eclipse N1 microscope from Nikon, equipped with infinity 3s camera (Lumenera) driven by Metamorph® software (Molecular Devices), an apochromatic x60/1.0 NA water immersion objective, and Scientifica micromanipulators. Excitatory postsynaptic currents (EPSC) were recorded using a Multiclamp 700B amplifier (Axon Instruments, Molecular Devices), digitized using a Digidata 1440A (Molecular Devices) and acquired using Clampex 10.7 software (Molecular Devices). Either acute slices or explants were placed in the microscope chamber, continuously perfused with aCSF bubbled with carbogen and containing 200 mM (+) Bicuculine. Micropipettes were obtained from 1 mm borosilicate capillaries (Harvard Apparatus) with a resistance of 4-6 MΩ using a vertical puller (Narishige) and filled with internal solution (Table 5; pH = 7,3; osmolarity ~ 300 mOsm). For PatchSeq sample acquisition, 0.5% Ribolock RNAse blocker 40 U/µl (Thermo) was added to the internal solution and aCSF osmolarity was adjusted to ~ 345 $mmol \cdot kg^{-1}$ using D-sorbitol.

In acute slices, recordings were performed from PCs in lobules VIa – VIb of cerebellar vermis (within 1 mm from midline). In explants, PCs were recorded from all cerebellar areas. To record evoked CF events in PC from both types of samples (eCF-EPSC), a bipolar electrode placed in a borosilicate theta glass capillary filled with aCSF was placed in the granule cell layer. Paired-pulse stimulation was applied to differentiate depressed CF-EPSC and facilitated PF-EPSC (Konnerth et al., 1990) (pulse duration range = 0.2 – 0.5 ms; inter-stimulus interval = 50 ms), using an ISO-Stim-01D isolated stimulator (NPI Electronic). The

electrode was moved around the cell to reach CF approaching PC from different angles, and paired-pulses were applied with increasing intensity in each location (10V to 95V). PC holding potential was clamped at -70 mV for P4-P7 cells (or its equivalent in DIV), -20 mV for P9-P15 and 0 mV for P19-P23bto prevent spikes when evoking CF-EPSC from mature cells. PCs were identified morphologically in acute slices using DIC microscopy. In explants, PC were identified using DIC and fluorescence from Igsf9-GFP positive CF axons surrounding the target neurons.

After recording, outside-out configuration ensured that biocytin was kept inside the cell for later imaging and, at the same time, the cell content was secured inside the capillary for single-cell RNA sequencing library synthesis.

Single-cell RNA sequencing

Cytoplasm contained in the micropipette after electrophysiological recordings was placed in a PCR tube to synthesize complementary DNA (cDNA) libraries according to SmartSeq2 protocol (Picelli et al., 2014). First, cDNA was synthesized by reverse transcription with oligo-dT priming. cDNA libraries were then pre-amplified for 18 PCR cycles and purified using AMpure magnetic beads. cDNA was enzymatically fragmented to adapt libraries to the sequencer length using NEBNext Ultra II FS. Sequencing libraries were synthesized using NEXTflex Rapid DNA-Seq kit (Perkin Elmer) and libraries quality was assessed by capillary electrophoresis (Labchip HT touch, Perkin Elmer). Libraries concentration was quantified by RT-qPCR. During library synthesis, a unique barcode was added to each sample to enable library pooling and parallel sequencing. Before sequencing, cells were selected attending to their sequencing library quality, assessed by the concentration and length of cDNA fragments in the library. Libraries were sequenced using the NextSeq 2000 (10 million reads per cell).

Single-cell electroporation (SCE)

Explants were placed in the microscope chamber filled with sterile aCSF (Table 6). Micropipettes were filled with SCE solution, containing 9,5% TE buffer and different plasmids in K-D-Gluconate – based intracellular solution. Inferior olivary neurons were identified by Igsf9-GFP positive fluorescence and electroporated with tdTomato plasmid (6 $\mu g \cdot \mu l^{-1}$). PC were electroporated using CAG-eGFP (6 $\mu g \cdot \mu l^{-1}$) and CMV-PCDHγA11-mCherry-N1 18 $\mu g \cdot \mu l^{-1}$ or CAG-γC3-mCherry 18 $\mu g \cdot \mu l^{-1}$. Electroporation was performed using cell-attached configuration and applying 4 consecutive pulses of -2,5 V, 25 ms duration, at 1 Hz. Explants were incubated for minimum 48H before imaging or patching electroporated cells to ensure constructs expression.

Immunostaining and microscopy techniques

Immunostaining was used to visualize PC morphology (Results Chapter I), as well as different PC afferents (Results Chapter II) and γPCDH-A11 protein clusters (Results Chapter IV). Either acute slices or explants were fixed in 4% paraformaldehyde – 4% sucrose at 4ºC overnight and free aldehyde groups were then quenched with NH_4Cl 50 mM in PBS during 30 minutes at RT. Tissue was permeabilized using Triton X-100 in PBS at 0.3% for acute slices (10 minutes) and 0.5% for explants (15 minutes), at RT. Non-specific binding was blocked by incubating samples in bovine serum albumin (BSA) 1% in PBS during 1 hour at RT. 0.5% Triton X-100 was for explants during blocking. Proteins of interest were labelled using specific primary antibodies in BSA 1%-PBS at 4ºC overnight, followed by fluorophores-bound secondary antibodies at 1:400 dilution during 2 hours at RT. The detailed list of antibodies combinations and their concentrations can be found in Table 7. In acute slices, biocytin infused through the patch pipette allowed to reveal cell morphology by incubating slices with Streptavidin conjugated to AlexaFluor 488 (1:400, Molecular Devices). Samples were mounted in Fluoromount (Merck).

Acute slices images, as well as explants images in Results Chapter II, were acquired using a Leica DM6 CFS TCS SP8 confocal microscope with a 63X / 1.4 NA oil objective and a pinhole opened to 1 time the Airy disk, at 400 Hz scanning frequency and a vertical step size of 0.3 µm. Explants PC images in Results Chapter IV were acquired using an upright spinning disk confocal microscope optimized for fast volumetric acquisition. The system was built around a Nikon Eclipse FN-1 upright stand (Nikon Instruments), equipped with a Yokogawa CSU-22 spinning disk confocal scan head (50 µm pinholes; 10,000 apertures). Emitted fluorescence was filtered through a multi-band emission filter wheel (447/460, 525/550, 535/545, 600/650 nm) controlled by a Lambda 10-3 controller (Sutter Instrument) and detected using an EMCCD camera (Rolera EM-C2, QImaging) with a 1004 × 1002 pixels array and 6,5 µm pixel pitch. Image acquisition and hardware synchronisation were managed using Metamorph Infinity software (v7.10, Molecular Devices) with a Z-step size set at 0.3 µm.

Analysis techniques

All code generated for this thesis work is available at https://github.com/elenabazb

Electrophysiology analysis: eCF-EPSC

CF fire in all-or-none fashion and evoke large, paired-pulse depressed currents in PC. All analyses were conducted in a blinded manner, unaware of the condition or age group to which each cell belonged. About 100 sweeps were recorded per cell, stimulating at different intensities from different positions in the granule cell layer using a paired-pulse stimulation protocol as explained above. All sweeps were concatenated in Clampfit 10, baseline was normalized to 0 pA and first and second peak amplitudes were quantified using the same software (*P1* and *P2*, respectively). From this point, peak amplitudes were analyzed using a custom R Statistical Software pipeline (R Core Team, 2024). First, paired-pulse ratio (PPR) of all sweeps was evaluated to discard facilitated events (presumably mediated by parallel fibers). To quantify the number of CF inputs for a given PC, and since each input should evoke a *P1* response in a discrete range of amplitude values regardless of stimulation intensity, we employed Kernel Density Estimation using R's '*density*' function with a Gaussian kernel function. Bandwidth was determined using pilot estimation of derivatives (Sheather & Jones, 1991). This approach enabled a systematic and unbiased detection of one or more peaks in the CF-EPSC amplitudes distribution, corresponding to the different CF inputs, and their localization within specific amplitude range. To avoid an overestimation of CF inputs due to technical variability, density function was thresholded using 1/5 of the standard deviation as a rule to discard peaks corresponding to few isolated sweeps. The range of a given CF input was defined by calculating the local minima of the density function according to the second derivative rule. The range of *P1* amplitudes belonging to each interval between local minima were averaged, as well as their paired *P2*. The corresponding sweeps were averaged in Clampfit 10. When multiple CF inputs are detected for a given cell, the higher

amplitude ones correspond to the sum of the amplitudes of the smaller inputs, since increasing stimulation intensity will consecutively recruit higher threshold afferents. Thus, smaller range average inputs were subtracted from higher ones to compute the real amplitude of the estimated CF-EPSCs. PPR of each averaged eCF-EPSC trace was calculated according to these corrected amplitudes.

Corrected eCF-EPSC amplitudes were used to quantify the functional differentiation of CF inputs in each recorded cell using a disparity index (*D.I.* = *S.D. / μ*; where S.D. stands for standard deviation and *μ* stands for the mean of all averaged CF inputs), as previously proposed by (Hashimoto & Kano, 2003). D.I. represents the coefficient of variation for all CF-EPSC amplitudes evoked in a given cell; therefore, low D.I. values indicate that different CF inputs exhibit equivalent strength and *vice versa*.

Image analysis

γPCDH-A11 and vesicular glutamate transporter 2 (vGLUT2) subcellular distribution (Results Chapter IV, Figure 20) were analyzed from spinning disk stacks (1004 x 1002 pixels, 0.1625 μm x 0.1625 μm per pixel, 0.3 μm *z*-step) including 4 channels: (1) blue channel, corresponding to Calb1 staining, (2) green channel, corresponding to GFP volumetric marker, (3) red channel, corresponding to γPCDH-A11-mCherry, and (4) far-red channel, corresponding to vGLUT2 staining. As explained above, GFP and γPCDH-A11-mCherry were introduced in the target PCs through SCE, while Calb1 and vGLUT2 correspond to immunostainings.

All image analyses were conducted in FIJI (Schindelin et al., 2012). First, PCs identity was confirmed by Calb1 positive staining. Then, a maximum intensity projection (MIP) was created from the GFP channel and thresholded to obtain a whole-cell mask. Soma and proximal dendrites regions of interest (ROIs) were manually delimited. Distal dendrites ROI was created from excluding soma and proximal dendrites ROIs from whole-cell mask. Red and far-red channels were

treated equally throughout the entire analysis. First, background subtraction was performed in the 16-bit images stack applying a 50 pixels radius rolling-ball. MIP was obtained and converted to 8-bit, from where fluorescence integrated density was measured for each ROI. Enrichment analysis in Results Chapter IV, Figure 20, corresponds to the normalized expression in each ROI to the whole-cell integrated density (IntDen) per area. For protein clusters analysis, red or far-red channel MIPs where thresholded (91-255) and *Analyze Particles* was applied for each ROI.

Single-cell RNA sequencing analysis

Reads alignment

Adapter sequences were removed from raw reads using Cutadapt version 1.18 (Martin, 2011) and fastp version 0.20.0 (Chen et al., 2018). Quality of the pre-processed reads before mapping was assessed with FastQC version 0.11.5 (Andrews, 2010). The splice aware aligner STAR (version 2.7.10a) was used to map reads to the genome and to perform read counting at the gene level using default settings (Dobin et al., 2013). The reference genome GRCm39 was adapted to improve cPCDHs detection. First, *Gm37013*, *Gm38666* and *Gm38667* pseudogenes were removed from the cPCDH locus. Second, we observed that most of the multi-mapping reads corresponded to the constant exon shared by all isoforms in α- and γ-PCDH clusters. Thus, the constant exon was split from the isoform sequences in each cluster and displayed as an isolated gene sequence. This way, reads mapping to the α- or γPCDH constant exon were included for quantification. Reads multi-mapping to variable exons were discarded.

Quality controls

The total number of counts and total number of detected genes were evaluated in the entire dataset for each experiment. Outlier cells in the total counts – total genes distribution were discarded. Both parameters were also

evaluated after subsetting datasets according to known experimental conditions to evaluate possible batch effects. Counts were normalized using logarithmic normalization from Seurat (v5) (Hao et al., 2021; Hao et al., 2024). PC marker genes expression was evaluated and cells not expressing PC marker genes (Ppp1r17, Calb1, Pcp2, Pcp4, Itpr1, Aldoc, Gad1, Slc32a1) were discarded.

Differential expression and pathway analysis

Differential expression was assessed using Likelihood Ratio Test (LRT) in *DESeq2* v1.42.1 (Love et al., 2014) with electrophysiological classification as the main test parameter (developmental stages according to D.I. values) for Results Chapter I, and using age and condition (full *vs* naïve) in Results Chapter III. *degPatterns* (Pantano, 2023) was used to group genes with the same changes in expression over development. Pathway analysis of each gene cluster was assessed according to Cell Component Gene Ontology (GO) terms enrichment in EnrichR (Xie et al., 2021). Expression of genes significantly changing (LRT *p* value < 0.05) was transformed using a Variance Stabilizing Tramsformation (VST) for visualization purposes.

cPCDH diversity

cPCDH counts were scaled in a 0 – 10 range and heatmaps were plotted using *pheatmap* v1.0.12 (Kolde, 2019). Shannon's diversity index (*H*) was calculated using '*vegan*' v2.6-6.1 package (Oksanen et al., 2024) as an indicator of cPCDH isoform diversity. It was calculated as $H = -\sum p_i \cdot \ln p_i$, where p_i is the proportion of normalized counts corresponding to one isoform compared to all the detected isoforms in each cell.

cPCDH expression cell-cell correlation

Similarity of cPCDH isoforms repertoire between PCs was calculated using Kendall's correlation coefficient with '*Rstatix*' (Kassambara, 2023), applied to the normalized and scaled cPCDH counts of each cluster separately. From the

correlation matrix, the following comparisons were extracted: (1) “within nest”, corresponding to coefficients calculated from PCs innervated by branches of the same CF, and (2) “*versus* control”, corresponding to coefficients calculated from PCs *within nest* compared to neighboring PCs not innervated by the same CF. The density distribution of each set of coefficients was calculated and compared using a Kolmogorov–Smirnov test.

Materials and Methods Tables

Table 1: Slicing solution composition.

Reagent	Concentration (mM)
Sucrose	252
Glucose	25
KCl	3
$CaCl_2$	0.5
$MgCl_2$	7
Na_2HPO_4	1,25
$NaHCO_3$	26

Table 2: Aritificial cerebrospinal fluid (aCSF).

Reagent	Concentration (mM)
Glucose	25
NaCl	125
$CaCl_2$	2
$MgCl_2$	1
Na_2HPO_4	1,25
$NaHCO_3$	25
KCl	2,5

Table 3: Dissection medium composition.

Reagent	Concentration (mM)
$CaCl_2$	0.5
KCl	2.5
KH_2PO_4	0.66
$MgCl_2$	2
$MgSO_4$	0.28
NaCl	50
Na_2HPO_4	0.85
Glucose	25
$NaHCO_3$	2.7
Sucrose	175
HEPES	2

Table 4: Culture medium composition.

Reagent	Concentration
Basal Medium Eagle (BME)	25%
Hank's balanced salt solution (HBSS)	25%
Decomplemented horse serum	6,25%
Glucose	2,5 M
L-Glutamine	1 mM

Table 5**:** Whole-cell patch-clamp internal solution for voltage-clamp recordings.

Reagent	Concentration (mM)
Cs-D-Gluconate	120
HEPES	10
BAPTA	10
TEA-Cl	3
Na_2ATP	2
MgATP	2
NaGTP	0,2

Na-P-Creatin	10
Biocytin	13 mM

Table 6: Sterile aCSF.

Reagent	Concentration (mM)
NaCl	130
KCl	2,5
$CaCl_2$	2,2
$MgCl_2$	1,5
HEPES	10
Glucose	10

Table 7: Primary-Secondary antibodies combinations used.

Primary antibody	Secondary antibody
Mouse anti-Calb1 1:5000 (Swant 300)	Goat anti-mouse-DyLight 405 (Jackson ImmunoResearch 115-475-003)
Chicken anti-GFP 1:1000 (Aves Lab, GFP-1020)	Goat anti-chicken-AF488 (Thermo Fisher A48260)
Guinea pig anti-RFP 1:500 (Synaptic Systems 390 004)	Goat anti-guinea pig-AF568 (Thermo Fisher A11075)
Rabbit anti-vGLUT2 1:1000 (Synaptic Systems 135 402)	Goat anti-rabbit-AF647 (Thermo Fisher A21244)
Guinea pig anti-vGLUT1 1:1000 (Sigma Aldrich AB5905)	Goat anti-guinea pig-AF568 (Thermo Fisher A11075)
Guinea pig anti-vGAT 1:500 (Synaptic Systems 131 004)	Goat anti-guinea pig-AF568 (Thermo Fisher A11075)

Results

Results

Chapter I: Regulation of γPCDH expression in Purkinje cells during Climbing Fiber competition.

Context and aims

In order to investigate whether cPCDHs could be involved in CF to PC synapse selection, we aimed to capture the changes in cPCDH isoforms expression happening during the developmental critical period from P3-P5 to P20-23. Due to the high number of isoforms and the lack of commercial antibodies, sc-RNAseq was the appropriate approach to study these proteins. In the literature, it has been extensively shown that P3-P5 corresponds to the multi-innervation peak of PC, that CF competition happens during P8-P12 and that by P21 most cells are monoinnervated. Hence, one could think about the possibility of performing fluorescence activated cell sorting (FACS) of PCs at each timepoint to maximize sample size and reduce experimentation time. However, this approach presents several challenges. First, PCs dendrites, particularly at later developmental stages, are large and highly branched, making them susceptible to fragmentation during tissue dissociation. Instead, single-nucleus RNA sequencing (sn-RNAseq) presents as a more viable alternative, as it enables transcriptomic profiling without requiring intact neuronal morphology. In addition, PCs represent a relatively small neuronal population within the cerebellum, especially when compared to granule cells. Therefore, nuclei sorting requires a reliable fluorescent nucleus marker for all ages. Furthermore, cerebellum histological organization has been shown to bias PC morphology and microcircuitry development; hence, a microdissection of the region of interest should be performed previous to cell sorting. Besides, we quickly realized the vast intercellular diversity of PCs, finding variable states of CF differentiation and PC dendritic development within the same age and anatomical location, too. Therefore, even if it would be statistically possible to correlate sample age to CF competition stage, we opted for directly assessing CF connectivity for each single PC prior to its sequencing by implementing PatchSeq (**Figure 8a**). This would allow us to reduce biological variability within conditions and to address gene expression changes correlated to functional circuit development specifically.

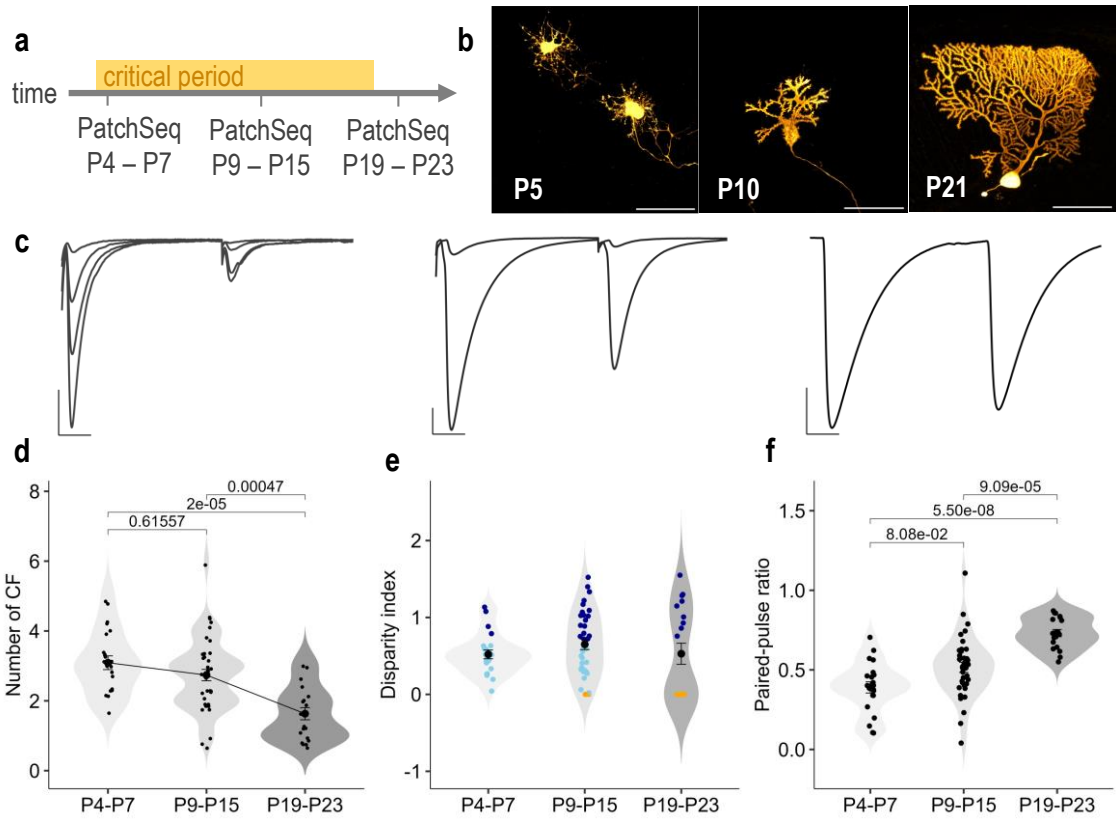

Figure 8: Electrophysiology and imaging of sequenced cells. (a) Experimental timeline for PatchSeq sample acquisition. (b) Example images of patched and sequenced PCs at P5, P10 and P21 (from left to right) after incubation with Streptavidin-AlexaFluor 488. Maximum intensity projections after confocal Z-stacks. Scale bars: 50 µm. (c) Representative traces of paired-pulse depressed, CF evoked EPSCs at P5, P10 and P21. Horizontal scale bar: 10 ms. Holding potential was -70 mV for P5, -20 mV for P10 and 0 mV for P21. (d) Quantification of the number of averaged CF inputs per cell in each age range. Error bars correspond to S.E.M. Kruskal-Wallis test p value: $1.725 \cdot 10^{-5}$. P-values displayed in graph correspond to Dunn's pairwise comparisons with Bonferroni adjustment for multiple comparisons. (e) Disparity index (DI) of CF inputs amplitudes per cell. Each violin plot corresponds to an age range; color scale corresponds to D.I. value (increasing values from yellow to blue). Error bars correspond to S.E.M. (f) Paired-pulse ratio per cell in each age range, quantified as the amplitude of the second pulse amplitude over the first pulse amplitude for each averaged CF input. Error bars correspond to S.E.M. Kruskal-Wallis test p value: $7.585 \cdot 10^{-8}$. P-values displayed in graph correspond to Dunn's pairwise comparisons with Bonferroni adjustment for multiple comparisons.

Functional classification of Purkinje cells

115 cells were individually patched in cerebellar parasagittal acute slices from P4 to P26 C57B6/J mice, obtained as previously explained (Wetlab Materials and Methods, page 78). CF-EPSCs were evoked through a paired-pulse stimulation protocol with a bipolar electrode positioned around the cell soma, applying different stimulation intensities (10-95V) (Wetlab Materials and Methods, page 79). After recording, cell content was gently aspirated, and membrane was resealed by outside-out configuration. Cell cytoplasm contained in the patch pipette was then transferred to a PCR tube to synthesize sequencing libraries according to SmartSeq2 protocol (Picelli et al., 2014) and slices were incubated with fluorescent streptavidin to reveal PCs morphology through confocal imaging (**Figure 8b**).

The number of CFs connected to a given PC was estimated by the number of discrete current steps elicited in response to paired-pulse stimulation. The analysis was performed using a custom semi-automatic pipeline for blind analysis (Materials and Methods, Analysis techniques, page 83). In summary, sweeps putatively belonging to the same CF input according to the amplitudes distribution were averaged (**Figure 8c**). Our analysis reproduced the existing literature about CF elimination, finding a significant decrease in the number of CF inputs over time (**Figure 8d**). While most CF are eliminated during this period, one of them is strengthened and becomes functionally dominant. Evoked CF-EPSCs during CF competition reflect this, showing a single input with a markedly higher amplitude compared to the others. To study this functional differentiation of CF inputs, disparity index (D.I., Materials and Methods, Analysis techniques, page 83) was calculated from the amplitude of averaged inputs from the same PC (**Figure 8e**). When D.I. ~ 0.5, each of the multiple CF inputs generate equivalent EPSC amplitudes, while higher values would represent amplitude differences between inputs and hence reflect the strengthening of one CF over the progressive elimination of the rest. For visualization purposes, monoinnervated cells are represented here as D.I. = 0. When analyzing the D.I. distribution in P19-P23 cells, a bimodal distribution can be observed. It may correspond to the existence of still

multi-innervated cells at old stages, still in late phases of CF competition according to the high D.I. value. Attending to this criterion, PCs were classified within three discrete categories: “early competition” (0 < D.I. < 0.7), “late competition” (D.I. > 0.7) and “mono-innervation” (D.I. = 0). Finally, paired-pulse ratio (PPR) was calculated as the second pulse amplitude over the first for each average CF input in a cell. In multi-innervated cells, PPR values for each input were averaged. In this case, a significant increase in the average PPR was observed (**Figure 8f**)**,** which may be indicative of changes in the CF release probability.

Overall, these results allowed us to validate our experimental conditions for CF-PC circuit maturation studies, and, importantly, to group the cells according solely to the functional differentiation of the circuit.

Expression changes of developmentally relevant genes

After library synthesis and single-cell RNA sequencing, reads were mapped to the mouse genome using STAR and a custom-made alignment file to avoid multi-mapping of genes of interest, as explained in Materials and Methods, Analysis techniques, page 85. First, cells with less than 20% of their reads mapping to exon sequences were discarded. Then, quality controls were performed attending to the distribution of total counts and total detected genes. Cells with total counts sum below 100 and/or total detected genes above 9000 were considered as outliers and discarded for subsequent analyses. These parameters were analyzed for each electrophysiologically defined group, and no significant batch effects were detected, discarding technical variations across experimental conditions (Supplementary Figure 1a). Counts were then normalized using “*LogNormalize*” method from Seurat (Hao et al., 2024). The expression of PC marker genes was assessed as part of quality controls (Supplementary Figure 1b). Cells not expressing any of the known PC markers were discarded. Final sample size for genes of interest analysis was n = 70, 61% of the initially patched cells.

We then aimed to explore the overall gene expression changes during CF competition. Differential expression analysis was performed using Likelihood Ratio Test (LRT) from DESeq2 (Love et al., 2014) and *degPatterns* (Pantano, 2023) to identify groups of genes covarying across the three developmental stages. Among the significantly differentially expressed genes, four groups of genes following the same trends over time were detected, including: lower expression during late competition (group 1), higher expression during late competition (group 2), increasing expression over time (group 3) and decreasing expression over time (group 4) (**Figure 9a**). To study the functional implication of these, pathway analysis was performed using EnrichR (Xie et al., 2021) and Gene Ontology (GO) Cellular Component Annotations (2023 dataset). A detailed list of genes belonging to each group and their associated GO terms can be found in

Table 8 to Table 11. Among the enriched GO terms, pathways expected to be modulated during this period were detected, such as voltage-gated cation channels (Na^+, Ca^{2+}), excitatory and inhibitory synapses organization, cytoskeleton remodeling, neuron projection and cell-adhesion (**Figure 9b**). In addition, genes known to be involved in CF elimination (Paul et al., 2024; Watanabe & Kano, 2024) were found to be significantly different across our three groups (Supplementary Figure 1c). These results show that PatchSeq approach under our experimental conditions allows the unbiased detection of relevant changing genes during development.

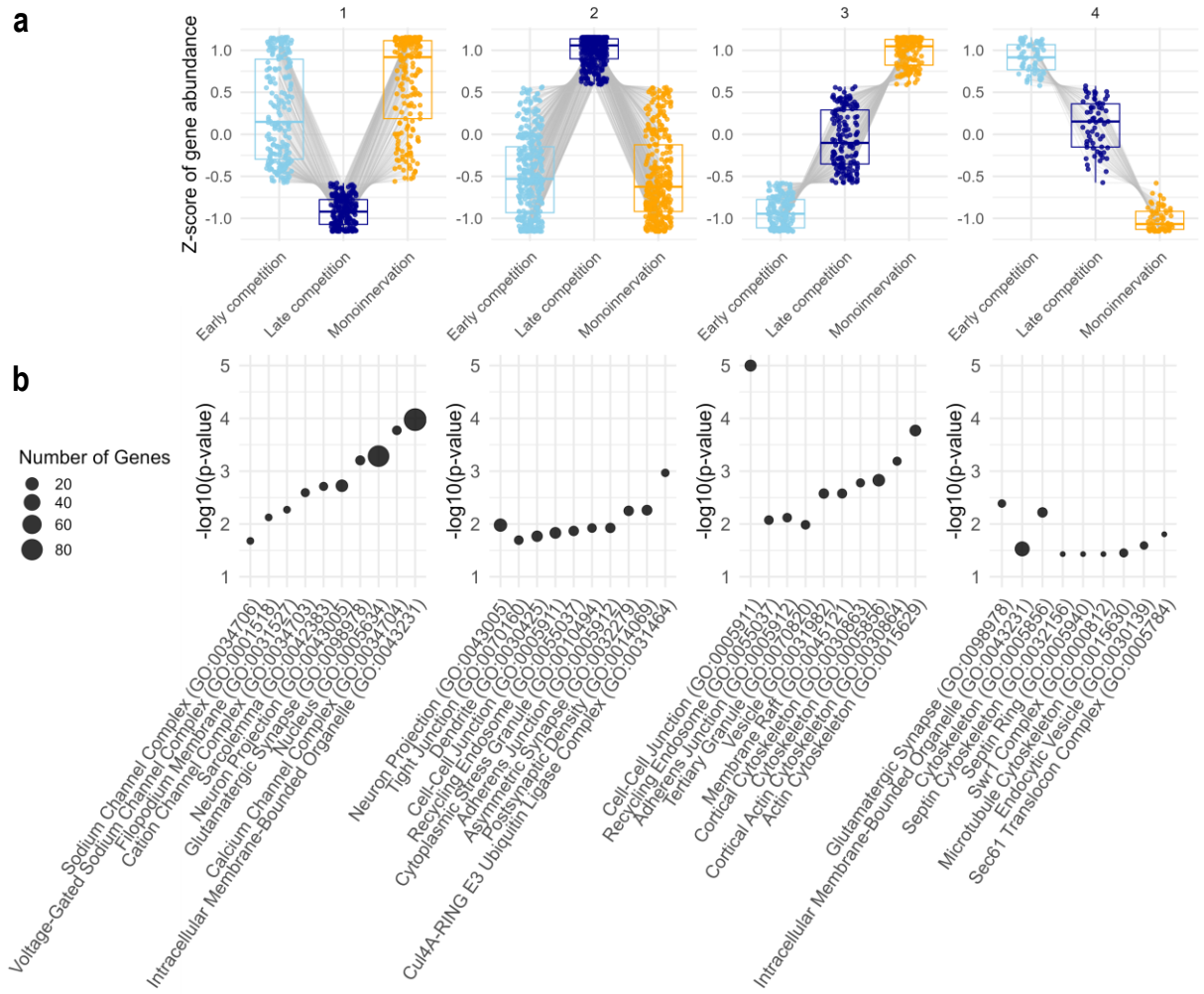

Figure 9: Differential expression analysis Differential expression analysis of electrophysiologically defined groups. (a) Genes with significant different expression across conditions (adjusted $p < 0.05$ in LRT) were clustered in four groups according to the changes in expression across time. Each dot corresponds to the relative expression of one gene. (b) Top 10 enriched GO terms ($p < 0.05$) for each gene group above them. The size of the dot is scaled to the number of genes detected for each GO term.

cPCDH regulation during the critical period

As previously explained, although no experimental evidence has been found to correlate cPCDH expression with PC connectivity, these proteins have been recurrently proposed as candidates for such a role due to their high isoform diversity, expression profile in PC and binding properties (Sanes & Zipursky,

2020; Wu & Jia, 2021; Yagi, 2012). cPCDH studies present special challenges; first, because of the lack of commercial antibodies against specific isoforms, (especially for immunostaining applications) and second, because of the high diversity of isoforms, that complicates low-throughput techniques application. These classical approaches are hence hardly applicable in this context. Therefore, single-cell RNA sequencing represents a suitable strategy for rapid detection of all cPCDH isoforms at once. To improve cPCDH detection while preventing multimapping-derived false positives, a STAR mapping file was adapted as explained in Materials and Methods, Analysis methods, page 85.

When analyzing cPCDH, a generally low expression level was observed, and significant variations were not detected for single isoforms (**Figure 10a**). This could bepartly due to zero inflation, an inherent problem in single-cell RNAseq experiments, and magnified in PatchSeq because of the habitual dropouts plus the limited sample size. However, we could observe a decrease in the number of different isoforms expressed over the developmental critical period. This was quantified applying Shannon's diversity index (*H*) (Shannon, 1997), which considers simultaneously the total number of different genes and the relative expression of these in each cell. *H* index showed that the diversity of cPCDH expressed per cell tends to decrease in parallel to CF elimination (**Figure 10b**). In addition, when diversity was quantified for each cluster individually, it could be observed that this trend is driven mainly by γPCDH cluster (**Figure 10c, d, e**). This trend was also observed when quantifying the number of detected isoforms and the total normalized counts per cluster (Supplementary Figure 2).

Therefore, these results may indicate that PCs regulate γPCDH isoform diversity during CF elimination, achieving the well-known scattered expression across cells for each isoform when CF connections have been stabilized.

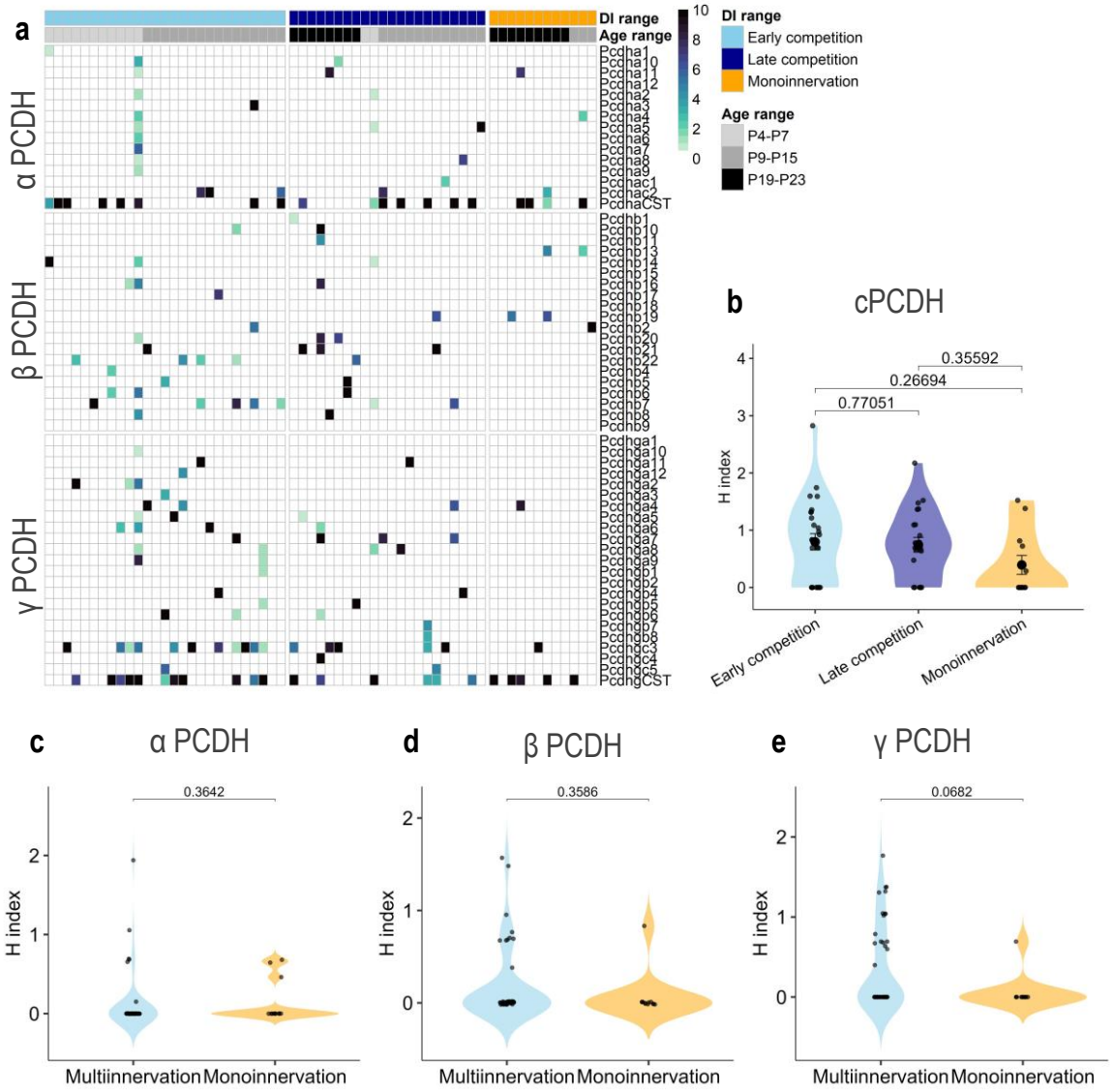

Figure 10: cPCDH expression in PC during CF elimination. (a) Heatmap showing normalized and scaled expression (0-10) of each cPCDH isoform. Gene names "PcdhaCST" and "PcdhgCST" correspond to the constant exons of Alpha and Gamma clusters, respectively. (b) Shannon's diversity H index calculated for all merged clusters. Kruskal – Wallis test p value: 0.249. Displayed p values correspond to Dunn's test pairwise comparisons with Bonferroni adjustment for multiple comparisons. Error bars correspond to S.E.M. (c) Shannon's H index calculated for each cPCDH cluster (x axis) per condition. Krukal – Wallis test p value: 0.08. Displayed p value corresponds to the lowest obtained after Dunn's test pairwise comparisons with Bonferroni adjustment. (d) Shannon's H index calculated for Gamma cluster in multiinnervated (early or late competition) or monoinnervated cells. Displayed p value corresponds to Mann Whitney's test.

Conclusions

Our results demonstrate, first, that it is possible to perform long electrophysiological recordings and preserve cell morphology, while achieving good quality starting material to produce single-cell RNA sequencing libraries. Differential expression analysis showed that significant changes are detected in relevant molecular pathways for PC development when cells are grouped according to CF functional differentiation. Shannon's *H* diversity index was proposed as a method to quantify cPCDH diversity, bringing information about both the level of expression and the diversity of isoforms simultaneously. Using this tool, we observed that γPCDH diversity specifically tends to decrease when CF are eliminated during the developmental critical period.

Supplementary figures Results Chapter I

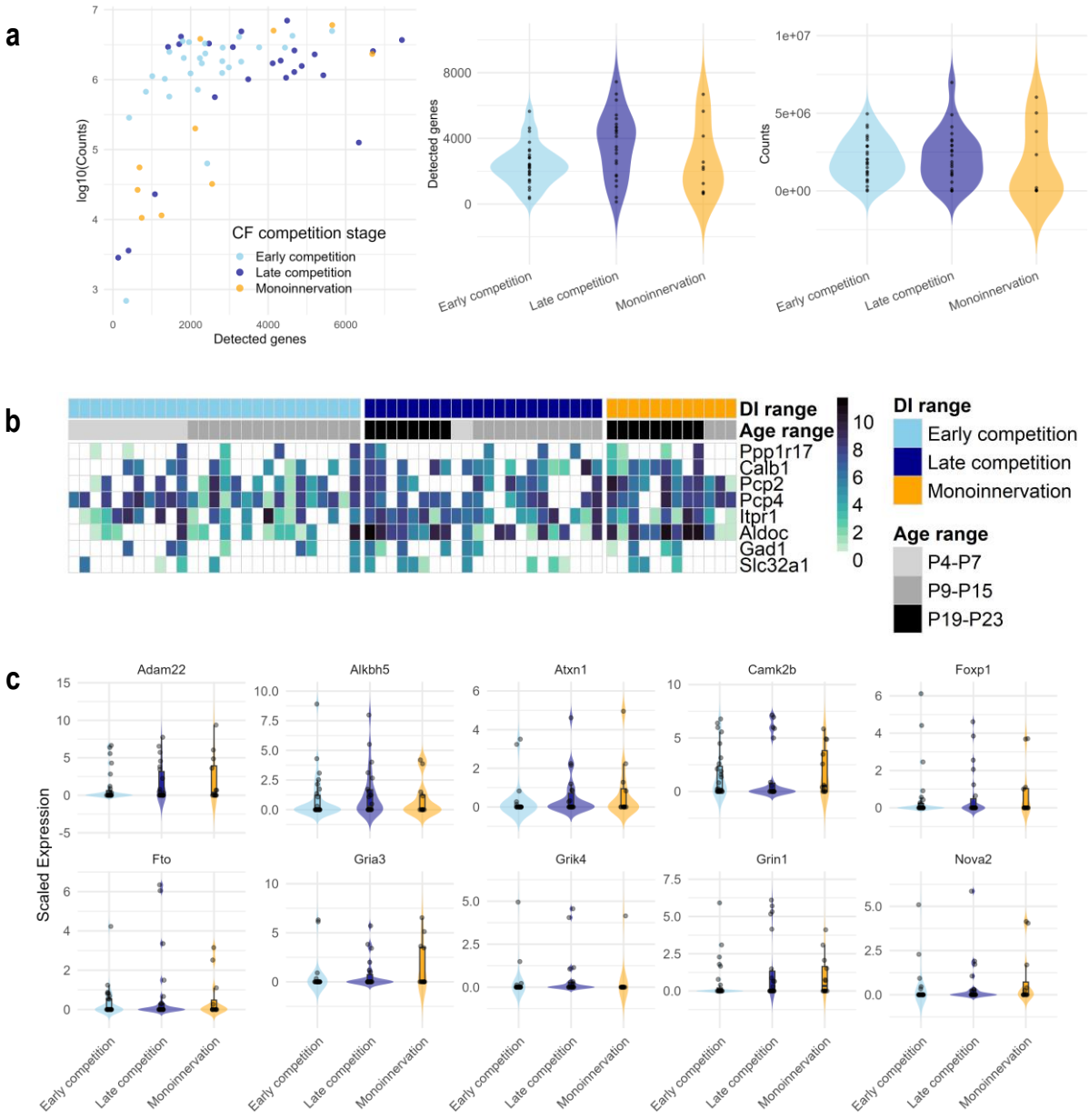

Supplementary Figure 1: Quality controls and GOIs expression. (a) Left: scatter plot showing the number of detected genes per sample in x and total counts, in logarithmic scale, in y. Middle: quantification of total detected genes per condition. Kruskal-Wallis test p value: 0.06. Right: quantification of raw total counts (in logarithmic scale) per condition. Kruskal-Wallis test p value: 0.5515. (b) Heatmap of PCs marker genes expression (normalized and scaled from 0 to 10). (c) Normalized expression of CF elimination related genes that were found significant in LRT differential expression analysis. LRT Adam22 p = 0.0265; Alkbh5 p = 0.0216; Atxn1 p = 0.0057; Camk2b p = 0.0105; Foxp1 p = 0.0178; Fto

p = 0.0248; Gria3 p = 0.0032; Grik4 p = 0.0434; Grin1 p = 0.0215; Nova2 p = 0.0373.

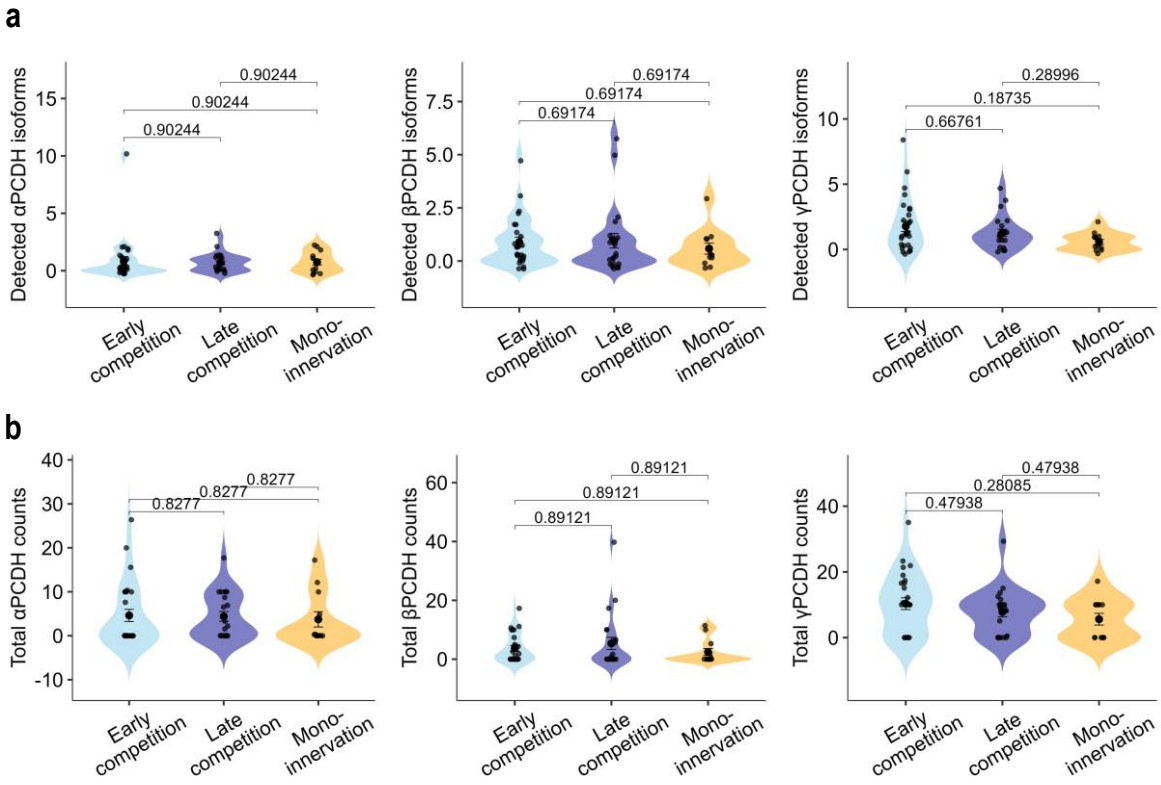

Supplementary Figure 2: Quantification of cPCDH expression per cluster. (a) Number of detected isoforms per condition. Kruskal-Wallis p-value from left to right: 0.6945, 0.7447 and 0.1694. (b) Sum of total scaled counts per cluster. Kruskal-Wallis p-value from left to right: 0.8370, 0.8033 and 0.2098. (a, b) Displayed p values correspond to Dunn's pariwise comparisons with Hommel's correction.

Tables Results Chapter I

Table 8: Genes included in cluster 1 from LRT – DGE analysis in Figure 2, left panels.

Gene Cluster 1	
Term	**Genes**
Intracellular Membrane-Bounded Organelle (GO:0043231)	Setd5, Smg1, Rbm26, Thra, Trrap, Fbh1, Zmynd8, Syne2, Cabin1, Golga2, Rsrc1, Snrnp70, Cspp1, Ppp6r2, Ppp6r3, Rev3l, Myo18a, Ubtf, Dip2b, Cic, Gusb, Sptan1, Ddx17, Kdm6b, Spacdr, Gaa, Arid5a, Zbtb33, Cbfa2t3, Pou3f3, Hcfc1, Dpm1, Psma4, Setbp1, Itpka, Eef1a2, Rbms1, Terf2ip, Phip, Tnik, Hoxb7, Vamp2, Notch2, Kmt2a, Mgst3, Gata6, Prdm15, Baz2a, Prdm13, Rela, Cux1, Ubb, Stk38, Fam120a, Dmd, Suds3, Brd4, Runx1t1, Arnt2, Crebbp, Taf15, Brf1, Brpf3, Huwe1, Dnajc13, Stam, Nsg1, Ptpn12, Mt3, Usp29, Nr2f6, Sod1, Ift20, Nr4a2, Rab14, Ago2, Calm3, Calr, Cdk13, Brwd1, Calm2, Tpt1
Calcium Channel Complex (GO:0034704)	Ryr2, Trpc4, Calm3, Cacna1e, Calm2
Nucleus (GO:0005634)	Setd5, Smg1, Rbm26, Thra, Trrap, Fbh1, Zmynd8, Syne2, Cabin1, Rsrc1, Snrnp70, Ppp6r2, Ppp6r3, Rev3l, Myo18a, Ubtf, Dip2b, Cic, Ddx17, Kdm6b, Spacdr, Arid5a, Zbtb33, Cbfa2t3, Pou3f3, Hcfc1, Dpm1, Psma4, Setbp1, Itpka, Eef1a2, Rbms1, Terf2ip, Phip, Tnik, Hoxb7, Notch2, Kmt2a, Gata6, Prdm15, Baz2a, Prdm13, Rela, Cux1, Ubb, Stk38, Fam120a, Dmd, Suds3, Brd4, Runx1t1, Arnt2, Crebbp, Taf15, Brf1, Brpf3, Huwe1, Nsg1, Ptpn12, Mt3, Usp29, Nr2f6, Sod1, Nr4a2, Ago2, Calm3, Calr, Cdk13, Brwd1, Calm2, Tpt1
Glutamatergic Synapse (GO:0098978)	Bcr, Ago2, Dlgap1, Nptx1, Sptb, Rela
Neuron Projection (GO:0043005)	Ank2, Nsg1, Ank1, Ift20, Inpp5a, Ubb, Scn8a, Scn9a, Dip2b, Ephb2, Arhgef7, Lzts1, Vamp2, Shank1

Sarcolemma (GO:0042383)	Ryr2, Ank2, Dmd, Plec
Cation Channel Complex (GO:0034703)	Ryr2, Trpc4, Calm3, Calm2
Filopodium Membrane (GO:0031527)	Dmd, Syne2
Voltage-Gated Sodium Channel Complex (GO:0001518)	Scn8a, Scn9a
Sodium Channel Complex (GO:0034706)	Scn8a, Scn9a

Table 9: Genes included in cluster 2 from LRT – DGE analysis in Figure 2, middle-left panels.

Cluster 2	
Term	**Genes**
Cul4A-RING E3 Ubiquitin Ligase Complex (GO:0031464)	Cdkn1b, Crbn, Trpc4ap
Postsynaptic Density (GO:0014069)	Nlgn1, Sipa1l1, Slitrk1, Grik4, Akap5, Ppp1r9a, Shank3, Dnm2
Asymmetric Synapse (GO:0032279)	Slc4a8, Nlgn1, Sipa1l1, Akap5, Ppp1r9a, Shank3, Dnm2
Neuron Projection (GO:0043005)	Nrp2, Nlgn1, Dscam, Ripk2, Kcnb2, Htr1a, Akap5, Ppp1r9a, Dnm2, Unc80, Trim9, Slc4a8, Alcam, Slc38a7, Adgrl1, Rgs12, Shank3.
Adherens Junction (GO:0005912)	Camsap3, Cyth3, Arvcf, Notch1, Tmod3, Frmd4b, Mpp7
Cytoplasmic Stress Granule (GO:0010494)	Atxn2l, Rock1, Caprin1, Pum1, Gigyf2
Recycling Endosome (GO:0055037)	Slc9a3, Tbc1d14, Relch, Atp11a, Akap5, Tbc1d17, Dnm2
Cell-Cell Junction (GO:0005911)	Cyth3, Arvcf, Notch1, Usp53, Src, Tmod3, Nphp4, Frmd4b, Rasip1, Mpp7, Epha2
Dendrite (GO:0030425)	Trim9, Slc4a8, Nlgn1, Dscam, Kcnb2, Htr1a, Rgs12, Akap5, Ppp1r9a, Gigyf2
Tight Junction (GO:0070160)	Cyth3, Usp53, Frmd4b, Mpp7, Epha2

Table 10: Genes included in cluster 1 from LRT – DGE analysis in Figure 2, middle-right panels.

Cluster 3	
Term	**Genes**
Cell-Cell Junction (GO:0005911)	Rap1b, Sptbn4, Sdcbp, Ccdc85c, Actn1, Kazn, Flot2, Pkn2, Rpgrip1l, Mtdh, Rnd1, Adgrl3
Actin Cytoskeleton (GO:0015629)	Sptbn4, Plekhh2, Auts2, Limch1, Actn1, Dlc1, Myo5a, Flot2, Ntn1, Rnd1, Ttc17
Cortical Actin Cytoskeleton (GO:0030864)	Sptbn4, Plekhh2, Dlc1, Flot2
Cytoskeleton (GO:0005856)	Auts2, Limch1, Cep295, Myo5a, Ntn1, Rnd1, Ttc17, Sdcbp, Alms1, Map7, Akt1, Aldoc, Pkn2, Gapdh
Cortical Cytoskeleton (GO:0030863)	Sptbn4, Plekhh2, Dlc1, Flot2
Membrane Raft (GO:0045121)	Rap1b, Ldhb, Sdcbp, Dlc1, Arid3a, Cbl
Vesicle (GO:0031982)	Sdcbp, Akt1, Myo5a, Flot2, Calm1, Ap3b2, Gapdh
Adherens Junction (GO:0005912)	Sptbn4, Sdcbp, Ccdc85c, Flot2, Rnd1
Recycling Endosome (GO:0055037)	Scamp5, Stx6, Lmtk2, Myo5a, Sorl1
Tertiary Granule (GO:0070820)	Dync1li1, Ptprb, Dlc1, Ubr4, Aldoc

Table 11: Genes included in cluster 1 from LRT – DGE analysis in Figure 2, left panels.

Cluster 4	
Term	**Genes**
Glutamatergic Synapse (GO:0098978)	Trio, Nptxr, Clcn3
Cytoskeleton (GO:0005856)	Slc30a9, Tmod4, Septin2, Amph, Mark4, Pfdn5, Spata7
Sec61 Translocon Complex (GO:0005784)	Ssr4
Endocytic Vesicle (GO:0030139)	Inpp5f, Clcn3, Amot
Intracellular Membrane-Bounded Organelle (GO:0043231)	Hdac5, Casz1, Cdca2, Chd7, Usp34, Ube2d1, Mia3, Chd3, Clcn3, Inpp5f, Ppp4r4, Map6, Brd8, Magi1, Slc30a9,

	sFnbp1, Septin2, Cnbp, Wapl, Pitpnm1, Pspc1, Rlim, Ube2o, Fam193b, Sf1
Microtubule Cytoskeleton (GO:0015630)	Septin2, Map6, Mark4, Spata7
Septin Cytoskeleton (GO:0032156)	Septin2
Septin Ring (GO:0005940)	Septin2
Swr1 Complex (GO:0000812)	Brd8

Results

Chapter II: Olivo-cerebellar explants recapitulate circuit development *in vitro.*

Context and aims

After observing that cPCDH expression is regulated in PCs during CF elimination, we aimed to implement a system that would allow simultaneous access to pre- and postsynaptic circuit partners, as well as genetic and functional manipulations. Previously described hindbrain explants or olivo-cerebellar explants (Chedotal et al., 1997; Letellier et al., 2007) were our preferred option. These organotypic cultures are prepared from E14 mouse embryos (after PCs and IONs birth but before the onset of synapse formation) and can be cultured for ~40 days, which broadly covers olivo-cerebellar circuit development, including the critical period for CF elimination. Furthermore, three-dimensional circuit architecture is maintained in explants, and PCs and IONs are exposed and accessible. Hence, we proceed to the developmental characterization of PC afferents within these *in vitro* conditions, with a focus on CF to PC synapses using immunohistochemistry and electrophysiology. Explants were prepared from Igsf9-eGFP mice, selectively expressing eGFP in IONs and CFs (Patz et al., 2018).

Olivo-cerebellar explants preserve spatiotemporal development of cerebellar microcircuitry

First, to monitor the development of the main PC afferents, explants were fixed at DIV7-8, DIV14, DIV21 and DIV26, corresponding, approximately, to P0-P1, P7, P14 and P19, respectively, covering the main stages of circuit development (onset of synapse formation, early competition or “pericellular nest” stage, late competition or “capuchon" stage and “dendritic” stage) (Kano et al., 2018). Immunostaining for Calb1 and Igsf9-GPF was used to visualize PCs and CF, respectively. In addition, vGLUT2, the selective glutamate transporter in CF was co-labelled with either vGLUT1 or vesicular GABA transporter (vGAT) to visualize the distribution of PF and inhibitory inputs respectively to CF contacts.

At DIV7-DIV8, PC show fusiform morphology with dendritic processes extending in multiple directions from the cell body. CF, vGLUT2, vGLUT1 and vGAT signals are dim at this stage, but diffuse, sparse synapses can be observed

around PCs cell bodies (**Figure 11a, Figure 12a**). One week later, PCs exhibit a spheric cell body, and one primary dendrite starts emerging and hence defining cells' polarity. CFs surround the soma, colocalizing with vGLUT2 puncta. On the contrary, vGLUT1 signal appears in the short dendritic tree. vGLUT2 puncta can also be observed in the dendrites because, at this stage, PF co-express both glutamate transporters (Miyazaki et al., 2003) (**Figure 11b**). Inhibitory contacts start gathering around the soma but not overlapping with vGLUT2 puncta (**Figure 12b**). At DIV21, a well-developed PC dendritic tree can be observed, and vGLUT2-positive CF terminals are established mainly on the primary dendrite shaft, thus illustrating somato-dendritic translocation (Hashimoto, Ichikawa, et al., 2009). vGLUT1 puncta density is increased and restricted to distal dendrites, in agreement with the dramatic increase of PF innervation that is observed *in vivo* within the corresponding developmental period (Kurihara et al., 1997) (**Figure 11c**). vGAT puncta distributes through all cell compartments (**Figure 12c**), which may probably correspond to the contacts from the two main inhibitory cell types: basket cells and stellate neurons (Watanabe & Kano, 2024). Finally, at DIV26, which corresponds to the mature stage of the circuit, PC branching is more complex while vGLUT2-positive CF terminals as well as vGLUT1 and vGAT positive terminals show similar distribution across the different subcellular compartments as for the previous time point (**Figure 11d, Figure 12d**).

Overall, these images illustrate the recapitulation of normal cerebellar microcircuitry development in explants from DIV7 to DIV26 critical period, showing the correct spatial organization of diverse synaptic contacts and, importantly, an *in vivo* – like morphological development of PC and CF.

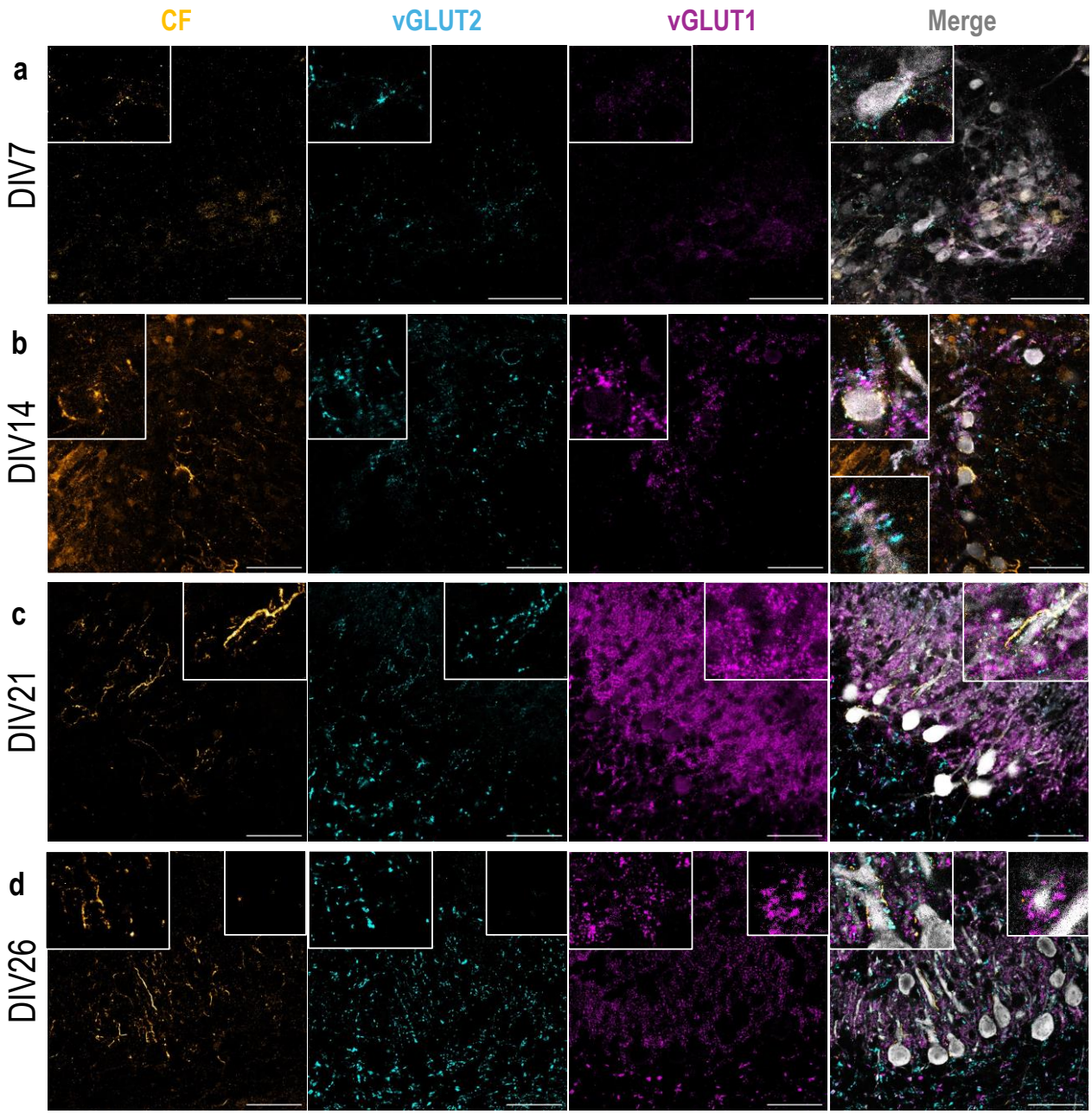

Figure 11: Immunostaining of Calb1, Igsf9-GFP (CF), vGLUT2 and vGLUT1 in explants over development. The three first panels of each row correspond to a single representative plane. The last panel (MIP merge) corresponds to the maximum intensity projection. All scale bars correspond to 50 µm.

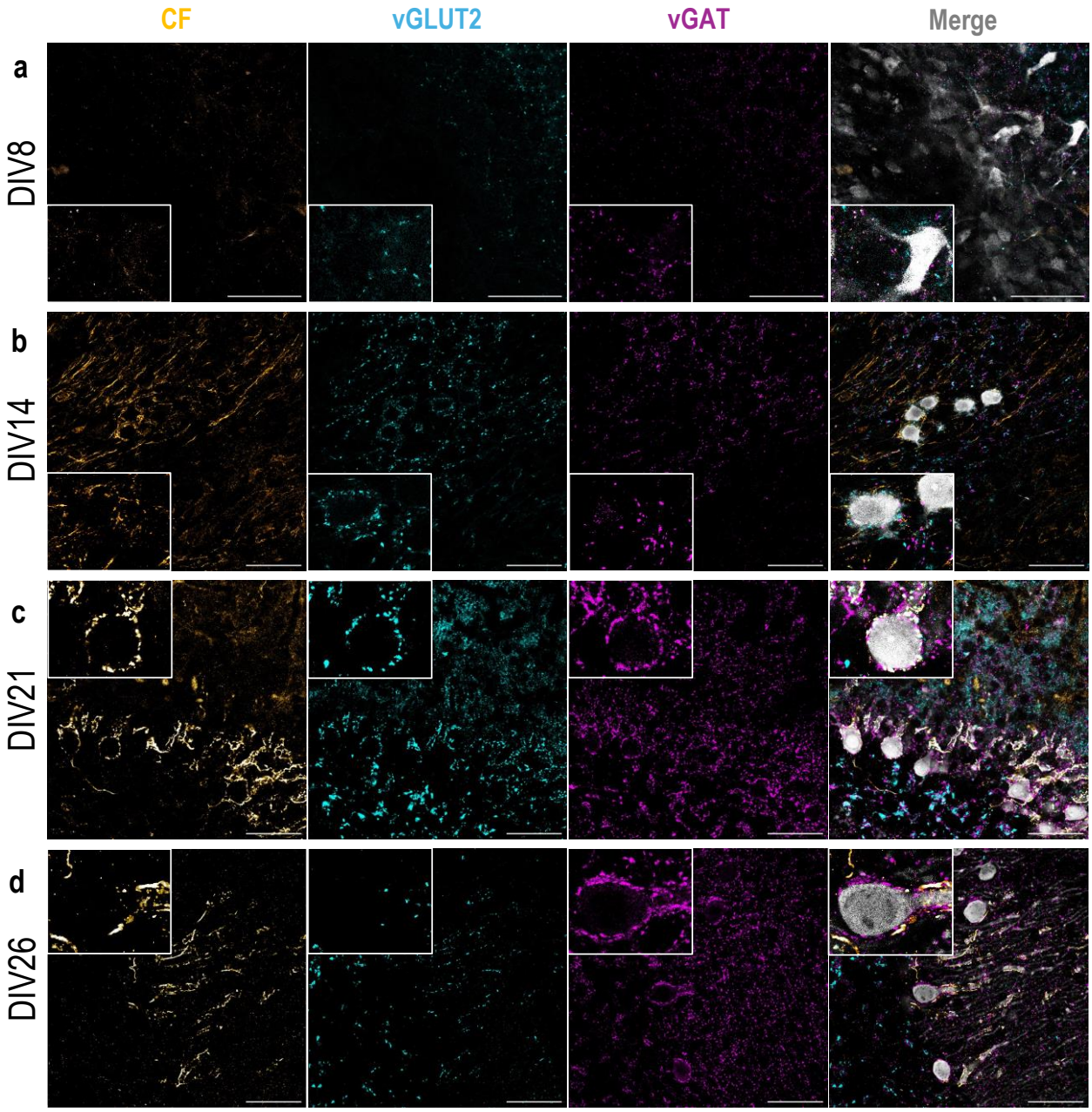

Figure 12: Immunostaining of Calb1, Igsf9-GFP (CF), vGLUT2 and vGAT in explants over development. The three first panels of each row correspond to a single representative plane. The last panel (MIP merge) corresponds to the maximum intensity projection. All scale bars correspond to 50 µm.

CF-PC synaptic maturation follows ex vivo developmental dynamics

To verify the use of explants under our experimental conditions to study CF elimination, evoked CF-EPSCs were recorded from PCs at three timepoints: DIV14, DIV28 and DIV35 applying the same paired-pulse stimulation protocol used for acute slices. A significant decrease in the number of CF inputs per PC was observed (**Figure 13a**), as well as D.I. variations similar to *ex vivo* conditions (**Figure 13b**) and increasing PPR values over time (**Figure 13c**). This is in line with studies that previously addressed CF competition in explants (Letellier et al., 2009).

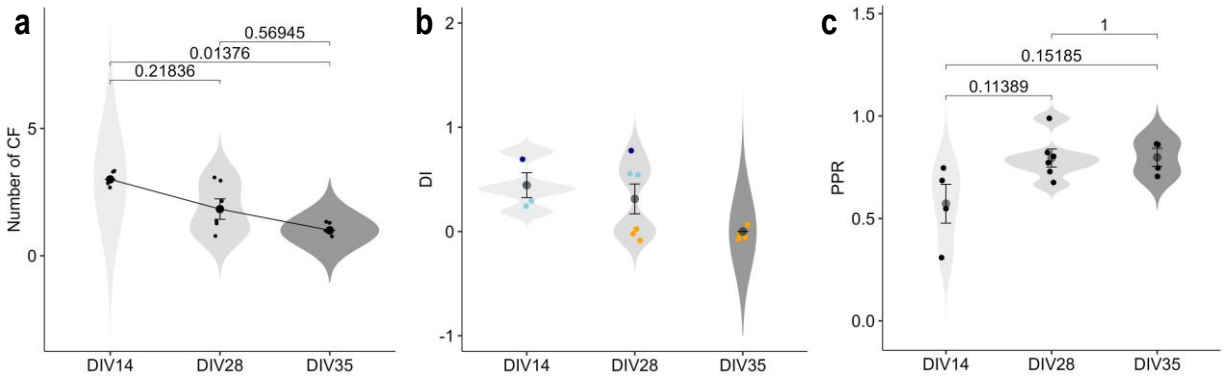

Figure 13: Electrophysiological characterization of CF to PC synapses in explants. (a) Quantification of the number of CF inputs per cell in each age range. Kruskal-Wallis test p value: 0.01726. (b) DI of CF inputs amplitudes per cell. Color scale corresponds to y values (orange: D.I. = 0; light blue: 0 < D.I. < 0.7; dark blue: D.I. > 0.7). Kruskal-Wallis test p value: 0.07673. (c) Paired-pulse ratio per cell in each age range, quantified as in Figure 8. Kruskal-Wallis test p value: 0.1054. (a,b,c) Error bars correspond to S.E.M. Displayed p values correspond to Dunn's pairwise comparisons with Bonferroni adjustment.

Conclusions

Our IHC and electrophysiology data demonstrate that the main developmental features of the olivo-cerebellar circuit are recapitulated in explants, including: (1) PC dendritic tree differentiation, (2) CF elimination, functional differentiation and dendritic translocation, (3) PF innervation and

vesicular transporter expression switch, and (3) PC innervation by inhibitory inputs. The different PC afferents are segregated spatially across PCs occupying the same territories as *in vivo* and following the same temporal trajectory. Altogether, these results support the use of olivo-cerebellar explants for the study of CF to PC synapse development.

Results

Chapter III: Brainstem innervation is required for γPCDH regulation in Purkinje cells.

Context and aims

After validating hindbrain explants as an appropriate model for the study of CF development, we aimed to assess whether cPCDH decrease in diversity over development in PCs depends on CF innervation. Previous studies showed PCs survival in explants even when the brainstem is removed during culture preparation, meaning that PCs develop in the complete absence of CF innervation. Furthermore, when a brainstem is reattached to the isolated cerebellar plate after the closure of the critical period, those naïve but mature PCs get multi-innervated by CFs with equal synaptic strength. Under these conditions, PCs are unable to eliminate supernumerary CF and these are retained in the long term (Letellier et al., 2007); i.e., PCs are unable to choose a winning CF out of the developmental critical window. These results suggest that CF to PC innervation during critical period induces long-term molecular changes that ensure adult mono-innervation. This, together with our previous observations in acute slices, encouraged us to hypothesize that brainstem innervation may be involved in the regulation of cell-adhesion molecules in PCs during the critical period; more specifically, cPCDH. To test this idea, PatchSeq was performed in full and "naïve" explants (isolated cerebellar plates) during early development and after the closure of the critical period (**Figure 14a, b**) to investigate the effect of brainstem innervation in cPCDH expression regulation in PCs. Using the same $CsMeSO_3$ – based internal solution than before, voltage-clamp continuous recordings were performed at -70 mV holding potential to ensure cell's viability through the observation of spontaneous EPSC. After recordings, each cell's content was used for single-cell RNA sequencing libraries preparation following the same SmartSeq2 protocol.

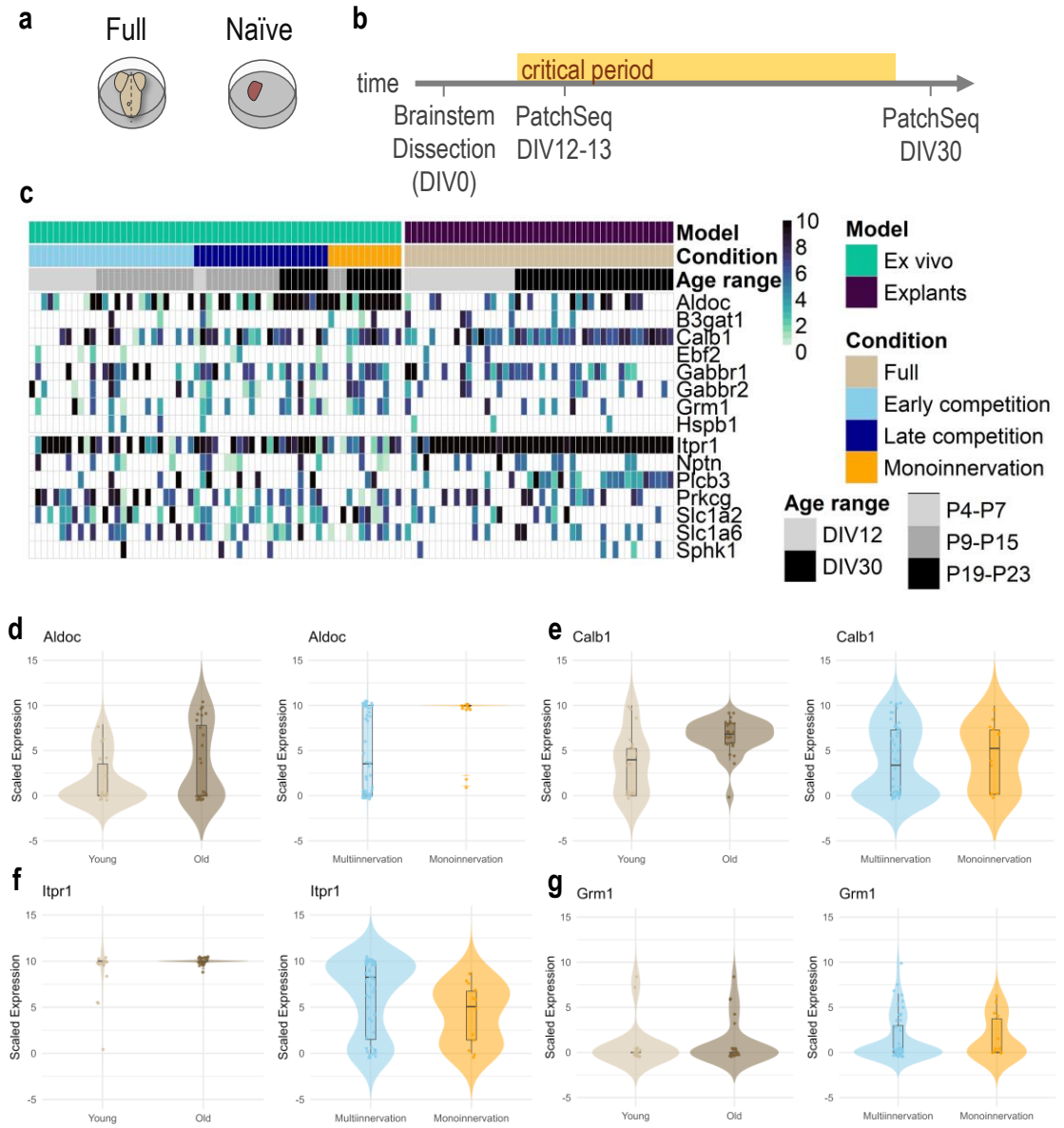

Figure 14: Comparison of sagittal bands-gene expression across developmental stages of PCs in explants and acute slices. (a) Schematics of culture full and naïve explants. (b) Experimental timeline of brainstem dissection and PatchSeq sample acquisition to study the effect of brainstem innervation in PCs gene expression. (c) Heatmap showing scaled (0-10) expression of Calb1 and cerebellar sagittal bands-genes in PCs in acute slices (ex vivo) and full explants (in vitro). (d, e, f, g) Scaled expression of aldolase C (Aldoc), calbindin 1 (Calb1), inositol 1,4,5-trisphosphate receptor type 1 (Itpr1) and glutamate metabotropic receptor 1 (Grm1) in full explants (left panels) and acute slices (right panels) across developmental stages.

Conserved PCs marker genes and sagittal bands genes profile in explants across developmental stages of PCs

Reads were mapped to the mouse genome using the same cPCDH detection-improved custom template in STAR (Materials and Methods, Analysis techniques, page 85). Total obtained counts were equivalent for each batch (young or old, full or naïve explants). However, we detected 37.4% more genes in young *versus* old PCs in full explants, and a 36% in naïve explants (Supplementary Figure 3a, b). Together with the similar trend that we observed in acute slices (Supplementary Figure 1), those results suggest an age-dependent effect.

To test whether PCs gene expression is preserved in explants, we first compared well-known PC genes in both models, including Calb1 and 14 sagittal bands-encoding genes, including: aldolase C (Aldoc), inositol 1,4,5-trisphosphate receptor type 1 (Itpr1), glutamate metabotropic receptor type 1 (Grm1), β-1,3-glucuronyltransferase 1 (B3gat1), early-B cell factor 2 (Ebf2), GABA-B receptor 1 and 2 (Gabbr1, 2), heat-shock protein family B member 1 (Hspb1), neuroplastin (Nptn), phospholipase C β3 (Plcb3), protein kinase Cγ (Prkcg), glutamate transporter 1 (Slc1a2), excitatory aminoacid transporter 4 (EAAT4, Slc1a6) and sphingosine kinase 1 (Sphk1) (Figure 14c). We did not observe striking differences in the regulation of these genes, comprising different patterns over time, such as an increase with age (Aldoc and Calb1, **Figure 14d** and **Figure 14e**, respectively), constitutive high expression (Itpr1, Figure 14f), or lower constitutive expression (Grm1, **Figure 14g**). The expression across developmental stages of all the mentioned genes can be found in Supplementary Figure 4. This points to no major differences between PCs gene expression in explants and *in vitro*.

To further investigate possible differences between PCs gene expression during development *in vitro*, we performed a differential expression analysis between DIV12-13 and DIV30 PCs using LRT from DESeq2, similarly to the approach used for acute slices (**Figure 15a**). Genes with significantly different expression were classified as up- or downregulated with age, and EnrichR

pathway analysis was performed on each subset. Among the upregulated pathways, we found peptidase related pathways, mainly, although only a few genes were assigned per pathway (**Figure 15b**, upper panel). Downregulated pathways included several excitatory synapses pathways as well as cell adhesion genes (**Figure 15b**, bottom panel). In acute slices, glutamatergic synapses pathways were detected among downregulated genes over time; however, different genes associated with excitatory synapses and CAMs were distributed across the different expression patterns found **Figure 9**. All things considered, our pathway analysis approach remains as an exploratory tool, highly sensitive to the input dataset provided and to the gene annotation database. Nevertheless, these results point to important pathways (excitatory synapses and CAMs) for PCs physiology and connectivity being regulated both *in vivo* and *in vitro* during development.

Differential gene expression analysis reveals alteration in the expression of synaptic genes and CAMs in PCs that develop in absence of CF input

In order to test the influence of brainstem innervation in PCs gene expression during development, LRT-based differential expression and pathway analysis was then performed on naïve explants data (**Figure 15c**). Importantly, while glutamatergic synapse related genes were found enriched among the downregulated ones in full explants and slices, this pathway was found upregulated in naïve explants – except for NMDA receptor complex genes. The only other pathway enriched among upregulated genes was U5 snRNP, which also followed the same trend in full explants, and comprised only a few genes (**Figure 15d**, upper panel). In addition, while cell-adhesion pathways were highly enriched in full explants downregulated pathways, these were not as prevalent in naïve explants (**Figure 15d**, bottom panel). These results indicate that brainstem innervation to PCs may have a direct effect on synaptic and CAM gene expression regulation during the developmental critical window.

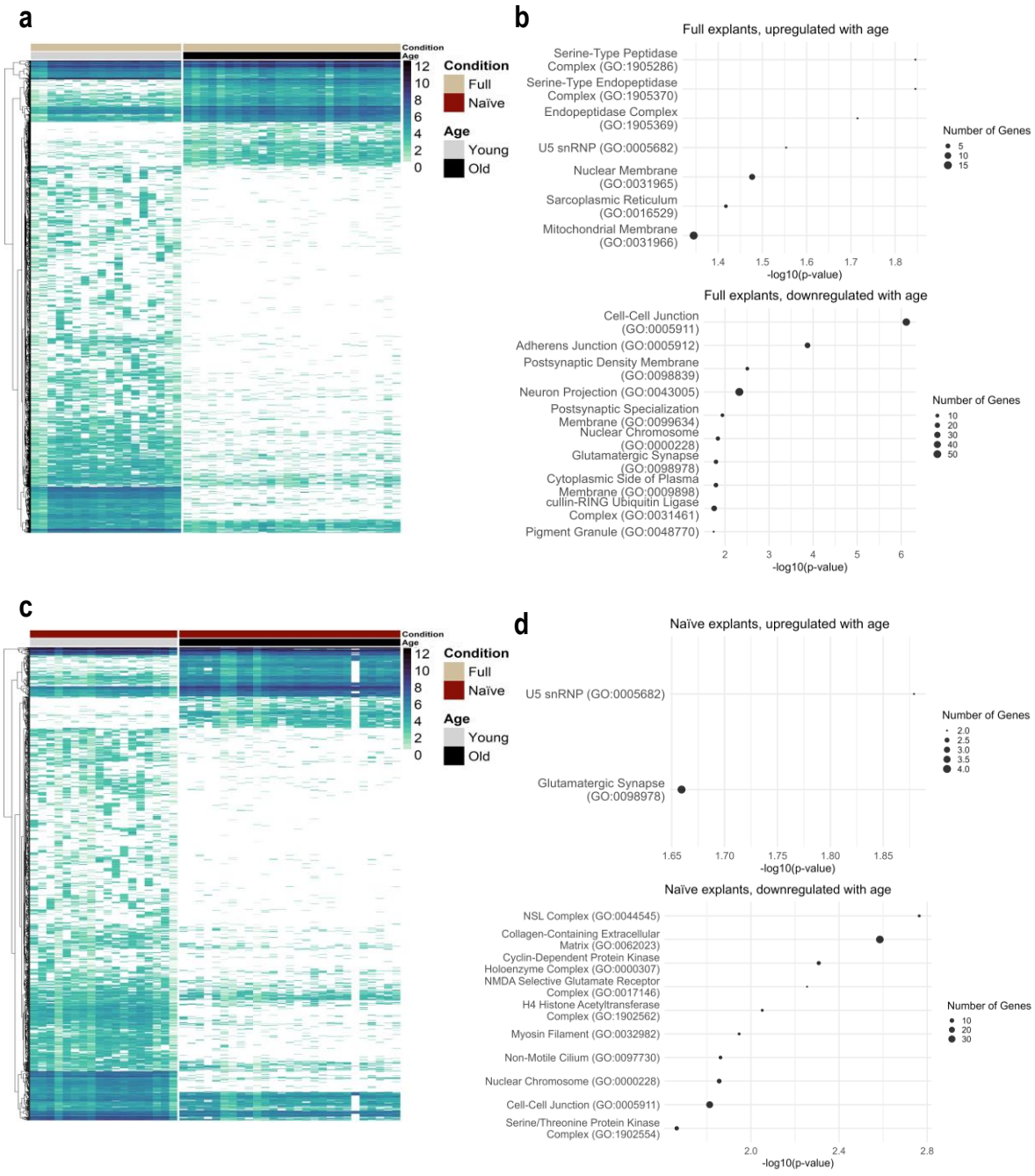

Figure 15: Differential expression analysis in full and naïve explants. (a) Heatmap of genes differentially expressed in young versus old cells from full explants. Scale corresponds to normalized counts. Genes with an adjusted p value < 0.05 are shown. (b) Pathway analysis for genes with higher (top panel) or lower expression in old explants (bottom). (c) Heatmap of differentially expressed genes in naïve explants (same parameters than in a). (d) Pathway analysis of genes in (c).

To better understand the effect of brainstem innervation, common regulated genes in full and naïve explants, as well as genes exclusively regulated

in the presence of brainstem innervation, were analyzed. To improve pathway analysis, genes were segregated according to the expression pattern (up- or downregulated in each condition) (**Figure 16a**). Upregulated pathways exclusively in the presence of brainstem innervation did not include any genes directly involved in synapse contact regulation (**Figure 16b**). Among the common upregulated pathways in naïve and full explants, we found genes involved in alternative splicing and only four genes involved in excitatory synapses, including glycogen synthase kinase-3β (Gsk3b) and the postsynaptic adhesion molecules Slitrk2 (Slit- and Trk-like family member 2), interleukin 1 receptor accessory protein like 2 (Il1rapl2) and Lrrc4b (leucine-rich repeat-containing protein 4B, NGL-3) (**Figure 16c**).

On the other hand, genes exclusively downregulated in full explants were found to be highly enriched in CAMs and excitatory postsynaptic genes, including kainate-type glutamate receptor 4 (Grik4), strongly involved in CF to PC synapse stabilization (Kakegawa et al., 2024) (**Figure 16d**). Certain cell adhesion genes were also found enriched among the common downregulated pathways (Figure 16e). Altogether, these findings indicate that the lack of brainstem innervation significantly affects gene regulation in PC, including, mainly, CAMs and excitatory synapses proteins.

Naïve PCs retain an immature pattern of cPCDH expression

cPCDH expression was analyzed as previously explained in Results Chapter I, page 99. As *in vivo*, a scattered expression per isoform can be observed (**Figure 17a**). H index was calculated for the expression of all clusters, showing a significantly lower isoform diversity in old explants; however, this difference was lost in naïve explants (**Figure 17b**). This indicates that brainstem innervation to PC is needed for cPCDH isoforms diversity regulation during the critical period.

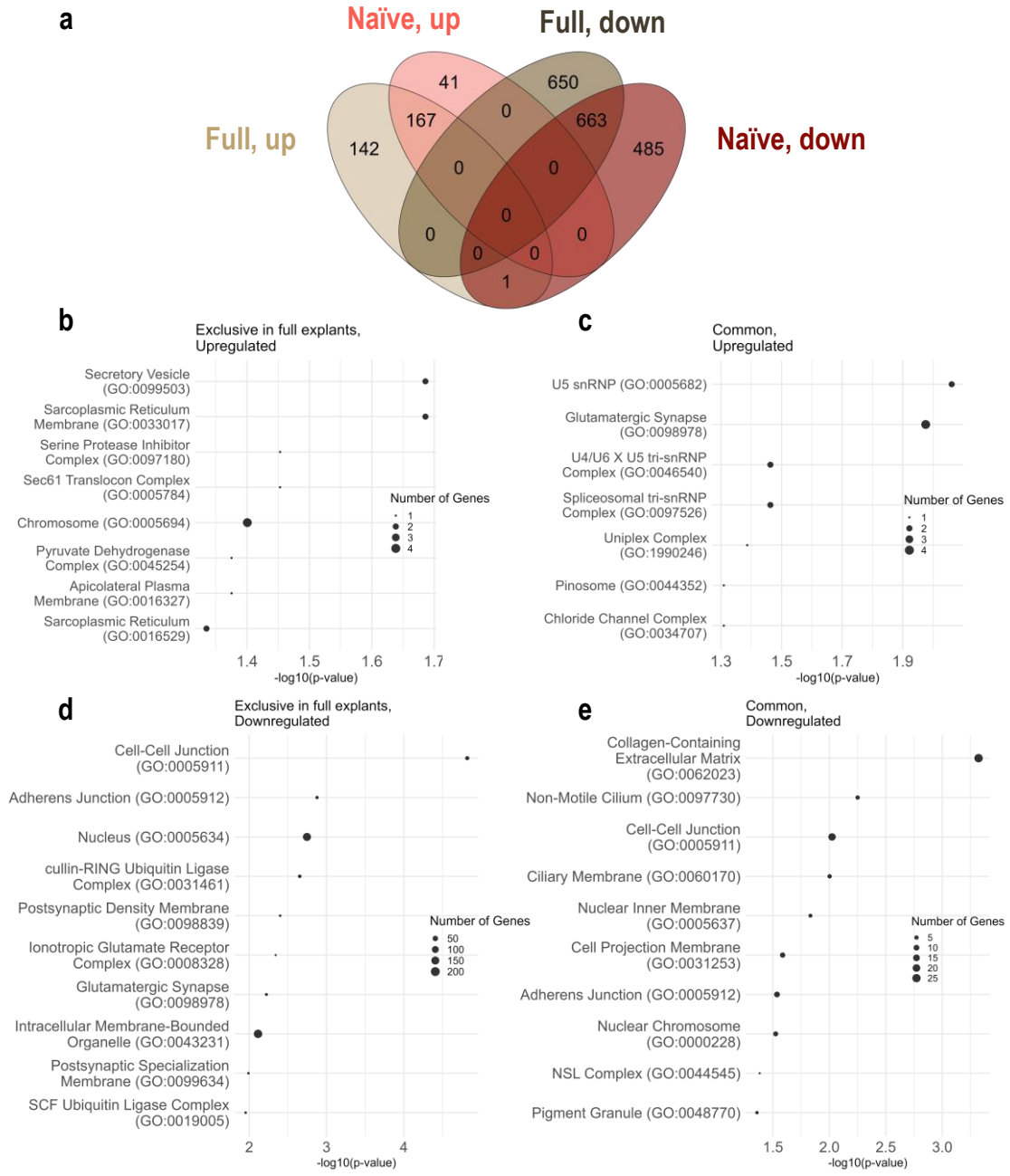

Figure 16: Genes regulated in both conditions and exclusively regulated in full explants. (a) Venn diagram showing the number of differentially expressed genes, young versus old PCs, in full and naïve explants, segregated according to the expression pattern (up- or downregulated) and the number of overlapping genes between each comparison. (b) Pathway analysis of upregulated genes with age exclusively changing in full explants. (c) Pathway analysis of upregulated genes in both full and naïve explants. (d) Pathway analysis of downregulated

genes with age exclusively changing in full explants. **(e)** Pathway analysis of downregulated genes in both full and naïve explants.

Isoform diversity was analyzed then for each cluster individually, showing that γPCDH and βPCDH diversity are both downregulated with age in full explants, but not in naïve ones (**Figure 17c, e**). On the contrary, αPCDH isoforms show a non-statistically significant trend with age and display lower diversity values in all conditions (**Figure 17d**).

Conclusions

When brainstem was dissected, preventing CF to PC innervation, before the onset of the developmental critical period, it could be observed that several cell-adhesion molecules did not undergo the expected changes with ages. cPCDH isoforms diversity was only decreased, as *in vivo*, in full explants, but this effect disappeared in naïve explants. These results may indicate that brainstem innervation, presumably CF to PC, has a significant impact in PC gene expression changes during development, and that it is needed for the regulation of cPCDH diversity during this period. Previous research has demonstrated that naïve PCs fail to eliminate supernumerary CFs upon reinnervation, retaining multi-innervation instead of undergoing normal synapse pruning. This inability to fine-tune CF inputs could be linked to the immature cPCDH expression pattern observed in these cells: multiple isoforms might potentially allow persistent multi-innervation and, possibly, prevent CF elimination.

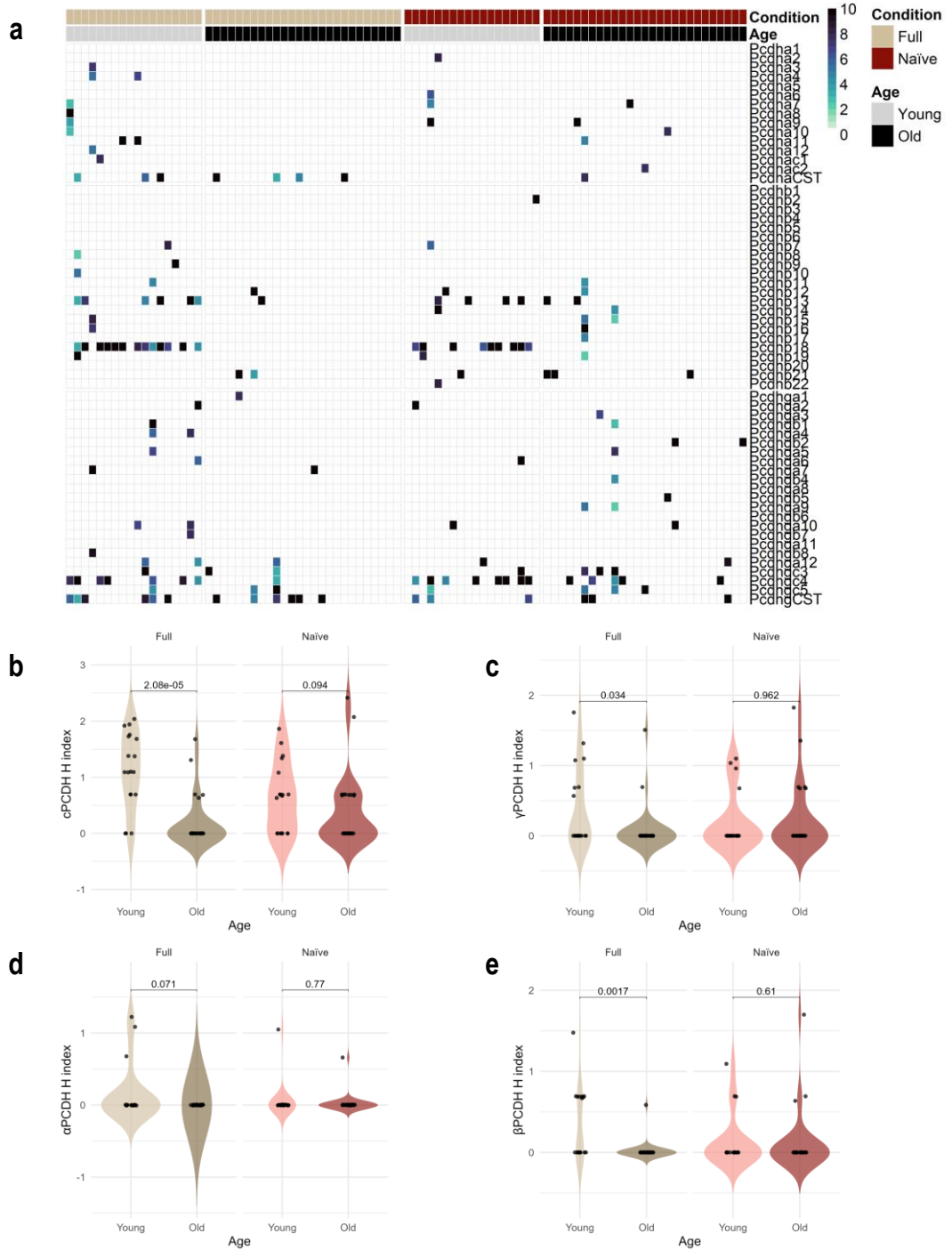

Figure 17: cPCDH expression in PC from full and naïve explants during and after developmental critical period. (a) Heatmap of normalized and scaled (0 – 10) expression per cPCDH isoform. (b) Shannon's H index calculated for all cPCDH clusters. (c,d,e) H index calculated for γ-, α- and βPCDH isoforms, respectively. (b,c,d,e) Displayed p values correspond to Mann Whitney's test with Hommel's adjustment.

Supplementary figures Results Chapter III

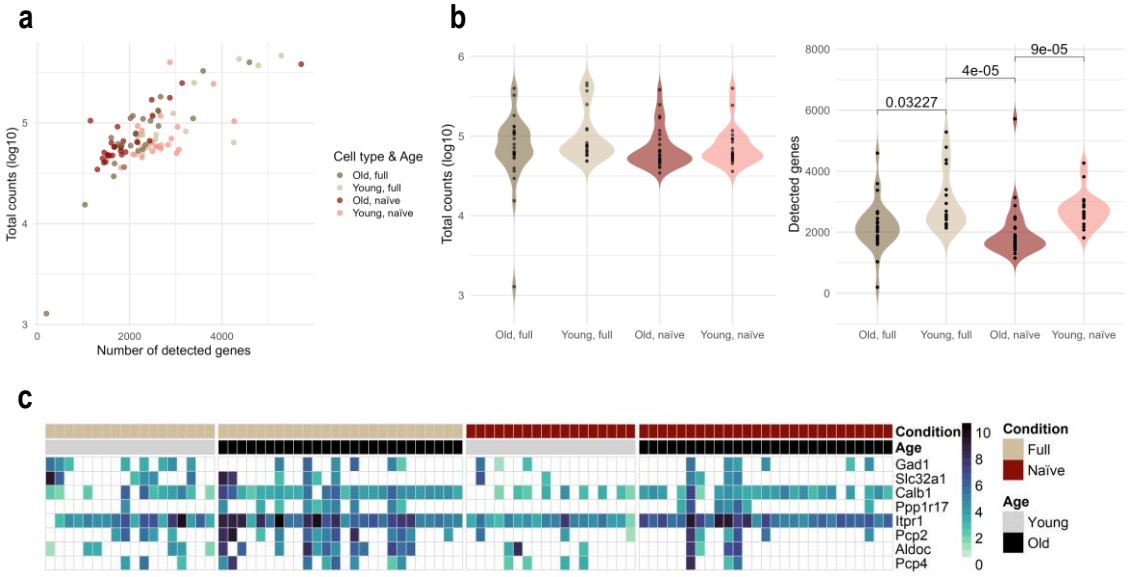

Supplementary Figure 3: Quality controls of explants single-cell RNA sequencing. (a) Scatter plot showing the number of detected genes per sample in x and total counts, in logarithmic scale, in y. (b) Left: quantification of total counts (in logarithmic scale) per condition. Kruskal-Wallis test p value: 0.1597. Right: total detected genes per condition. Kruskal-Wallis test p value: 2.48 · 10-6. Displayed p-values values correspond to Dunn's test pairwise comparisons with Bonferroni adjustment; only $p < 0.05$ are shown. (c) Heatmap of PCs marker genes expression (normalized and scaled from 0 to 10).

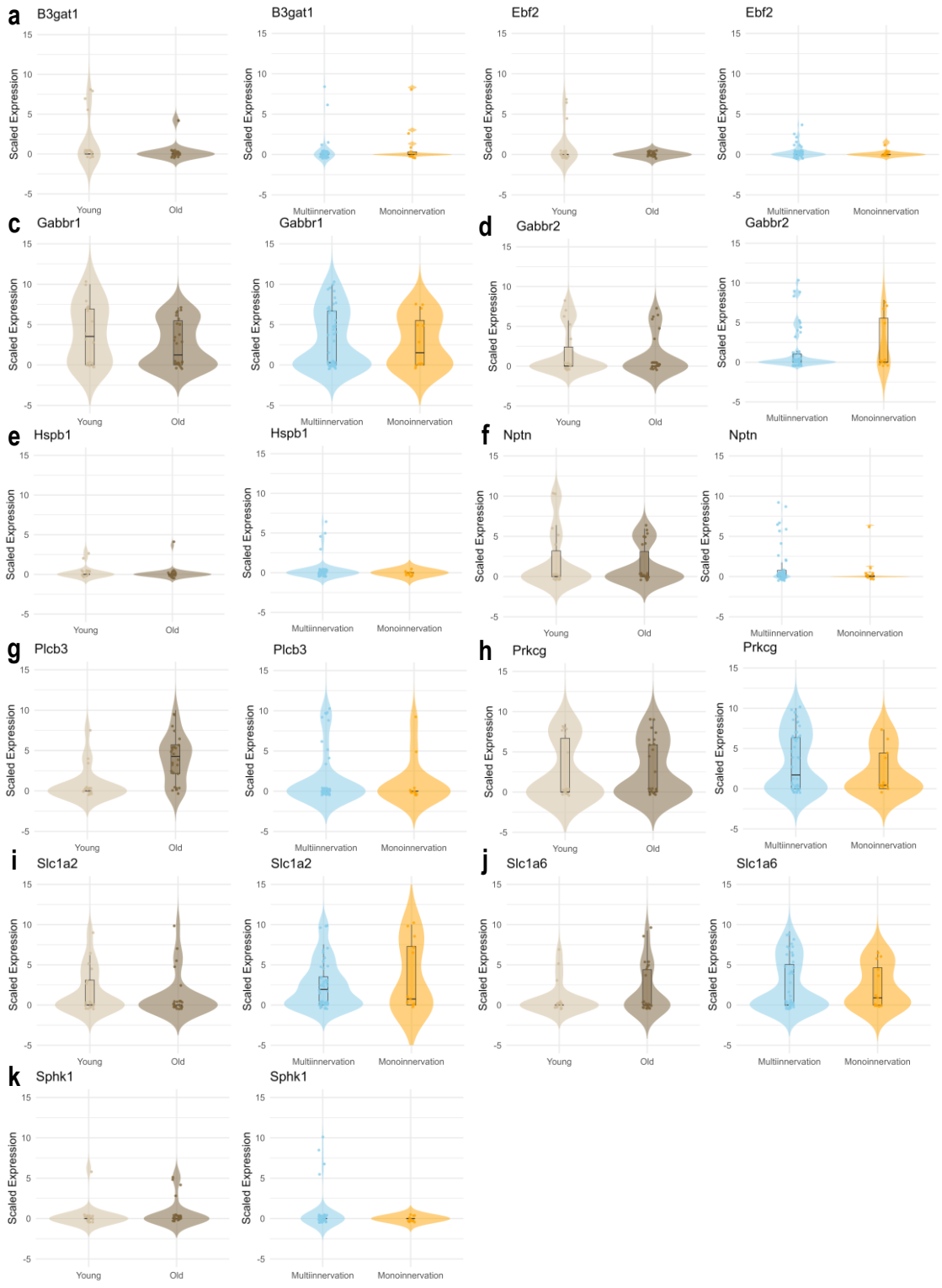

Supplementary Figure 4: Scaled (0-10) expression of sagittal bands-genes in PCs from explants (left panels, golden) and acute slices (right panels, blue-yellow).

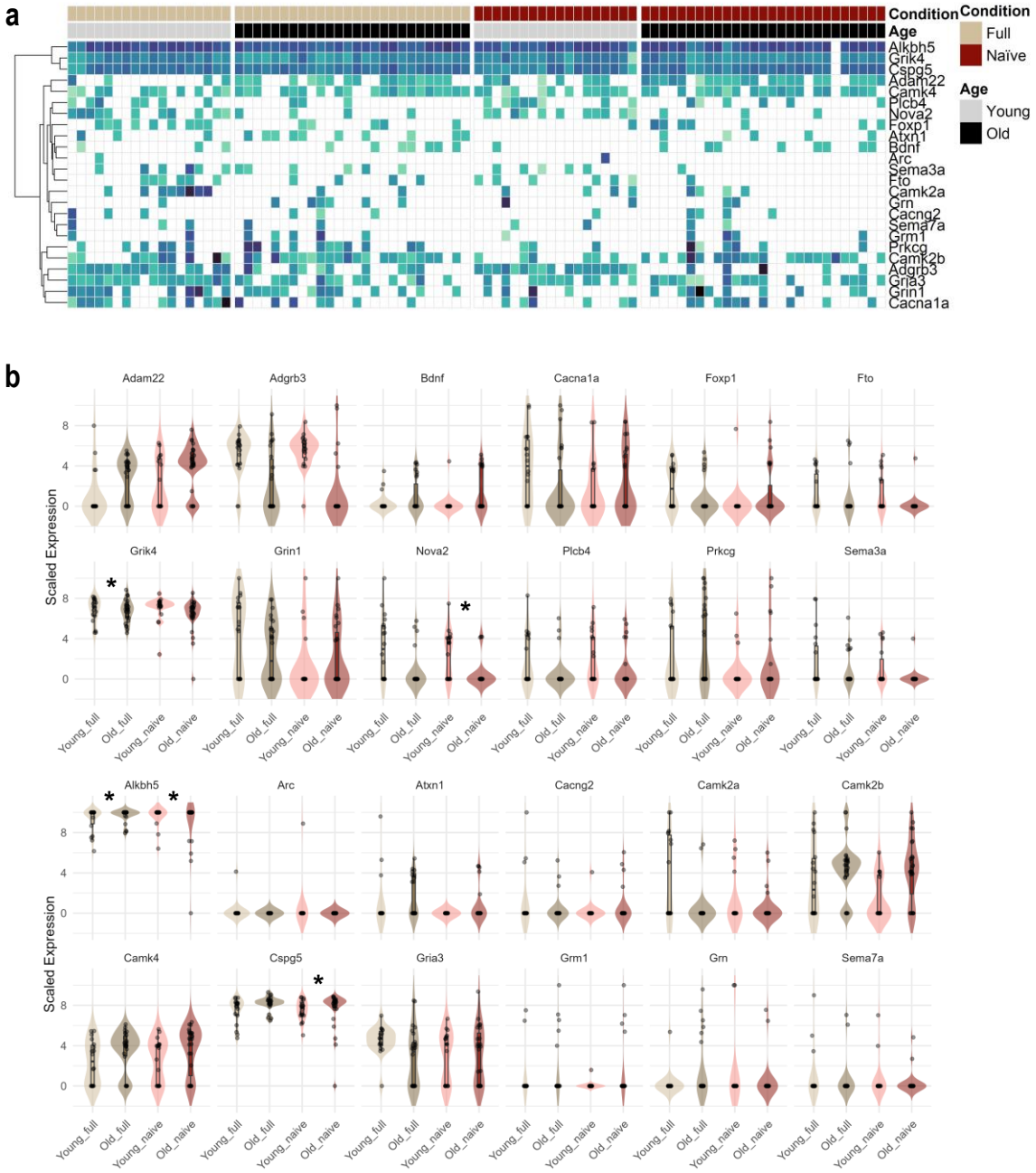

Supplementary Figure 5: Expression in full and naïve explants of genes related to CF elimination. (a) Heatmap showing scaled expression of CF elimination related genes. (b) Quantification of individual genes expression. Stars correspond to genes with an adjusted p value in LRT minor than 0.05.

Results

Chapter IV: Single isoform overexpression to alter γPCDH diversity in Purkinje cells accelerates CF elimination

Context and aims

Our previous experiments indicated that cPCDH are regulated in PC during CF elimination, finding a lower diversity of cPCDH isoforms expressed over time. In addition, when the brainstem was dissected out *in vitro*, PCs developed in the absence of CF innervation and retained high cPCDH diversity. This led us to hypothesize that high cPCDH isoform diversity at early postnatal ages may be allowing CF multi-innervation. Then, in cooperation with the activity-dependent competition among CFs, PCs may regulate their cPCDH isoforms repertoire to retain the winning afferent, establishing a molecular match that would ensure long-term mono-innervation while preventing multi-innervation in the mature circuit. If proven, this could explain previous research showing that, in explants, when brainstem is dissected out after the closure of the critical period, and a new one is presented to PCs, these get directly mono-innervated. Those results suggest that, in this situation, mature PCs do not choose their CF afferent based on activity-dependent cues. Instead, they could use molecular cues supporting recognition between specific partners (Letellier et al., 2007).

To address this question, we aimed to prematurely induce in young PCs the molecular pattern observed in adult cells; this is, artificially reducing cPCDH diversity before the end of the critical period and assessing the impact on CF innervation and competition. Inspired by previous work on cPCDH gain-of-function experiments in the olfactory bulb (Mountoufaris et al., 2017), we opted for single-isoform overexpression at DIV15 through single-cell electroporation (Materials and Methods, Wetlab materials and methods, page 81) (**Figure 18a**). Although a replacement strategy was not applied, the drastic overexpression of a single isoform would presumably dominate over the intrinsic pool of cPCDH proteins and thus shift transmembrane interactions stoichiometry by saturating available binding partners.

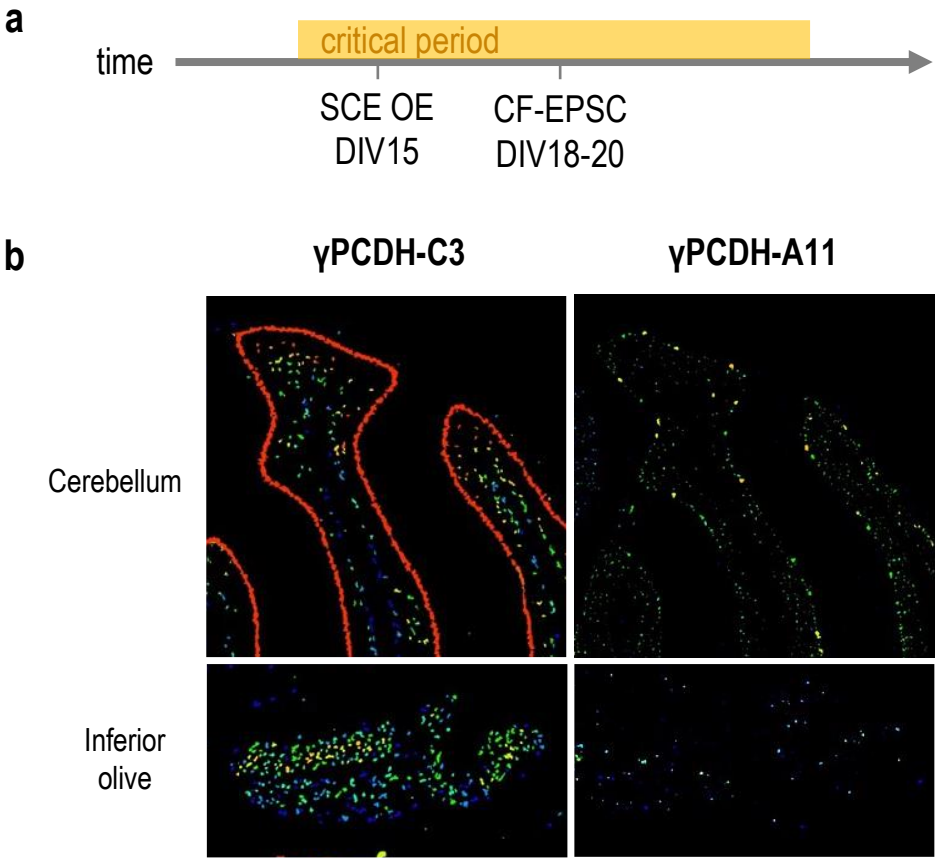

Figure 18: γPCDH-C3 and γPCDH-A11 expression in the cerebellum and brainstem. (a) Experiment timeline for single isoform overexpression through SCE and CF-EPSCs recordings. (b, c) γPCDH-C3 and γPCDH-A11 expression, respectively, in cerebellum PCs and IONs (arrowheads). Images credit: Allen Institute for Brain Science (available at http://mouse.brain-map.org/experiment/show/70784952;http://mouse.brain-map.org/experiment/show/79354776).

Because of the high number of cPCDH isoforms within the mouse genome, it was not feasible to test them all experimentally. We restricted our choice among isoforms from the γPCDH cluster, as it shows the strongest decrease in diversity in acute slices and explants (**Figure 10; Figure 17**). Among the three families composing the γPCDH cluster, we could notice that, while members of the A family displayed a scattered pattern of expression across cells, as described in the literature for cPCDHs, C-type isoforms were expressed by a higher percentage of cells. This was confirmed by the RNA hybridization data available at Allen Mouse Brain Atlas (2011). Attending to their expression pattern and

constructs availability, we selected one representative isoform for each family: γPCDH-A11 and γPCDH-C3 (**Figure 18b**). In addition, γPCDH-C3 has been previously linked to Axin1-dependent cell-adhesion (Steffen et al., 2023), cellular and synaptic connectivity organization in the neocortex (Lv et al., 2022) and seems to play a selective role in synapse formation between spinal cord and sensory neurons (Meltzer et al., 2023)**.**

After overexpression of one of these isoforms at DIV15, shortly after the multi-innervation peak, the number of CF-EPSCs was assessed at DIV18-DIV20, when CFs are in competition and most PCs are still multi-innervated (**Figure 8; Figure 13**).

Single γPCDH isoform overexpression during development accelerates CF elimination in PC

mCherry-tagged γPCDH-A11 and γPCDH-C3 were overexpressed into DIV15 explants PCs (close to multi-innervation peak, beginning of CF functional differentiation**; Figure 8, Figure 13**; Letellier et al. (2009)) through SCE, together with eGFP as a cytosolic marker. CF-EPSCs were evoked and recorded from electroporated PCs at DIV18-DIV20, corresponding to CF elimination phase (**Figure 8, Figure 13**; Letellier et al. (2009) (Figure 19a). CF-EPSCs were elicited and quantified as explained previously (Materials and Methods, Analysis techniques, page 83). While γC3-overexpressing PCs showed a similar number of CF-EPSC steps compared to the control condition (range: 2 to 4), a significantly lower number of CF-EPSC steps was found in γA11-overexpressing cells (1 to 2 CF-EPSCs) (**Figure 19b**). Noticeably, 44% of them showed a single CF-EPSC step.

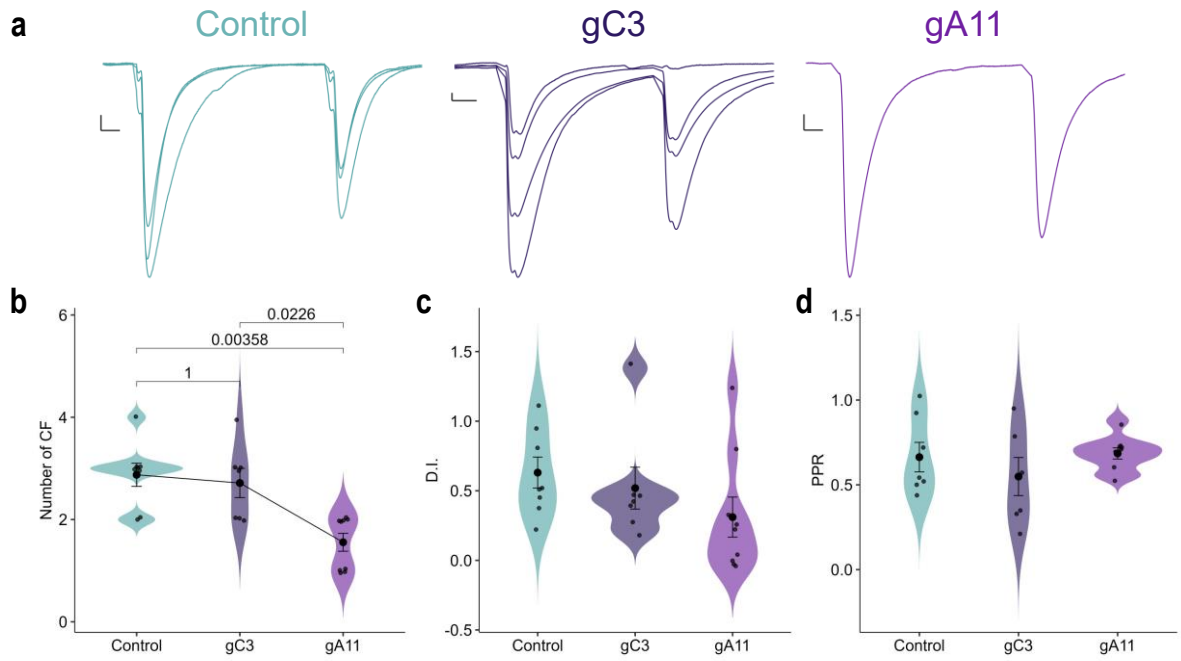

Figure 19: CF-EPSCs from control and single isoforms-overexpressing PCs. (a) Example traces of each condition. Scale bars correspond to 100 pA, 10 ms. Membrane potential was clamped at -30 mV for Control and gA11 conditions and -50 mV for gC3. Stimulation artifacts were removed for visualization purposes. (b) Estimated number of CF inputs per cell in each condition. Kruskal-Wallis test p value: 0.0021. Displayed p values correspond to Dunn's pairwise comparisons with Bonferroni adjustment. (c) D.I. of the recorded CF inputs per cell. D.I. = 0 corresponds to monoinnervated cells. Kruskal-Wallis test p value = 0.0551. (d) Average PPR per condition. Kruskal-Wallis test p value = 0.4461. (b, c, d) Error bars correspond to S.E.M.

These results suggest a causal link between γPCDH diversity and the number of CF inputs onto each PC. Furthermore, we found that two different γPCDH subfamilies, A and C, may display differential roles in PCs development, which was expected from the different expression patterns observed. Since no significant differences were observed in the functional differentiation of CF inputs, this may suggest that A-γPCDH are more likely involved in cell–cell recognition processes rather than directly contributing to the synaptic strengthening of the dominant CF.

Subcellular distribution of γPCDH-A11 protein in PCs

Taking advantage of the mCherry reporter fused to the electroporated γPCDH-A11 gene, confocal images were obtained to study the subcellular distribution of this protein across PC soma, proximal and distal dendrites at DIV18-DIV20. vGLUT2 was simultaneously immunolabelled as a CF release site marker to track CF territory. γPCDH-A11 proteins showed a clustered distribution, observing puncta both at the membrane and intracellularly (**Figure 20a**). A significant enrichment of γPCDH-A11 fluorescence in the cell body and primary dendrites was observed (**Figure 20b**). A similar trend was found in the distribution of vGLUT2 fluorescence (**Figure 20c**). The area occupied in each region by both signal clusters was quantified, observing a similar pattern. We found a higher percentage of soma and proximal dendrites area covered by γPCDH-A11 compared to distal dendrites (**Figure 20d**). Regarding vGLUT2 puncta, their area seems to represent a higher percentage in proximal dendrites than in the soma, although no statistically significant differences could be found compared to distal dendrites. At this age, it is known that PF co-express vGLUT1 and vGLUT2 (Figure 11; Miyazaki et al. (2003)), which could explain vGLUT2 expression in distal dendrites. At the same time, vGLUT2 area enrichment in proximal dendrites compared to the soma may confirm the dendritic translocation of CF.

These results show that γPCDH-A11 protein distribution shares same subcellular territory as CF synapses (soma and proximal dendrites). Although our data do not strongly support the localization of γPCDH-A11 at CF synapses, sharing the same dendritic region may support the possibility of γPCDH-A11 role in CF innervation.

Conclusions

Here we sought to test for a causal link between γPCDH expression and diversity and the CF selection process that occurs during the developmental critical period. We found that γPCDH-A11 but not γPCDH-C3 overexpression significantly accelerates the CF selection. Furthermore, our imaging data

indicates that, when overexpressed, this isoform gets enriched in proximal dendrites while not directly colocalizing with CF synapses. Overall, our results highlight a selective role of some specific γPCDH isoforms in the CF elimination process.

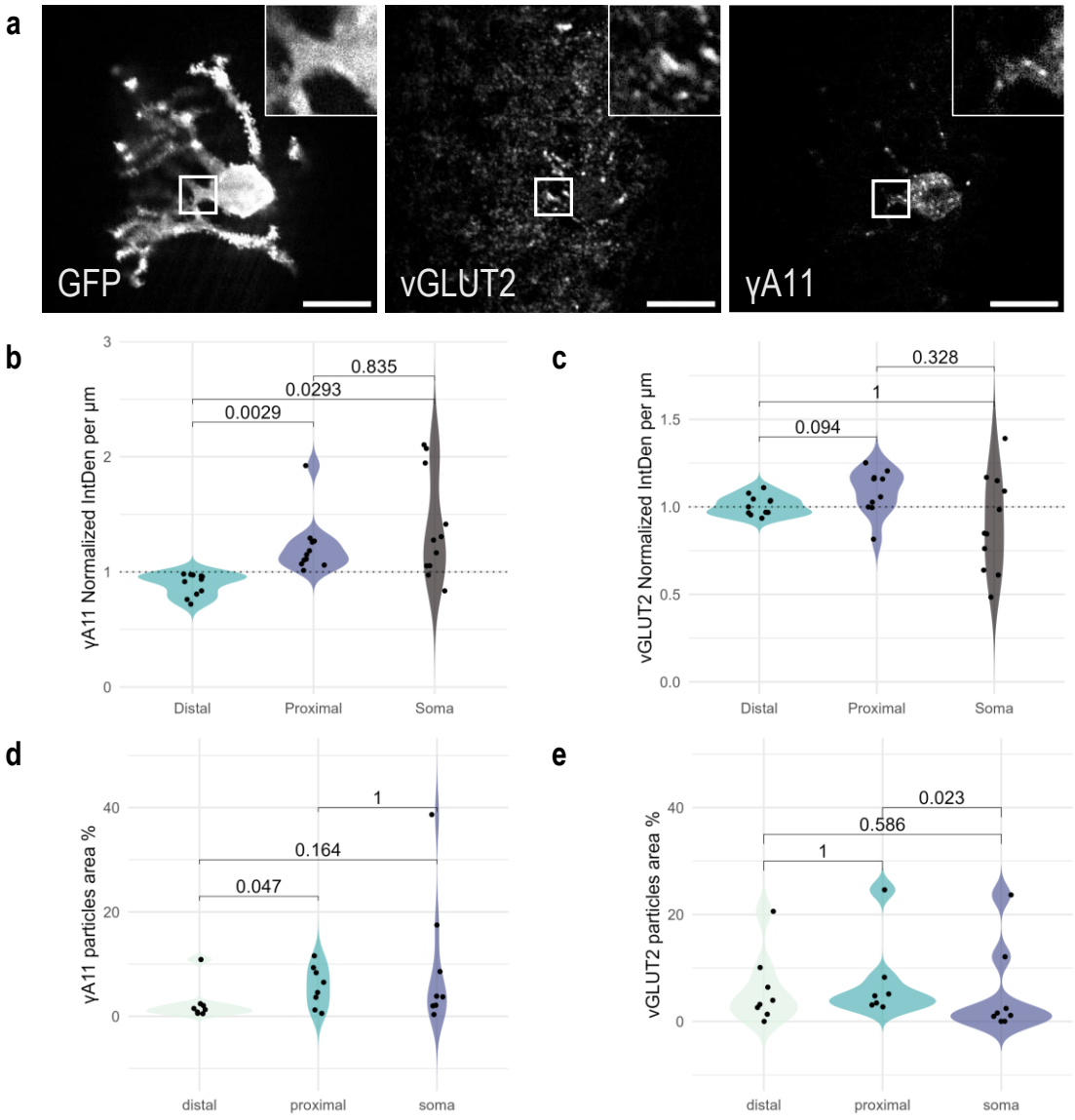

Figure 20: Subcellular localization of γPCDH-A11 and vGLUT2 in PCs. (a) Example images of one electroporated PC. One single plane is shown. From left to right: GFP, vGLUT2 and γPCDH-A11. Scale bars correspond to 20 µm. (b) γPCDH-A11 fluorescence per area, normalized to the whole cell signal (dashed line), in distal dendrites, proximal dendrites and soma. Repeated Measures ANOVA p value on not normalized data: 0.00981. (c) vGLUT2 fluorescence per area, normalized to the whole cell signal (dashed line), in distal dendrites, proximal dendrites and soma. Repeated Measures ANOVA p value on not

normalized data: 0.0901. (d) Percentage of compartment area occupied by γPCDH-A11 particles in whole cell, distal or proximal dendrites, and soma. Repeated Measures ANOVA p value: 0.21. (e) Percentage of compartment area occupied by vGLUT2 particles in whole cell, distal or proximal dendrites, and soma. Repeated Measures ANOVA p value: 0.259. (b, c, d, e) Displayed p values correspond to Paired-data Wilcoxon's pairwise comparisons with Bonferroni correction.

Results

Chapter V: Influence of presynaptic partner identity in γPCDH isoform selection by PCs

Context and aims

In the previous chapters, we reported that γPCDH isoform diversity in PCs is refined in correlation with the developmental CF selection process, that brainstem to PC innervation is required for the establishment of a mature γPCDH expression pattern and, importantly, that overexpressing a single γPCDH isoform in PCs to mimic low diversity accelerates the CF selection process. Furthermore, because of the lack of differences with the control in the functional differentiation of CF when imposing low γPCDH diversity, we hypothesized that γPCDH are more likely involved in cell-cell recognition, rather than synaptic strengthening. We observed that only 1-2 isoforms can be detected in PCs after the closure of the critical period, but what determines which γPCDH isoforms should be expressed in the mature stage? Is it purely stochastic? γPCDH mediate strictly homophilic *trans*-interactions, and they have been reported to promote adhesive contacts *in vitro* (Kanadome et al., 2021; Zhang et al., 2025). Previous studies in the neocortex reported that local connectivity between pyramidal neurons depends on γPCDHs expression pattern, with knock-out neurons or neurons expressing similar γPCDH isoforms displaying higher probability of interconnection (Kawamura et al., 2023; Lv et al., 2022; Tarusawa et al., 2016). However, γPCDH role is still under debate since experimental evidence has also pointed to dendritic repulsion following homophilic interactions *in vivo* (Lefebvre et al., 2012; Zhu et al., 2024). Therefore, considering that the pre- and postsynaptic partners may need a coordinated γPCDH code, and given the impact of single isoform overexpressing on CF elimination, we hypothesized that PCs connected by the same ION may share a similar γPCDH repertoire.

γPCDH signature of PCs innervated by the same CF

To test this idea, our objective was to compare the γPCDH isoforms expressed by individual PCs innervated by the same ION in the mature circuit (**Figure 21a**). Taking advantage of the hindbrain explant system, which allows simultaneous access to both pre- and postsynaptic partners, single GFP-positive

IONs from Igsf9-GFP explant were electroporated with tdTomato at DIV25. Through this very sparse labelling, we could distinguish individual ION axons and their respective target PCs (**Figure 21b**). After 3 days of expression, single axons were tracked from the brainstem to the cerebellum plate (DIV28-31) (**Figure 21c**). We refer to neighboring PCs sharing the same CF afferent as a "nest" (**Figure 21d**). PCs within the same nest were acquired for PatchSeq ("PC nest"). Neighboring PCs not contacted by the nest CF, but within 100 µm radius from it, were patched as controls.

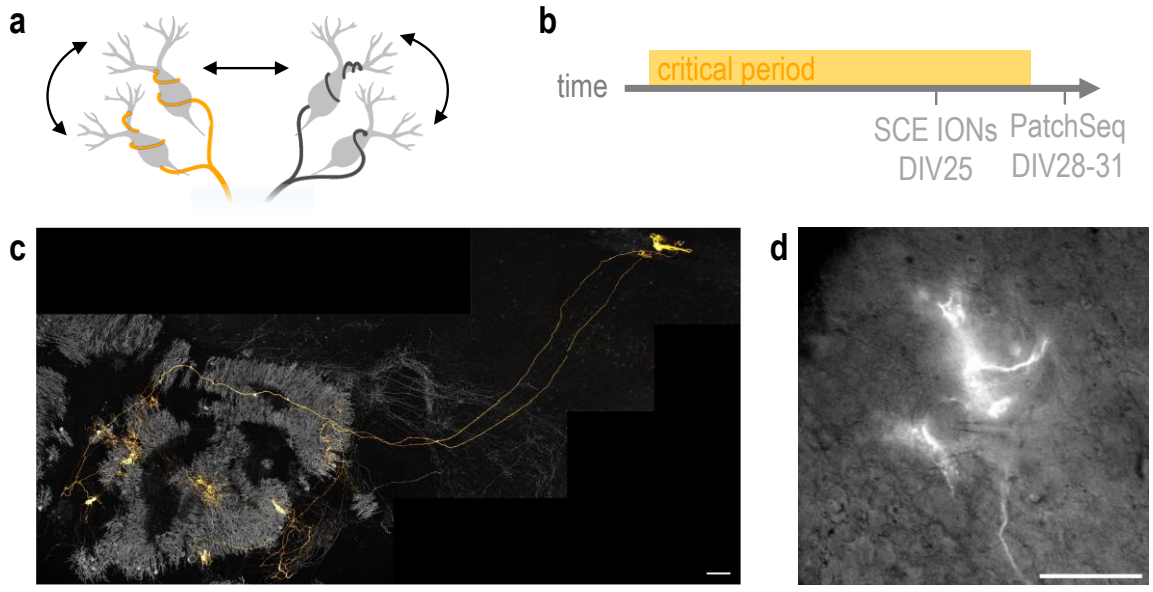

Figure 21: Experimental and analysis design of γPCDH repertoire in PCs depending on CF identity. (a) Experimental timeline. (b) Schematics of one tdTomato-labelled nest, a non-labelled nest and the comparisons to be performed. (c) Example image of tdTomato+ axon reconstruction. Orange: 2 electroporated IONs, CF and nests around PCs. Grey: Calb1 immunostaining. MIP from confocal stack. Scale bar corresponds to 100 µm. (d) Live epifluorescence and DIC image of patched PCs surrounded by a tdTomato+ CF (nest).

Quality controls based on the total counts, detected genes and expression of PC marker genes were conducted as in the previous chapters (Materials and Methods, Analysis techniques, page 85) and show no significant differences

among groups (Supplementary Figure 6a, b, c). Moreover, PC marker genes were found strongly expressed (Supplementary Figure 6d).

From the normalized expression of γPCDH genes, (Supplementary Figure 7a) a correlation matrix was computed using Kendall's correlation coefficient, representing the similarity of αPCDH, βPCDH and γPCDH isoforms between cells (**Figure 22a, b, c**). Then, comparisons of PCs within the same nest, and PCs in-nest *versus* PCs out-of-nest were extracted and compared. αPCDH isoforms showed overall high correlation values (within-nest: 0.667 ± 0.303; *verus*-control: 0.611 ± 0.581; median ± IQR) and no differences were detected between the compared groups (**Figure 22d**). Contrastingly, βPCDH isoforms display correlation values close to zero for both groups (within-nest: -0.05 ± 0.286; *verus*-control: -0.0716 ± 0.154), while maintaining no difference regarding nest-dependent groups (**Figure 22e**). Finally, γPCDH isoforms showed a shifted distribution towards higher correlation values for PCs within-nest comparisons (0.286 ± 0.377) compared to *versus*-control correlation coefficients (0.0363 ± 0.513) (**Figure 22f**).

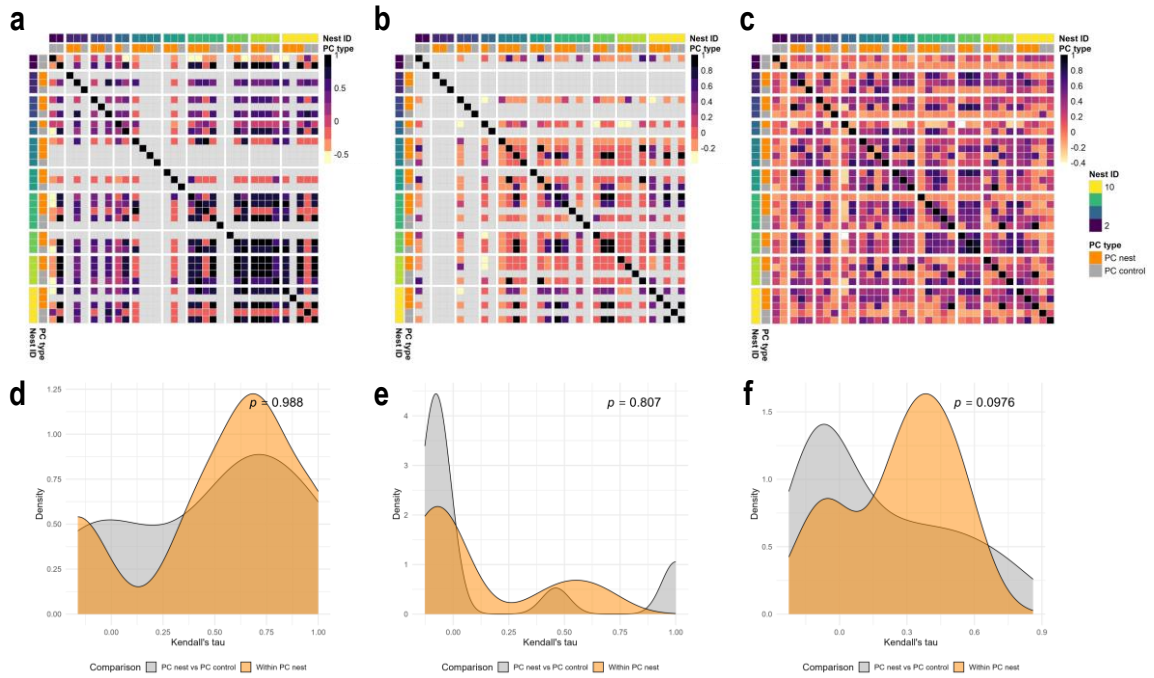

Figure 22: cPCDH isoforms expression comparisons in PCs attending to CF identity. (a, b, c) Correlation matrix of Kendall's tau coefficients calculated from

γPCDH (a), βPCDH (b) and γPCDH (c) clusters normalized expression. (d, e, f) Density distribution of correlation coefficients of PCs within the same nest (orange) and PCs from nest vs out of nest in the same animal for γPCDH (a), βPCDH (b) and γPCDH (c) isoforms. Displayed p value corresponds to Kolmogorov–Smirnov test.

Conclusions

The similarity of cPCDH repertoire was compared between PCs innervated by the same presynaptic ION, and those cells *versus* neighboring PCs connected to a different ION. αPCDH isoforms expression showed high correlation across nearby PCs, regardless of presynaptic partner identity, which could indicate that the α- isoforms expressed by a single PC depend on a different factor, such as the anatomical position within the explant or the animal's identity. βPCDH showed no difference and close to zero correlation values, suggesting that isoforms selection in this cluster is PC autonomous. Finally, we detected a higher similarity of γPCDH between PCs from the same nest, i.e., innervated by the same ION. This observation supports the existence of a molecular code in which matching pre- and postsynaptic γPCDH isoforms specify olivo-cerebellar connections.

Supplementary figures Results Chapter V

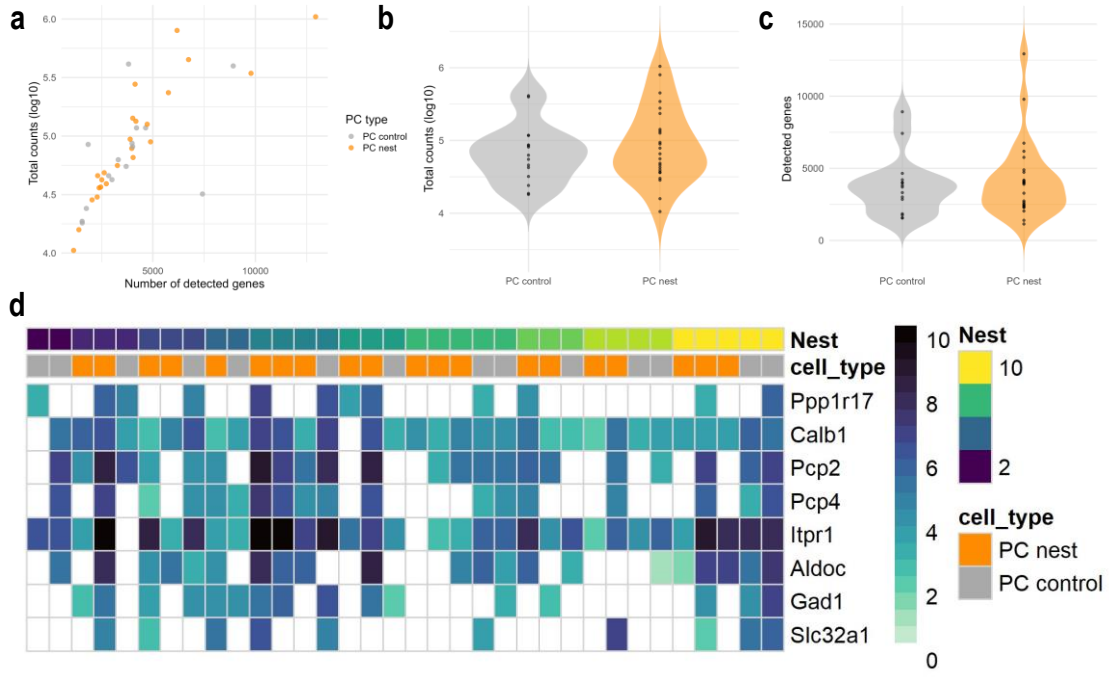

Supplementary Figure 6: PatchSeq quality controls (Chapter V). (a) Scatter plot showing the number of detected genes per sample in x and total counts, in logarithmic scale, in y. (b) Quantification of total counts per group (logarithmic scale). Mann Whitney's p value: 0.539. (c) Total detected genes per group. Mann Whitney's p value: 0.679. (d) Heatmap of PCs marker genes expression (normalized and scaled from 0 to 10).

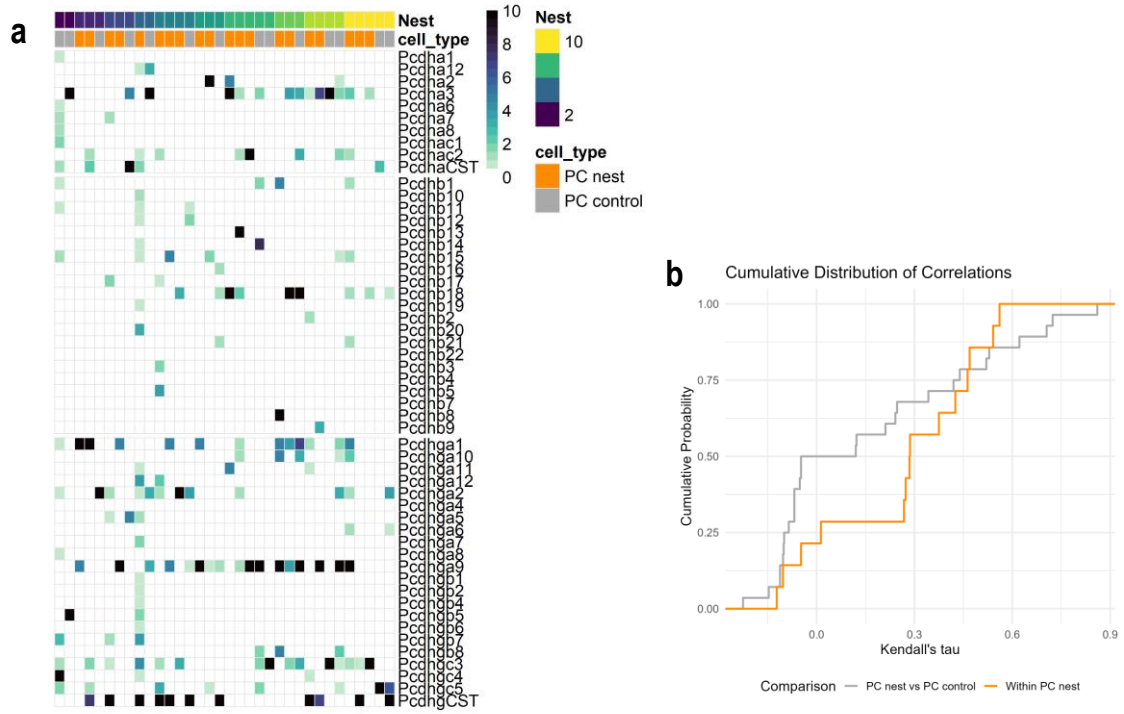

Supplementary Figure 7: Normalized cPCDH expression per CF nest and pairwise comparisons. (a) Heatmap of normalized cPCDH expression, scaled from 0 to 10. (b) Cumulative probability distribution of Kendall's tau correlation coefficient comparing PCs within the same nest (orange) and PCs from different nests in the same animal (grey). Kolmogorov–Smirnov test p value: 0.0976.

Discussion

Discussion

Recapitulation of results

How neurons recognize and select each other to form adaptative synaptic circuits has been a central question in Neuroscience for decades. Since the discovery of cPCDHs clustered genome organization and their combinatorial expression in neurons, they were proposed to be molecular barcodes for neurons and likely involved in brain connectivity (Sanes & Zipursky, 2020; Xiaozhong Wang et al., 2002; Wu & Maniatis, 1999; Yagi, 2012). However, it has only been during the last 10 years that the first experimental evidence was published pointing to cPCDH involvement in circuits wiring across diverse brain regions and cell types (Kawamura et al., 2023; Lefebvre et al., 2012; Lv et al., 2022; Meltzer et al., 2023; Mountoufaris et al., 2017; Zhu et al., 2024). In this work, we contribute to this growing body of literature by providing evidence for a possible function of γPCDH alternative isoforms in the specification of olivo-cerebellar circuitry during postnatal development.

To explore this question, we applied PatchSeq to quantify cPCDH expression and CF innervation in individual PCs during the developmental critical period for CF elimination (P3-P23). We observed a decrease in the diversity of γPCDH isoforms correlated with CF elimination and CF functional differentiation (Results Chapter I, page 93). Aiming for a more accessible model, we optimized and validated hindbrain explants for the study of CF-PC development (Results Chapter II, page 109). To test the involvement of CF innervation in PCs' γPCDH expression, we dissected out the brainstem from DIV0 explants and performed PatchSeq on PCs at DIV13 and DIV30, corresponding to the multi-innervation peak and the mature stage, respectively. Importantly, we found that preventing brainstem innervation blocked the developmental decrease of γPCDH diversity in PCs. They retained an immature γPCDH expression pattern, suggesting a direct involvement of brainstem afferents, possibly from olivary neurons, in PCs' γPCDH regulation during development (Results Chapter III, page 117). Next, in order to test for a causal link between cPCDH diversity and CF-PC circuit development,

we overexpressed single isoforms of γPCDH (A11 and C3) in DIV15 PCs. These two isoforms were chosen because γPCDH-A11 shows a scattered expression across mature PCs, while γPCDH-C3 is ubiquitously and constitutively expressed. The developmental stage of the circuit was then estimated at DIV18-20, corresponding to the CF elimination phase. While most PCs were multi-innervated in the control and γPCDH-C3 overexpression conditions, PCs overexpressing γPCDH-A11 had significantly less CF afferents. Nonetheless, no differences were found regarding the parameters related to CF functional differentiation (D.I. of amplitudes and PPR), which indicates a role of γPCDH in CF-PC recognition, but probably not in CF synaptic strengthening (Results Chapter IV, page 131). Finally, we assessed the presynaptic partner influence on cPCDH isoform selection in mature PCs. Thanks to a sparse labeling of IONs, single olivary axons were visually tracked from the brainstem to the cerebellum plates in DIV28-31 explants in order to identify corresponding PC targets. PatchSeq was performed on PCs innervated by the same CF afferent as well as on some nearby PCs, presumably innervated by different, unlabeled, axons. We found that γPCDH repertoire was more likely to be similar between PCs innervated by the same CF as compared to PCs innervated by different axons. It may suggest that γPCDH isoform selection in PCs is not stochastic and rather depends on the identity of the selected partner (Results chapter V, page 139).

Our results provide experimental evidence for an adhesive code, where γPCDHs mediate cerebellar connectivity by acting as molecular encoders of CF-PC synapse specificity, and that the identity of synaptic partners may influence γPCDH expression. These findings significantly advance our understanding of the molecular mechanisms underlying precise neuronal wiring and may extend to other brain regions.

Bridging connectivity refinement to single cell molecular identity with PatchSeq

The high number of isoforms of cPCDH in the mouse genome, together with a high sequence similarity across isoforms and the lack of commercial antibodies, has promoted the use of mRNA detection techniques in the field. However, single-cell RT-qPCR (sc-qPCR), RNA *in situ* hybridization (ISH) and the variety of sc-RNAseq approaches used may differ in their sensibility to detect cPCDHs, as well as the data processing employed. Early sc-qPCR experiments showed that PCs express 1-2 αPCDH isoforms (Esumi et al., 2005), 2-3 βPCDH isoforms (Hirano et al., 2012), 1-2 γPCDH-A and 1-2 γPCDH-B variants in mature (>P21) PCs (Kaneko et al., 2006), demonstrating cPCDH combinatorial expression in PCs. Frank et al. (2005) analyzed whole brain homogenates to study single isoforms expression in PCs. In line with our observations, they showed that γPCDH transcripts, but also proteins, are expressed prenatally, reach peak expression between P6 and P12, and are subsequently downregulated in the mature system. Interestingly, using RNA-ISH, they also showed that γPCDH were detected with a similar scattered pattern in the hippocampus and olfactory bulb granule cells, as well as mid- and hindbrain regions. Frank et al. accurately suggested, anticipating the upcoming research of following years, that γPCDH may play an important role in single-cell identity and synapse specificity in the cerebellum and other brain areas.

The previously mentioned qPCR and ISH-based studies could only test a few isoforms per cPCDH cluster in a reduced number of cells. Then, average diversity was extrapolated attending to the total number of isoforms in each cluster and the detected variants, assuming equal probability of expression for all variable isoforms except for α- and γ C-types. While high throughput sc-RNAseq techniques later facilitated cPCDH research by enabling simultaneous detection of all cPCDH transcripts, these approaches come with intrinsic biases and limitations (Jiang et al., 2022). Importantly, the scattered expression of cPCDHs across cells, combined with low transcript abundance per isoform, reduces their

probability of detection. In turn, it increases the frequency of dropouts – when transcripts are not detected despite being expressed. In this context, interpretation of zero-inflation when analyzing cPCDHs with sc-RNAseq should be carefully considered. Indeed, because scattered expression of isoforms is expected, some "correcting" approaches that reduce the frequency of zeros may increase homogeneity across cells, strongly conditioning the diversity of the isoforms measured for a given cell.

Such a correcting approach was used by Lv et al. (2022), who performed PatchSeq with SmartSeq2 full length sequencing, similarly to our approach, to study cPCDH expression in clonally related neurons of the neocortex. To improve cPCDH detection, the authors applied corrections on multimapping reads alignment; this is, sequenced fragments of RNA matching several exons in the genome. First, the three pseudogenes contained in the cPCDH locus (Gm37013, Gm38666 and Gm38667) were removed from the reference mapping genome. Generally, multimapping reads are excluded from the analysis because of the uncertainty about the genes they correspond to. In the case of cPCDH, multimapping reads can be notably found on the constant exons that are shared between isoforms of the α- and γ clusters. In their study, Lv et al. divided the assigned counts to a given cPCDH read by the number of different isoforms it mapped to. Although combinatorial expression can still be detected in their dataset, they reported an average of 9 different γPCDH isoforms per neuron, which is much higher than the values we found in PCs using PatchSeq or that were previously estimated in PCs using sc-qPCR and RNA-ISH (see above). When we applied their mapping strategy to our PatchSeq dataset from PCs, we could observe not only a higher number of isoforms detected, but a significant background noise that homogenized cPCDH repertoires. For many cells, both in their data as well as ours when processed with their parameters, almost every isoform per cluster was detected. For this reason, despite our mean detection being slightly lower than in the reference studies using RT-qPCR in PCs, we chose to minimally adjust the default mapping parameters while keeping high stringency for multimapping reads (Materials and Methods, Analysis techniques, page 85).

Zero inflation in our dataset, more pronounced than in Lv et al. (2022), was interpreted in our analysis as reflecting low probability of cPCDH transcripts detection, rather than true absence or missing data (Jiang et al., 2022; Qiu, 2020).

Later, Zhu et al. (2024) proposed optimized experimental and analysis procedures for the detection of γPCDH in neocortical neurons. They performed 5' end sequencing on FACS sorted neocortical neurons focusing on exon 1, the most variable across isoforms. Furthermore, an additional sequencing library was prepared from each sample using a γPCDH nested-PCR primer mix to enrich γPCDH content. They detected 2-3 isoforms per cluster in most cells, significantly less than in Lv et al., and scattered expression could be observed. Thanks to the targeted library preparation and increased sample size, their dropout effect was less limiting, and mapping was kept in default parameters, reducing possible artifacts introduced during data processing while maintaining a robust detection. It is important to notice, though, that the differences between Lv et al. and Zhu et al. datasets compared to our own could be due to the differences in brain regions and cell types (pyramidal neocortical neurons *versus* cerebellar PCs). Regardless, enriched γPCDH libraries combined with 5' end sequencing appear to be the optimal approach for cPCDH studies, selectively targeting transcripts of interest since library synthesis while enabling the simultaneous, reliable detection of all isoforms at the single-cell level.

Importantly, FACS sorting allows a dramatic increase in sample size compared to PatchSeq (thousands *versus* hundreds of cells, respectively). For this reason, data preprocessing in Zhu et al. analysis could be more restrictive and hence led to a higher average detection per cell compared to our PatchSeq study in PCs. Compared to our study, Lv et al. showed, as previously mentioned, a higher number of isoforms per cell, but it could be partly due to the background after multimapping correction. Because of their vast dendritic arborization, PCs do not resist FACS sorting and hence this technique was not possible for our study. Sorting PCs is also specially challenging due to the massive amount of granule cells in the cerebellar cortex (Kozareva et al., 2021). Furthermore, we exploited PatchSeq to its maximum possibilities. Beyond single-cell cytosolic

mRNA collection, we achieved long electrophysiology recordings (~30 minutes per cell), allowing to fully characterize CF connectivity on individual PCs. This way, sequenced PCs were annotated and classified based on the CF selection stage (early competition, late competition or mono-innervation), bypassing the high intercellular heterogeneity of PCs during postnatal development. Using this strategy, we could stablish a correlation between CF innervation development and the expression of alternate γPCDH isoforms. Consistent relative differences were observed between samples, and isoform-specific regulation — such as that of C-type γPCDHs – is present in our dataset. Therefore, while sequencing libraries preparation could be improved for better γPCDH quantification, our results bring the added value of a full electrophysiological characterization directly correlated with gene expression.

C-type *versus* alternate γPCDHs: divergent regulation and function during development

Identity encoding by cPCDHs relies on the available diversity of isoforms encoded in the genome, but, most importantly, in the regulatory mechanisms shaping their expression. Interestingly, both sc-qPCR approaches and sc-RNAseq found that C-type variable exons in α- and γ clusters are ubiquitously expressed in several neuron types (Frank et al., 2005; Kaneko et al., 2006; Lv et al., 2022; Meltzer et al., 2023; Mountoufaris et al., 2017; Zhu et al., 2024). Furthermore, certain cell types such as serotonergic neurons only express αPCDH-C2 (Chen et al., 2017). This suggests a differential regulation of these variants and likely a differential role of C-type isoforms in neuronal function. Similarly, C-type γPCDH isoforms were detected in a larger percentage of PCs in our PatchSeq datasets from both acute slices and hindbrain explants. Previous study from Toyoda et al. (2014) showed that cPCDH variable exons promoters are differentially methylated in PCs, preventing the expression of certain isoforms and hence generating combinatorial expression. Furthermore, they found that the percentage of methylated promoters tends to increase from early embryogenesis

until P21 in PCs. While they did not monitor methylation in the early postnatal period, this epigenetic mechanism may contribute to the decrease in γPCDH diversity that we observed throughout the CF selection process using PatchSeq. In addition, consistently with the different expression pattern observed for C-type isoforms, their promoters have been reported to be constitutively hypomethylated (Toyoda et al., 2014). While alternate exons (non-C-type) rely on CTCF and cohesin binding to activate their expression, C-type exons lack the conserved sequence element (CSE) to bind these proteins (Wu et al., 2001), which could explain the different pattern of expression observed for these isoforms.

Since the transcriptomic machinery regulating C-type isoforms is different, could they also be the subject of different post-transcriptional regulation? Our overexpression experiments showed that γPCDH-A11 is enriched in the soma and proximal dendrites of developing PCs (Results chaper IV, page 136). However, preliminary experiments suggest that γPCDH-C3 display a more homogeneous distribution in all cell compartments. Altogether, these contrasting expression patterns between alternate and C-type cPCDHs suggest different functional roles. In line with these results, while γPCDH-A11 overexpression significantly accelerated CF selection, γPCDH-C3 did not show differences with the control condition (Results chaper IV, page 134). Intriguingly, contradictory results have been found in the neocortex. On the one hand, Lv et al. reported that γPCDH-C3 overexpression led to reduced connectivity between sister cells. Conversely, Zhu et al. showed that reduced connectivity was only achieved by overexpression of variable isoforms, but not γPCDH-C4. These differences could be partly explained by the mechanism through which cPCDH proteins are delivered to the membrane via the secretory pathway. In fact, it has been shown that γC4 can only reach the membrane upon heterodimer formation with a different γ or β isoform (Fernández-Monreal et al., 2009; Fernández-Monreal et al., 2010). This could mean that the effect of γC4 depends on the availability of other cPCDH isoforms acting as a carrier, which is likely disrupted in overexpression experiments.

The lack of commercial antibodies impedes the direct detection of endogenously expressed cPCDH proteins and the study of their distribution. Our experiments, as well as those by Lv et al. and Zhu et al., do not assess the membrane localization of the proteins, nor the *trans* interaction with connected partners directly. Considering the possible disruption of γC4 membrane localization during overexpression, and the lack of effect on connectivity using this approach, the involvement of γPCDHs in connectivity might indeed depend on their membrane localization. Nevertheless, the specific mechanism remains unknown: whether cPCDH-mediated effects result from transmembrane homophilic binding or *cis* interactions with other proteins.

It is therefore essential to test the membrane localization of the overexpressed and endogenous proteins. This will also help confirm whether overexpression leads to reduced diversity of endogenous isoforms. While one antibody labeling the constant γPCDH domain (Rabbit anti-PCDH gamma, Synaptic Systems) has been validated for western blot, it does not work with classic immunohistochemistry protocols. We envision testing alternative approaches, such as glyoxal fixation, which improves antigen accessibility, and expansion microscopy. In expansion microscopy, epitopes can be labeled after protein denaturation, and the technique offers enhanced resolution through isotropic expansion of samples embedded and crosslinked within a hydrogel matrix. Taking advantage of this technique, the overexpressed mCherry-tagged isoform and all other endogenous γPCDHs could be simultaneously visualized. Analyzing the surface expression of both protein clusters would help us unravel the subcellular localization of different γPCDH variants. By co-labelling γPCDHs and CF release sites with anti-vGLUT2, this approach would also help clarifying the putative association of γPCDHs with synapses in PCs, as well as the localization of γPCDH in CF terminals.

The differential subcellular localization of A-type and C-type isoforms observed in our experiments correlate with their differential effects in CF selection. Differential synaptic functions were also found in previous studies (Frank et al., 2005; Toyoda et al., 2014; Zhu et al., 2024). Interestingly, C-type

isoforms positively regulate developmental synapse formation in the spinal cord (Weiner et al., 2005). Loss-of-function approaches (conditional KO of γPCDH-C isoforms) showed that γPCDH-C3 can autonomously promote synapse formation between sensory neurons and spinal cord neurons. Furthermore, γPCDH-C3 expression in HEK293 cells was sufficient to induce PSD95 clustering and postsynaptic specialization (Meltzer et al., 2023). Altogether, evidence points to the involvement of alternate γPCDH isoforms in synaptic partner selection, while C-type variants may mediate synaptogenesis in an unspecific manner.

Translating γPCDH homophilic interaction into CF selection

Adhesive *versus* repulsive signals

The synaptic localization of both C-type and alternate γPCDHs has been tested in synaptosomes, cell cultures and tissue (Frank et al., 2005; Phillips et al., 2001; X. Wang et al., 2002). Yet, FRET imaging (fluorescence resonance energy transfer) assays have shown that γPCDH-B proteins in synapses do not perform homophilic transmembrane interactions (Hoshino et al., 2023; Kanadome et al., 2021). It is important to notice, though, that γPCDH homophilic interactions were tested *in vitro* (Brasch et al., 2019; Hoshino et al., 2023; Rubinstein et al., 2015; Schreiner & Weiner, 2010), leading to K562 cells adhesion. Currently, most of the *in vivo* experimental evidence indirectly point to a repulsive effect of γPCDHs in neurons (Lefebvre et al., 2012; Lefebvre et al., 2008; Mountoufaris et al., 2017; Steffen et al., 2023; Toyoda et al., 2014; Zhu et al., 2024). In line with this, low γPCDHs diversity may reduce connectivity through increasing the probability of homophilic interaction while high diversity or conditional γPCDH KO seem to enhance connectivity by lowering the probability of interaction. In addition, γPCDH cKO and high diversity lead to aberrant dendritic morphology in PCs, showing increased self-crossing branches (Lefebvre et al., 2012; Toyoda et al., 2014). However, these experiments do not discard the fact that cPCDHs could have different effects depending on the subcellular expression and the molecular context. For instance, homophilic interaction could lead to a repulsive effect in

the dendritic tree as a mechanism for self-avoidance, while peri-synaptic interactions could promote adhesion.

Downstream signaling associated with γPCDHs' role in CF selection

PCs branch retraction during dendritic arborization has been proposed to be mediated by protein kinase C (PKC) (Fujishima et al., 2012). In PCs, PKC is regulated during development and its activity has also been linked to CF elimination. Remarkably, PKC mutations lead to spino-cerebellar ataxia subtype 14 (SCA14), causing dendritic development impairments, persistent CF multi-innervation and neurodegeneration of PCs (Chen et al., 1995). In addition, PKC is also implicated in γPCDH signaling pathways (Garrett et al., 2012; Keeler et al., 2015), which highlights the possible dual roles of certain molecular actors downstream cPCDHs.

Upon interaction, the CAM/protease ADAM10 first, and γ-secretase later, cleave γPCDH, releasing a soluble extracellular segment and an intracellular C-terminal peptide (Ct-γPCDH) (Haas et al., 2005). Interestingly, ADAM10 protease activity can be triggered by AMPA receptors activation (Reiss et al., 2006), which could be one of the steps linking synaptic activity and cell-cell recognition. In addition, the secreted ligand of ADAM receptors, LGI2, has been recently observed to be regulated in IONs during PC developmental critical period (Paul et al., 2024). LGI2-ADAM interaction can, in turn, promote AMPA receptors recruitment to synapses (Fukata et al., 2021), which could potentially play a role in the strengthening of the winning CF.

The cleaved intracellular Ct-γPCDH fragment can then either promote cytoplasmic signaling or be transported to the nucleus. In the cytoplasm, Ct-γPCDH interact with FAK/Pyk2 pathway to regulate cytoskeleton remodeling (Garrett et al., 2012; Keeler et al., 2015). This pathway has been proposed to mediate dendritic stabilization and self-avoidance (Fan et al., 2018). In the nucleus, Ct-γPCDH can interact with γPCDH promoters, inducing its own

expression in a positive, CSE-independent feedback loop (Hambsch et al., 2005). Other studies performed on vascular endothelial cells described that γPCDH nuclear signaling can suppress Notch1-mediated transcription (Joshi et al., 2024). Little research has been conducted on γPCDH-mediated gene expression in the nervous system. Whether Ct-γPCDH may be able to interact with other target genes in neurons remains unexplored. *In silico* transcription factor-promoter interaction tools would help pointing at promising candidate loci. Experimentally, Ct-γPCDH peptide could be expressed in primary neuronal cultures followed by RNAseq to test upregulated transcripts and ChIP-seq to map genomic binding sites.

Whether these signaling cascades are exclusive, simultaneous or coordinated upon γPCDH transmembrane interaction remains unknown. Given the different effects of C-type *versus* variable isoforms in neurons, and the apparent differences in subcellular distribution, one could hypothesize that the same homophilic interaction may have the ability to produce different downstream effects. This concept was described as “functional selectivity” (Kenakin, 2005), referring to the possibility that ligand-receptor interactions could produce preferential or biased targeting of downstream signaling elements depending on the molecular environment. For example, synaptic γPCDH, putatively involved in synaptic partner recognition, could be inducing nuclear signaling, while γPCDHs mediating dendritic self-avoidance could preferentially activate cytoskeleton remodeling pathways. Further research is needed to unravel downstream effects of γPCDHs and its relationship with their proposed functions.

Possible contribution of γPCDH interaction with synaptogenic molecules

On the other hand, γPCDH are able to modulate neuroligins (Nlgn). These are well-known postsynaptic CAMs that bind presynaptic neurexins (Nrxn) and display synaptogenic effects. Pathway analysis of our acute slices PatchSeq data revealed that Nlgn1 expression is upregulated during CF selection (Results

Chapter I, **Figure 9**, Table 9). Nlgn1-Nrxn interaction is known to promote spine formation, as well as presynaptic specialization (Scheiffele et al., 2000). Molumby et al. (2017) showed that various γPCDH isoforms can physically bind Nlgn1 in the cell surface *in vitro* and inhibit Nlgn-induced presynaptic differentiation. Hence, one could think that "unmatched" γPCDH dimers in the membrane could prevent synapse formation through Nlgn inhibition, and that γPCDH homophilic interaction would release Nlgn in the postsynapse. This would be in line with recent FRET imaging experiments showing that γPCDH localized at synapses are less likely to interact in *trans* (Hoshino et al., 2023). However, when Molumby et al. co-expressed γPCDH in their artificial synapse assay (transfection of Nlgn1 and Nrxn1β in COS cells), Nlgn1 synaptogenic effect was inhibited regardless of γPCDH homophilic interaction. Interestingly, co-expression of both CAMs induced clustering of γPCDH at contact sites (Molumby et al., 2017). Nevertheless, it is important to notice that COS cells lack the complex molecular environment in neurons, and that a single isoform expression does not mimic the combinatorial pattern found in the brain.

How γPCDH isoform diversity would affect Nlgn1 function remains unknown. Hypothetically, γPCDH *trans* homophilic binding could shift interactions stoichiometry, allowing Nlgn to bind Nrxn and induce synapse strengthening. This mechanism could simultaneously explain synaptic partner recognition and CF strengthening. However, it would imply not only that γPCDH may have selective intracellular signaling, but that they can mediate either membranes repulsion or adhesion depending on the molecular surroundings. Such a complex molecular mechanism requires intensive research to be fully understood in more physiological conditions.

Stochastic *versus* deterministic expression of cPCDH isoforms in Purkinje cells

Early after the discovery of cPCDH gene cluster, the combinatorial expression of these genes was described in PCs. Since no pattern was detected that could explain the selection of γPCDH repertoire in PCs, it was described as stochastic promoter selection (Frank et al., 2005; Tasic et al., 2002; Toyoda et al., 2014). In addition, cPCDH are expressed in the membrane as heterodimers, while mediating strict homophilic interaction in *trans*. For all these reasons, they were proposed to be "cellular barcodes" to mediate single-cell identity in the brain. However, if cPCDHs encode connectivity, specific isoforms expression should be somehow regulated to ensure synaptic connection with the most appropriate partner. Since experimental evidence points towards a repulsive effect of cPCDHs interactions in PCs, isoform diversity may hypothetically prevent certain connections and, simultaneously, allow selected synapses formation. It could also be possible that cPCDH-mediated dendrites repulsion is a mechanism to limit the initial pool of available synaptic partners in an unbiased or stochastic manner. Finally, one could also speculate that the same cPCDH interaction would translate into adhesive or repulsive signals depending on the cellular context, such as the level of activity or the dendrite identity.

More recently, it has been shown that neocortical neurons derived from the same progenitor express a similar repertoire of cPCDHs (Lv et al., 2022), indicating a non-random pattern of cPCDH expression. These authors propose cPCDH expression as a mirror of the "developmental history" of the cells. Their data suggests that there is a cPCDH-mediated preferential connectivity between clonally related cells. Surprisingly, by electroporation of random sets of cPCDH isoforms, Zhu et al. (2024) later showed that cPCDH similarity is inversely correlated with the connectivity rate between neocortical neurons. The source of the disparity between these results is under debate. In any case, both show indirect measurements relating synaptic connectivity and cPCDH diversity, something for which experimental evidence was missing.

Cortical excitatory neurons receive afferents promiscuously, making it difficult to identify presynaptic partners. Meanwhile, PCs retain a single CF afferent in the mature system, which facilitates the study of cell-cell recognition mechanisms (Hashimoto & Kano, 2003). On their side, CFs branch in the cerebellum plate, innervating a discrete number of PCs (Sugihara et al., 2001). Hindbrain explants allow long-term culture while maintaining intact CF to PCs connectivity (Letellier et al., 2009), and our results showed that developmental dynamics of CF and other PC afferents are maintained in this system (Results Chapter II, page 109). Explants are a unique experimental model in which simultaneous access to identified pre- and postsynaptic partners is possible. This is not achievable in any other culture with the same level of physiological and histological similarity to the *in vivo* situation. Taking advantage of this system, we detected a higher pairwise similarity of γPCDH isoforms (but not α- or β-) between PCs innervated by branches of the same CF. Although the statistical difference does not reach the standard 5% α-error to be considered significant, a clear trend in the density distribution of pairwise comparisons can be observed (Results Chapter V, Figure 22). Because of the high variability of the data, we calculated that over 400 neurons would be needed to get a statistical difference with a 5% α-error and 80% statistical power.

The fact that γPCDH isoform selection seems to depend on CF identity points to important considerations regarding γPCDH regulation and function in PCs: γPCDHs do not serve only as self-avoidance molecules, but are likely to be also involved in synaptic partner recognition and are regulated accordingly. There must be a transcellular mechanism mediating the silencing of certain γPCDH isoforms while CF selection occurs. Crucially, the developmental pattern of γPCDH expression in IONs remains unknown. Hypothetically, IONs could either undergo a developmental regulation similar to PCs or express a predefined, reduced set of γPCDH isoforms. In the first scenario, both synaptic elements should coordinate and coregulate their γPCDH expression. It is known that this process is mediated by promoter methylation in PCs (Toyoda et al., 2014). In addition, methyltransferase activity is known to be regulated by neuronal activity

(Feng et al., 2010; Kong et al., 2020). However, CF terminals seem too distanced from the ION cell body; the required signaling for this regulation might not be efficient enough to dynamically match the changes in the target PC. Therefore, one could expect local regulatory mechanisms to take place. Intracellular pools of cPCDHs could hypothetically be used for a fast isoform replacement in the synapse (Fernández-Monreal et al., 2009; Fernández-Monreal et al., 2010).

In the second scenario, where IONs could express a pre-narrowed γPCDH subset, and assuming that the observed effects on CF selection depend on homophilic γPCDH binding, PCs would have to adapt their repertoire to the γPCDH pattern imposed by the winning CF. In this case, the continuous expression of the interacting isoform could be promoted by the positive feedback loop mediated by γPCDH intracellular domain in the nucleus (Hambsch et al., 2005), while "unmatched" isoforms promoters would be methylated by Dnmt3b (Toyoda et al., 2014).

To address this question, we are currently building a new dataset of PatchSeq from IONs during development. Although Allen Brain Atlas shows combinatorial expression of γPCDH variable isoforms in IONs, whether they undergo isoform diversity changes during development is unknown. Understanding the developmental expression pattern of γPCDH in IONs will bring valuable hints to elucidate a possible mechanism for both the influence of γPCDH in CF selection and the mechanisms regulating γPCDH diversity in both cell types. Furthermore, employing the same sparse labeling of CF explained in Results Chapter V, we could perform paired PatchSeq of a given ION and its targets in the mature system. This exceptional experiment would determine whether each PC and its winning CF express the same set of γPCDH, which would indicate an adhesive interaction, or the complete opposite.

Working model: how γPCDH alternative isoforms diversity regulates CF selection

Our results, together with the known functions of γPCDH, clearly points to a role of γPCDH regulating CF selection and a CF-dependent regulation of γPCDH expression in PCs. Although relevant questions remain to be addressed (recapitulated in the next section), we propose here a plausible mechanism supporting our data.

Currently, attending to the available literature described above, our data indirectly suggests that IONs may express low γPCDH diversity from the beginning of the critical period, and that γPCDH may be promoting adhesive interactions between CFs and PCs. In this hypothetic case, PCs would reduce their γPCDH diversity to match the repertoire expressed by the most active CF. CF inputs at PC soma would activate AMPA receptors, which in turn would activate ADAM10 protease. Then, the interacting γPCDH intracellular domain would be cleaved. In the cytoplasm, Ct-γPCDH would inhibit FAK/Pyk2 locally, promoting dendrite stabilization. In the nucleus, Ct-γPCDH will upregulate the expression of the unmethylated isoforms in a positive feedback loop. Dnmt3b would progressively methylate "unused" or "unmatched" γPCDH promoters. "Matched" isoforms could be protected from methylation thanks to Ct-γPCDH-dependent expression.

This way, CFs that no longer find a γPCDH match lose synaptic territory and are progressively eliminated. All our experimental data fit in this model. Dnmt3b methylation and "protection" of certain γPCDH isoforms may depend on CF activity, which would explain why high isoform diversity was observed in "naïve" explants. CF predetermined γPCDH identity biases isoform selection in PCs, which would explain the similarity of γPCDH isoforms in PCs that selected the same CF. Finally, when a single γPCDH isoform is expressed in PCs during the critical period, CF elimination is accelerated maybe because CF pruning requires no further "winner-imposed" editing of the PC barcode. The repertoire is already collapsed to a single, readily matchable identity code. All incoming CFs

that do not display that isoforms combination immediately encounter a strong γPCDH mismatch signal, activate Ct-γPCDH-mediated FAK/Pyk2 repulsion and retract, whereas the rare CF branch that does share the same isoform is stabilized without having to wait for Dnmt3b-driven silencing of alternative promoters. The competitive phase would therefore be bypassed and pruning would be completed earlier, as we observed with premature expression of γPCDH-A11, but not the ubiquitously expressed and tolerated C3 isoform. On the other hand, when PC's γPCDH isoforms interact with those in CF afferents, they might release Nlgn, allowing it to interact with Nrxn presynaptically and thus inducing synapse strengthening. A reduced inhibition of Nlgn in *cis* could therefore contribute to the stabilization and strengthening of the selected CF afferent.

On the other hand, γPCDH-KO phenotype in PCs strongly suggest repulsive, dendrite-avoidance processes. γPCDHs homophilic binding acts as a recognition code on its own. The downstream effect depends, then, on the intracellular context. In the assumption that IONs express a stochastic subset of γPCDH from early competition, we could explain the avoidance effect in KO models as follows. When an exact isoform match occurs at a developing synapse, FAK/Pyk2 inhibition locally immobilizes the contacted dendrite; therefore, the "net" effect of the interaction is adhesive or stabilizing in this context. Conversely, when only a partial or zero match happens, as in the case of γPCDH-KO, the cleavage cascade is inefficient. Therefore, FAK/Pyk2 would remain active a filopodium can retract. This could be interpreted, thus, as a repulsive signal.

Since γPCDH sequencing data from IONs during development is currently missing, we could also argue that IONs could express a broad diversity of γPCDH isoforms at early development, as it is the case for PCs and neocortical neurons. This possibility would imply the existence of a choreographed, activity-dependent γPCDH regulation in both synaptic partners at the same time. If local mechanisms in CF terminals would allow fast regulation of γPCDH, the initial bidirectional high diversity would allow multiple CF to connect weakly to the PC; all CFs would receive an equilibrated adhesion/repulsion signal. Then, the most active contact would locally induce higher AMPA receptor signaling in the PC, increasing

ADAM10 signaling and activating nuclear signaling. On its side, the presynaptic Ca^{2+} entry generating CF bursts could trigger ADAM10 at the CF bouton. However, as discussed above, this option seems complicated for IONs, whose axon terminals are far from the nucleus.

Overview of unresolved questions and proposed approaches

This project brings valuable new evidence to the intriguing functions of cPCDHs in brain wiring and the locus regulation during postnatal development, indirectly pointing at a possible mechanism underlying these functions. Yet, important questions need to be addressed:

(Q1) Is γPCDH role in connectivity mediated through *trans* homophilic interaction, or rather depends on *cis* heterophilic binding?

(Q2) Are γPCDH able to mediate both adhesion and repulsion in a context-dependent manner?

(Q3) What is the pattern of expression of γPCDH in IONs during development? Do protein isoforms reach the axon terminal membrane?

(Q4) What is the contribution of γPCDH-mediated Nlgn inhibition in CF selection and strengthening?

To answer these questions, we propose, first, to perform PatchSeq during development on IONs to quantify γPCDH diversity (answering Q3). In addition, RNAScope would enable us locate γPCDH transcripts in both IONs and PCs, which would help understanding the regulatory mechanisms of γPCDH diversity in both cell types (local *versus* nuclear regulation).

Secondly, using sparse labelling of IONs, we could perform PatchSeq on connected IONs and their PC targets in the mature system, which would give valuable information regarding Q1 and Q2. Finding matching isoforms in both pre- and postsynaptic cells would reinforce the hypothesis that γPCDH can mediate adhesive contacts in this circuit, and that their transmembrane interactions would be involved in CF selection.

Third, immunostaining with improved antigen access (expansion microscopy and glyoxal fixation, for instance) would enable the localization of γPCDH proteins. Thus, the localization of isoforms at PCs membranes and CF

terminals could be addressed (Q3, Q1). Finally, these imaging approaches could be employed to analyze the possible colocalization of γPCDH isoforms and Nlgn in PCs membranes, elucidating the contribution of *cis* interactions in CF strengthening (Q4).

General conclusions

This thesis work helps shed some light on the molecular mechanisms of CF selection in the developing cerebellum, as well as the contribution of cPCDH to this process. Attending to our results and considering the available literature, we can conclude that:

(1) cPCDH diversity is downregulated in PCs during the developmental critical period for CF elimination, likely through Dnmt3b promoter methylation and γPCDH C-terminal dependent expression. PatchSeq allows a full characterization of CF to PC connectivity *ex vivo* and the correlation of the electrophysiological status of single cell to its transcriptome.

(2) Hindbrain explants are a unique *in vitro* tool that recapitulates cerebellar microcircuitry development morphologically and electrophysiologically.

(3) CF innervation is needed for γPCDH regulation in PCs. CF activity on PCs may be promoting γPCDH nuclear signaling and γPCDH methylation, reducing the isoforms repertoire. The absence of brainstem innervation may prevent this process, which would explain why "naïve" PCs retain high γPCDH diversity, corresponding to an immature gene expression pattern.

(4) Early overexpression of a single γPCDH isoform in PCs accelerates CF selection. Because interactions are presumably mediated by the overexpressed isoform, the discrepancy of isoforms with most CF inputs increases, which would likely promote avoidance signals through FAK/Pyk2 in most CFs, except for the winning, matching axon.

(5) γPCDH combinatorial expression in PCs seem to depend on the γPCDH isoforms expressed by the winning CF. PCs may be able to adapt their γPCDH expression thanks to activity-dependent mechanisms, including ADAM10 protease and Dnmt3b promoters methylation.

References

Allen Mouse Brain Atlas ((2011). mouse.brain-map.org

Andersen, B. B., Korbo, L., & Pakkenberg, B. (1992). A quantitative study of the human cerebellum with unbiased stereological techniques. *Journal of Comparative Neurology*, *326*(4), 549-560. https://doi.org/https://doi.org/10.1002/cne.903260405

Andjus, P. R., Zhu, L., Cesa, R., Carulli, D., & Strata, P. (2003). A change in the pattern of activity affects the developmental regression of the Purkinje cell polyinnervation by climbing fibers in the rat cerebellum. *Neuroscience*, *121*(3), 563-572. https://doi.org/10.1016/s0306-4522(03)00556-6

Andrews, S. (2010). FastQC: a quality control tool for high throughput sequence data. https://www.bioinformatics.babraham.ac.uk/projects/fastqc/

Antonini, A., & Stryker, M. P. (1996). Plasticity of geniculocortical afferents following brief or prolonged monocular occlusion in the cat. *Journal of Comparative Neurology*, *369*(1), 64-82. https://doi.org/https://doi.org/10.1002/(SICI)1096-9861(19960520)369:1<64::AID-CNE5>3.0.CO;2-I

Apps, R., & Hawkes, R. (2009). Cerebellar cortical organization: a one-map hypothesis. *Nature Reviews Neuroscience*, *10*(9), 670-681. https://doi.org/10.1038/nrn2698

Arendt, D., Musser, J. M., Baker, C. V. H., Bergman, A., Cepko, C., Erwin, D. H., Pavlicev, M., Schlosser, G., Widder, S., Laubichler, M. D., & Wagner, G. P. (2016). The origin and evolution of cell types. *Nature Reviews Genetics*, *17*(12), 744-757. https://doi.org/10.1038/nrg.2016.127

Badaloni, A., Casoni, F., Croci, L., Chiara, F., Bizzoca, A., Gennarini, G., Cremona, O., Hawkes, R., & Consalez, G. G. (2019). Dynamic Expression and New Functions of Early B Cell Factor 2 in Cerebellar Development. *Cerebellum*, *18*(6), 999-1010. https://doi.org/10.1007/s12311-019-01051-3

Basu, R., R., T. M., & and Williams, M. E. (2015). The classic cadherins in synaptic specificity. *Cell Adhesion & Migration*, *9*(3), 193-201. https://doi.org/10.1080/19336918.2014.1000072

Beekhof, G. C., Osório, C., White, J. J., van Zoomeren, S., van der Stok, H., Xiong, B., Nettersheim, I. H. M. S., Mak, W. A., Runge, M., Fiocchi, F. R., Boele, H.-J., Hoebeek, F. E., & Schonewille, M. (2021). Differential spatiotemporal development of Purkinje cell populations and cerebellum-dependent sensorimotor behaviors. *eLife*, *10*, e63668. https://doi.org/10.7554/eLife.63668

Billings, G., Piasini, E., Lőrincz, A., Nusser, Z., & Silver, R. A. (2014). Network Structure within the Cerebellar Input Layer Enables Lossless Sparse Encoding. *Neuron*, *83*(4), 960-974. https://doi.org/10.1016/j.neuron.2014.07.020

Brainard, M. S., & Knudsen, E. I. (1998). Sensitive periods for visual calibration of the auditory space map in the barn owl optic tectum. *Journal of Neuroscience*, *18*(10), 3929-3942.

Braitenberg, V., & Schüz, A. (1991). Peters' Rule and White's Exceptions. In V. Braitenberg & A. Schüz (Eds.), *Anatomy of the Cortex: Statistics and Geometry* (pp. 109-112). Springer Berlin Heidelberg. https://doi.org/10.1007/978-3-662-02728-8_21

Brasch, J., Goodman, K. M., Noble, A. J., Rapp, M., Mannepalli, S., Bahna, F., Dandey, V. P., Bepler, T., Berger, B., Maniatis, T., Potter, C. S., Carragher, B., Honig, B., & Shapiro, L. (2019). Visualization of clustered protocadherin neuronal self-recognition complexes. *Nature*, *569*(7755), 280-283. https://doi.org/10.1038/s41586-019-1089-3

Bravin, M., Morando, L., Vercelli, A., Rossi, F., & Strata, P. (1999). Control of spine formation by electrical activity in the adult rat cerebellum. *Proceedings of the National Academy of Sciences*, *96*(4), 1704-1709. https://doi.org/10.1073/pnas.96.4.1704

Brock, L., Coombs, J., & Eccles, J. (1951). Action potentials of motoneurones with intracellular electrode. Proc. Univ. Otago Med. Sch,

Brock, L., Coombs, J., & Eccles, J. (1952a). The recording of potentials from motoneurones with an intracellular electrode. *The Journal of Physiology*, *117*(4), 431.

Brock, L., Coombs, J., & Eccles, J. (1952b). Synaptic excitation and inhibition. *The Journal of Physiology*, *117*(2), 8p.

Busch, S. E., & Hansel, C. (2023). Climbing fiber multi-innervation of mouse Purkinje dendrites with arborization common to human. *Science*, *381*(6656), 420-427. https://doi.org/10.1126/science.adi1024

Cadwell, C. R., Palasantza, A., Jiang, X., Berens, P., Deng, Q., Yilmaz, M., Reimer, J., Shen, S., Bethge, M., Tolias, K. F., Sandberg, R., & Tolias, A. S. (2016). Electrophysiological, transcriptomic and morphologic profiling of single neurons using Patch-seq. *Nature Biotechnology*, *34*(2), 199-203. https://doi.org/10.1038/nbt.3445

Cajal, S. R. (1893). Nuevo concepto de la histología de los centros nerviosos: conferencias pronunciadas en la Academia y Laboratorio de Ciencias Médicas de Cataluña en los días 14, 18 y 19 de marzo de 1892. Imprenta de Henrich y Cia. https://books.google.fr/books?id=YkA9MwEACAAJ

Cajal, S. R. (1894). *Histología. Consideraciones generales sobre la morfología de la célula nerviosa*. https://books.google.fr/books?id=qA0KywEACAAJ

Cajal, S. R. (1899). Estudios sobre la corteza cerebral humana: I. Corteza Visual. II. Estructura de la corteza motriz del hombre y mamíferos superiores. https://books.google.fr/books?id=9TIeywEACAAJ

Cajal, S. R. (1904). Textura del sistema nervioso del hombre y de los vertebrados : estudios sobre el plan estructural y composición histológica de los centros nerviosos adicionados de consideraciones fisiológicas fundadas en los nuevos descubrimientos. Volumen III. Madrid : Nicolás Moya. http://hdl.handle.net/10481/69715

Cerminara, N. L., Lang, E. J., Sillitoe, R. V., & Apps, R. (2015). Redefining the cerebellar cortex as an assembly of non-uniform Purkinje cell microcircuits. *Nature Reviews Neuroscience*, *16*(2), 79-93. https://doi.org/10.1038/nrn3886

Changeux, J.-P. (2022). Epigenesis, Synapse Selection, Cultural Imprints, and Human Brain Development: From Molecules to Cognition. In O. Houdé & G. Borst (Eds.), *The Cambridge Handbook of Cognitive Development* (pp. 27-49). Cambridge University Press. https://doi.org/DOI: 10.1017/9781108399838.004

Changeux, J. P., Courrege, P., & Danchin, A. (1973). A theory of the epigenesis of neuronal networks by selective stabilization of synapses. *Proc Natl Acad Sci U S A*, *70*(10), 2974-2978. https://doi.org/10.1073/pnas.70.10.2974

Chedotal, A., Bloch-Gallego, E., & Sotelo, C. (1997). The embryonic cerebellum contains topographic cues that guide developing inferior olivary axons. *Development*, *124*(4), 861-870. https://doi.org/10.1242/dev.124.4.861

Chen, B., Brinkmann, K., Chen, Z., Pak, C. W., Liao, Y., Shi, S., Henry, L., Grishin, N. V., Bogdan, S., & Rosen, M. K. (2014). The WAVE regulatory complex links diverse receptors to the actin cytoskeleton. *Cell*, *156*(1-2), 195-207. https://doi.org/10.1016/j.cell.2013.11.048

Chen, C., Kano, M., Abeliovich, A., Chen, L., Bao, S., Kim, J. J., Hashimoto, K., Thompson, R. F., & Tonegawa, S. (1995). Impaired motor coordination correlates with persistent multiple climbing fiber innervation in PKC gamma mutant mice. *Cell*, *83*(7), 1233-1242. https://doi.org/10.1016/0092-8674(95)90148-5

Chen, S., Zhou, Y., Chen, Y., & Gu, J. (2018). fastp: an ultra-fast all-in-one FASTQ preprocessor. *Bioinformatics*, *34*(17), i884-i890. https://doi.org/10.1093/bioinformatics/bty560

Chen, W. V., Nwakeze, C. L., Denny, C. A., O'Keeffe, S., Rieger, M. A., Mountoufaris, G., Kirner, A., Dougherty, J. D., Hen, R., Wu, Q., & Maniatis,

T. (2017). Pcdhalphac2 is required for axonal tiling and assembly of serotonergic circuitries in mice. *Science*, *356*(6336), 406-411. https://doi.org/10.1126/science.aal3231

Chih, B., Gollan, L., & Scheiffele, P. (2006). Alternative splicing controls selective trans-synaptic interactions of the neuroligin-neurexin complex. *Neuron*, *51*(2), 171-178. https://doi.org/10.1016/j.neuron.2006.06.005

Choo, M., Miyazaki, T., Yamazaki, M., Kawamura, M., Nakazawa, T., Zhang, J., Tanimura, A., Uesaka, N., Watanabe, M., Sakimura, K., & Kano, M. (2017). Retrograde BDNF to TrkB signaling promotes synapse elimination in the developing cerebellum. *Nat Commun*, *8*(1), 195. https://doi.org/10.1038/s41467-017-00260-w

Cisneros-Franco, J. M., Voss, P., Thomas, M. E., & de Villers-Sidani, E. (2020). Critical periods of brain development. *Handb Clin Neurol*, *173*, 75-88. https://doi.org/10.1016/B978-0-444-64150-2.00009-5

de Wit, J., Sylwestrak, E., O'Sullivan, M. L., Otto, S., Tiglio, K., Savas, J. N., Yates, J. R., 3rd, Comoletti, D., Taylor, P., & Ghosh, A. (2009). LRRTM2 interacts with Neurexin1 and regulates excitatory synapse formation. *Neuron*, *64*(6), 799-806. https://doi.org/10.1016/j.neuron.2009.12.019

Dean, C., Scholl, F. G., Choih, J., DeMaria, S., Berger, J., Isacoff, E., & Scheiffele, P. (2003). Neurexin mediates the assembly of presynaptic terminals. *Nat Neurosci*, *6*(7), 708-716. https://doi.org/10.1038/nn1074

DeBello, W. M., Feldman, D. E., & Knudsen, E. I. (2001). Adaptive axonal remodeling in the midbrain auditory space map. *Journal of Neuroscience*, *21*(9), 3161-3174.

DeFelipe, J. (2002). Chapter 17 Cortical interneurons: from Cajal to 2001. In *Progress in Brain Research* (Vol. 136, pp. 215-238). Elsevier. https://doi.org/https://doi.org/10.1016/S0079-6123(02)36019-9

Ding, X., Liu, S., Tian, M., Zhang, W., Zhu, T., Li, D., Wu, J., Deng, H., Jia, Y., Xie, W., Xie, H., & Guan, J. S. (2017). Activity-induced histone modifications govern Neurexin-1 mRNA splicing and memory preservation. *Nat Neurosci*, *20*(5), 690-699. https://doi.org/10.1038/nn.4536

Dityatev, A., Dityateva, G., Sytnyk, V., Delling, M., Toni, N., Nikonenko, I., Muller, D., & Schachner, M. (2004). Polysialylated Neural Cell Adhesion Molecule Promotes Remodeling and Formation of Hippocampal Synapses. *The Journal of Neuroscience*, *24*(42), 9372. https://doi.org/10.1523/JNEUROSCI.1702-04.2004

Eccles, J. C. (1967). Circuits in the cerebellar control of movement. *Proc Natl Acad Sci U S A*, *58*(1), 336-343. https://doi.org/10.1073/pnas.58.1.336

Esumi, S., Kakazu, N., Taguchi, Y., Hirayama, T., Sasaki, A., Hirabayashi, T., Koide, T., Kitsukawa, T., Hamada, S., & Yagi, T. (2005). Monoallelic yet combinatorial expression of variable exons of the protocadherin-α gene cluster in single neurons. *Nature Genetics 2005 37:2*, *37*(2), 171-176. https://doi.org/10.1038/ng1500

Fagiolini, M., Katagiri, H., Miyamoto, H., Mori, H., Grant, S. G., Mishina, M., & Hensch, T. K. (2003). Separable features of visual cortical plasticity revealed by N-methyl-D-aspartate receptor 2A signaling. *Proc Natl Acad Sci U S A*, *100*(5), 2854-2859. https://doi.org/10.1073/pnas.0536089100

Fan, L., Lu, Y., Shen, X., Shao, H., Suo, L., & Wu, Q. (2018). Alpha protocadherins and Pyk2 kinase regulate cortical neuron migration and cytoskeletal dynamics via Rac1 GTPase and WAVE complex in mice. *eLife*, *7*. https://doi.org/10.7554/eLife.35242

Feldman, D. E., & Knudsen, E. I. (1997). An anatomical basis for visual calibration of the auditory space map in the barn owl's midbrain. *Journal of Neuroscience*, *17*(17), 6820-6837.

Feng, J., Zhou, Y., Campbell, S. L., Le, T., Li, E., Sweatt, J. D., Silva, A. J., & Fan, G. (2010). Dnmt1 and Dnmt3a maintain DNA methylation and regulate synaptic function in adult forebrain neurons. *Nature Neuroscience*, *13*(4), 423-430. https://doi.org/10.1038/nn.2514

Fernández-Monreal, M., Kang, S., & Phillips, G. R. (2009). Gamma-protocadherin homophilic interaction and intracellular trafficking is controlled by the cytoplasmic domain in neurons. *Molecular and Cellular Neuroscience*, *40*(3), 344-353. https://doi.org/https://doi.org/10.1016/j.mcn.2008.12.002

Fernández-Monreal, M., Oung, T., Hanson, H. H., O'Leary, R., Janssen, W. G., Dolios, G., Wang, R., & Phillips, G. R. (2010). gamma-protocadherins are enriched and transported in specialized vesicles associated with the secretory pathway in neurons. *Eur J Neurosci*, *32*(6), 921-931. https://doi.org/10.1111/j.1460-9568.2010.07386.x

Földy, C., Darmanis, S., Aoto, J., Malenka, R. C., Quake, S. R., & Südhof, T. C. (2016). Single-cell RNAseq reveals cell adhesion molecule profiles in electrophysiologically defined neurons. *Proceedings of the National Academy of Sciences*, *113*(35), E5222-E5231. https://doi.org/10.1073/pnas.1610155113

Francis, D. D., Diorio, J., Plotsky, P. M., & Meaney, M. J. (2002). Environmental enrichment reverses the effects of maternal separation on stress reactivity. *J Neurosci*, *22*(18), 7840-7843. https://doi.org/10.1523/JNEUROSCI.22-18-07840.2002

Frank, M., Ebert, M., Shan, W., Phillips, G. R., Arndt, K., Colman, D. R., & Kemler, R. (2005). Differential expression of individual gamma-protocadherins

during mouse brain development. *Molecular and Cellular Neuroscience*, *29*(4), 603-616. https://doi.org/10.1016/J.MCN.2005.05.001

Fuerst, P. G., Koizumi, A., Masland, R. H., & Burgess, R. W. (2008). Neurite arborization and mosaic spacing in the mouse retina require DSCAM. *Nature*, *451*(7177), 470-474. https://doi.org/10.1038/nature06514

Fujishima, K., Horie, R., Mochizuki, A., & Kengaku, M. (2012). Principles of branch dynamics governing shape characteristics of cerebellar Purkinje cell dendrites. *Development*, *139*(18), 3442-3455. https://doi.org/10.1242/dev.081315

Fukata, Y., Chen, X., Chiken, S., Hirano, Y., Yamagata, A., Inahashi, H., Sanbo, M., Sano, H., Goto, T., Hirabayashi, M., Kornau, H. C., Pruss, H., Nambu, A., Fukai, S., Nicoll, R. A., & Fukata, M. (2021). LGI1-ADAM22-MAGUK configures transsynaptic nanoalignment for synaptic transmission and epilepsy prevention. *Proc Natl Acad Sci U S A*, *118*(3). https://doi.org/10.1073/pnas.2022580118

Garcia-Lopez, P., Garcia-Marin, V., & Freire, M. (2010). The histological slides and drawings of Cajal [Review]. *Frontiers in Neuroanatomy*, *Volume 4 - 2010*. https://doi.org/10.3389/neuro.05.009.2010

Garrett, A. M., Schreiner, D., Lobas, M. A., & Weiner, J. A. (2012). gamma-protocadherins control cortical dendrite arborization by regulating the activity of a FAK/PKC/MARCKS signaling pathway. *Neuron*, *74*(2), 269-276. https://doi.org/10.1016/j.neuron.2012.01.028

Gomez, A. M., Traunmuller, L., & Scheiffele, P. (2021). Neurexins: molecular codes for shaping neuronal synapses. *Nat Rev Neurosci*, *22*(3), 137-151. https://doi.org/10.1038/s41583-020-00415-7

Goulas, A., Betzel, R. F., & Hilgetag, C. C. (2019). Spatiotemporal ontogeny of brain wiring. *Science Advances*, *5*(6), eaav9694. https://doi.org/10.1126/sciadv.aav9694

Goulas, A., Schaefer, A., & Margulies, D. S. (2015). The strength of weak connections in the macaque cortico-cortical network. *Brain Structure and Function*, *220*(5), 2939-2951. https://doi.org/10.1007/s00429-014-0836-3

Graf, E. R., Zhang, X., Jin, S. X., Linhoff, M. W., & Craig, A. M. (2004). Neurexins induce differentiation of GABA and glutamate postsynaptic specializations via neuroligins. *Cell*, *119*(7), 1013-1026. https://doi.org/10.1016/j.cell.2004.11.035

Granovetter, M. S. (1973). The Strength of Weak Ties. *American Journal of Sociology*, *78*(6), 1360-1380. http://www.jstor.org/stable/2776392

Groh, A., Meyer, H. S., Schmidt, E. F., Heintz, N., Sakmann, B., & Krieger, P. (2010). Cell-type specific properties of pyramidal neurons in neocortex underlying a layout that is modifiable depending on the cortical area. *Cerebral Cortex*, *20*(4), 826-836.

Guirado, R., Perez-Rando, M., Sanchez-Matarredona, D., Castillo-Gómez, E., Liberia, T., Rovira-Esteban, L., Varea, E., Crespo, C., Blasco-Ibáñez, J. M., & Nacher, J. (2014). The Dendritic Spines of Interneurons Are Dynamic Structures Influenced by PSA-NCAM Expression. *Cerebral Cortex*, *24*(11), 3014-3024. https://doi.org/10.1093/cercor/bht156

Guo, Y., Monahan, K., Wu, H., Gertz, J., Varley, K. E., Li, W., Myers, R. M., Maniatis, T., & Wu, Q. (2012). CTCF/cohesin-mediated DNA looping is required for protocadherin alpha promoter choice. *Proc Natl Acad Sci U S A*, *109*(51), 21081-21086. https://doi.org/10.1073/pnas.1219280110

Haas, I. G., Frank, M., Veron, N., & Kemler, R. (2005). Presenilin-dependent processing and nuclear function of gamma-protocadherins. *J Biol Chem*, *280*(10), 9313-9319. https://doi.org/10.1074/jbc.M412909200

Hagemann-Jensen, M., Ziegenhain, C., & Sandberg, R. (2022). Scalable single-cell RNA sequencing from full transcripts with Smart-seq3xpress. *Nature Biotechnology*, *40*(10), 1452-1457. https://doi.org/10.1038/s41587-022-01311-4

Hambsch, B., Grinevich, V., Seeburg, P. H., & Schwarz, M. K. (2005). gamma-Protocadherins, presenilin-mediated release of C-terminal fragment promotes locus expression. *J Biol Chem*, *280*(16), 15888-15897. https://doi.org/10.1074/jbc.M414359200

Hao, Y., Stuart, T., Kowalski, M. H., Choudhary, S., Hoffman, P., Hartman, A., Srivastava, A., Molla, G., Madad, S., Fernandez-Granda, C., & Satija, R. (2024). Dictionary learning for integrative, multimodal and scalable single-cell analysis. *Nat Biotechnol*, *42*(2), 293-304. https://doi.org/10.1038/s41587-023-01767-y

Hashimoto, K., Ichikawa, R., Kitamura, K., Watanabe, M., & Kano, M. (2009). Translocation of a "winner" climbing fiber to the Purkinje cell dendrite and subsequent elimination of "losers" from the soma in developing cerebellum. *Neuron*, *63*(1), 106-118. https://doi.org/10.1016/j.neuron.2009.06.008

Hashimoto, K., & Kano, M. (2003). Functional differentiation of multiple climbing fiber inputs during synapse elimination in the developing cerebellum. *Neuron*, *38*(5), 785-796. https://doi.org/10.1016/s0896-6273(03)00298-8

Hashimoto, K., & Kano, M. (2013). Synapse elimination in the developing cerebellum. *Cell Mol Life Sci*, *70*(24), 4667-4680. https://doi.org/10.1007/s00018-013-1405-2

Hashimoto, K., Tsujita, M., Miyazaki, T., Kitamura, K., Yamazaki, M., Shin, H. S., Watanabe, M., Sakimura, K., & Kano, M. (2011). Postsynaptic P/Q-type Ca2+ channel in Purkinje cell mediates synaptic competition and elimination in developing cerebellum. *Proc Natl Acad Sci U S A*, *108*(24), 9987-9992. https://doi.org/10.1073/pnas.1101488108

Hashimoto, K., Yoshida, T., Sakimura, K., Mishina, M., Watanabe, M., & Kano, M. (2009). Influence of parallel fiber-Purkinje cell synapse formation on postnatal development of climbing fiber-Purkinje cell synapses in the cerebellum. *Neuroscience*, *162*(3), 601-611. https://doi.org/10.1016/j.neuroscience.2008.12.037

Hattox, A. M., & Nelson, S. B. (2007). Layer V neurons in mouse cortex projecting to different targets have distinct physiological properties. *Journal of Neurophysiology*, *98*(6), 3330-3340.

Hebb, D. O. (1949). The organization of behavior: a neuropsychological theory. J. Wiley; Chapman & Hall.

Hensch, T. K. (2004). Critical period regulation. *Annu Rev Neurosci*, *27*, 549-579. https://doi.org/10.1146/annurev.neuro.27.070203.144327

Hensch, T. K., & Bilimoria, P. M. (2012). Re-opening Windows: Manipulating Critical Periods for Brain Development. *Cerebrum*, *2012*, 11. https://www.ncbi.nlm.nih.gov/pubmed/23447797

Hensch, T. K., Fagiolini, M., Mataga, N., Stryker, M. P., Baekkeskov, S., & Kash, S. F. (1998). Local GABA circuit control of experience-dependent plasticity in developing visual cortex. *Science*, *282*(5393), 1504-1508. https://doi.org/10.1126/science.282.5393.1504

Herculano-Houzel, S. (2009). The human brain in numbers: a linearly scaled-up primate brain. *Front Hum Neurosci*, *3*, 31. https://doi.org/10.3389/neuro.09.031.2009

Hirano, K., Kaneko, R., Izawa, T., Kawaguchi, M., Kitsukawa, T., & Yagi, T. (2012). Single-neuron diversity generated by Protocadherin-beta cluster in mouse central and peripheral nervous systems. *Front Mol Neurosci*, *5*, 90. https://doi.org/10.3389/fnmol.2012.00090

Hirota, J., & Mombaerts, P. (2004). The LIM-homeodomain protein Lhx2 is required for complete development of mouse olfactory sensory neurons. *Proceedings of the National Academy of Sciences*, *101*(23), 8751-8755. https://doi.org/10.1073/pnas.0400940101

Hobert, O., & Kratsios, P. (2019). Neuronal identity control by terminal selectors in worms, flies, and chordates. *Current Opinion in Neurobiology*, *56*, 97-105. https://doi.org/https://doi.org/10.1016/j.conb.2018.12.006

Hökfelt, T., & Fuxe, K. (1969). Cerebellar monoamine nerve terminals, a new type of afferent fibers to the cortex cerebelli. *Experimental Brain Research*, *9*(1), 63-72. https://doi.org/10.1007/BF00235452

Holtmaat, A., & Svoboda, K. (2009). Experience-dependent structural synaptic plasticity in the mammalian brain. *Nature Reviews Neuroscience*, *10*(9), 647-658. https://doi.org/10.1038/nrn2699

Horikawa, K., & Armstrong, W. (1988). A versatile means of intracellular labeling: injection of biocytin and its detection with avidin conjugates. *Journal of neuroscience methods*, *25*(1), 1-11.

Hoshino, N., Kanadome, T., Takasugi, T., Itoh, M., Kaneko, R., Inoue, Y. U., Inoue, T., Hirabayashi, T., Watanabe, M., Matsuda, T., Nagai, T., Tarusawa, E., & Yagi, T. (2023). Visualization of trans homophilic interaction of clustered protocadherin in neurons. *Proc Natl Acad Sci U S A*, *120*(38), e2301003120. https://doi.org/10.1073/pnas.2301003120

Hubel, D. H., & Wiesel, T. N. (1963). RECEPTIVE FIELDS OF CELLS IN STRIATE CORTEX OF VERY YOUNG, VISUALLY INEXPERIENCED KITTENS. *Journal of Neurophysiology*, *26*(6), 994-1002. https://doi.org/10.1152/jn.1963.26.6.994

Hubel, D. H., & Wiesel, T. N. (1972). Laminar and columnar distribution of geniculo-cortical fibers in the macaque monkey. *J Comp Neurol*, *146*(4), 421-450. https://doi.org/10.1002/cne.901460402

Hubel, D. H., & Wiesel, T. N. (1977). Ferrier lecture - Functional architecture of macaque monkey visual cortex. *Proceedings of the Royal Society of London. Series B. Biological Sciences*, *198*(1130), 1-59. https://doi.org/10.1098/rspb.1977.0085

Hull, C. (2020). Prediction signals in the cerebellum: beyond supervised motor learning. *eLife*, *9*. https://doi.org/10.7554/eLife.54073

Ito, M. (1972). Neural design of the cerebellar motor control system. *Brain Research*, *40*(1), 81-84. https://doi.org/https://doi.org/10.1016/0006-8993(72)90110-2

Itō, M. (1984). *The Cerebellum and Neural Control*. Raven Press. https://books.google.fr/books?id=Wt1qAAAAMAAJ

Ito, S., & Takeichi, M. (2009). Dendrites of cerebellar granule cells correctly recognize their target axons for synaptogenesis in vitro. *Proc Natl Acad Sci U S A*, *106*(31), 12782-12787. https://doi.org/10.1073/pnas.0906653106

Jiang, R., Sun, T., Song, D., & Li, J. J. (2022). Statistics or biology: the zero-inflation controversy about scRNA-seq data. *Genome Biology*, *23*(1), 31. https://doi.org/10.1186/s13059-022-02601-5

Johnson, J. S., & Newport, E. L. (1989). Critical period effects in second language learning: The influence of maturational state on the acquisition of English as a second language. *Cognitive Psychology*, *21*(1), 60-99. https://doi.org/https://doi.org/10.1016/0010-0285(89)90003-0

Joshi, D., Coon, B. G., Chakraborty, R., Deng, H., Fernandez-Tussy, P., Meredith, E., Traylor, J. G., Orr, A. W., Fernandez-Hernando, C., & Schwartz, M. A. (2024). Gamma protocadherins in vascular endothelial cells inhibit Klf2/4 to promote atherosclerosis. *bioRxiv*, 2024.2001.2016.575958. https://doi.org/10.1101/2024.01.16.575958

Juttner, R., & Rathjen, F. G. (2005). Molecular analysis of axonal target specificity and synapse formation. *Cell Mol Life Sci*, *62*(23), 2811-2827. https://doi.org/10.1007/s00018-005-5299-5

Kakegawa, W., Mitakidis, N., Miura, E., Abe, M., Matsuda, K., Takeo, Y. H., Kohda, K., Motohashi, J., Takahashi, A., Nagao, S., Muramatsu, S., Watanabe, M., Sakimura, K., Aricescu, A. R., & Yuzaki, M. (2015). Anterograde C1ql1 signaling is required in order to determine and maintain a single-winner climbing fiber in the mouse cerebellum. *Neuron*, *85*(2), 316-329. https://doi.org/10.1016/j.neuron.2014.12.020

Kakegawa, W., Paternain, A. V., Matsuda, K., Aller, M. I., Iida, I., Miura, E., Nozawa, K., Yamasaki, T., Sakimura, K., Yuzaki, M., & Lerma, J. (2024). Kainate receptors regulate synaptic integrity and plasticity by forming a complex with synaptic organizers in the cerebellum. *Cell Rep*, *43*(7), 114427. https://doi.org/10.1016/j.celrep.2024.114427

Kalinovsky, A., Boukhtouche, F., Blazeski, R., Bornmann, C., Suzuki, N., Mason, C. A., & Scheiffele, P. (2011). Development of axon-target specificity of ponto-cerebellar afferents. *PLoS Biol*, *9*(2), e1001013. https://doi.org/10.1371/journal.pbio.1001013

Kanadome, T., Hoshino, N., Nagai, T., Matsuda, T., & Yagi, T. (2021). Development of FRET-based indicators for visualizing homophilic trans interaction of a clustered protocadherin. *Sci Rep*, *11*(1), 22237. https://doi.org/10.1038/s41598-021-01481-2

Kaneko, R., Kato, H., Kawamura, Y., Esumi, S., Hirayama, T., Hirabayashi, T., & Yagi, T. (2006). Allelic gene regulation of Pcdh-alpha and Pcdh-gamma clusters involving both monoallelic and biallelic expression in single Purkinje cells. *J Biol Chem*, *281*(41), 30551-30560. https://doi.org/10.1074/jbc.M605677200

Kano, M., & Hashimoto, K. (2012). Activity-Dependent Maturation of Climbing Fiber to Purkinje Cell Synapses during Postnatal Cerebellar Development. *The Cerebellum*, *11*(2), 449-450. https://doi.org/10.1007/s12311-011-0337-3

Kano, M., Hashimoto, K., Watanabe, M., Kurihara, H., Offermanns, S., Jiang, H., Wu, Y., Jun, K., Shin, H. S., Inoue, Y., Simon, M. I., & Wu, D. (1998). Phospholipase cbeta4 is specifically involved in climbing fiber synapse elimination in the developing cerebellum. *Proc Natl Acad Sci U S A*, *95*(26), 15724-15729. https://doi.org/10.1073/pnas.95.26.15724

Kano, M., Watanabe, T., Uesaka, N., & Watanabe, M. (2018). Multiple Phases of Climbing Fiber Synapse Elimination in the Developing Cerebellum. *Cerebellum*, *17*(6), 722-734. https://doi.org/10.1007/s12311-018-0964-z

Kasper, E. M., Larkman, A. U., Lübke, J., & Blakemore, C. (1994). Pyramidal neurons in layer 5 of the rat visual cortex. I. Correlation among cell morphology, intrinsic electrophysiological properties, and axon targets. *Journal of Comparative Neurology*, *339*(4), 459-474.

Kasthuri, N., Hayworth, K. J., Berger, D. R., Schalek, R. L., Conchello, J. A., Knowles-Barley, S., Lee, D., Vázquez-Reina, A., Kaynig, V., Jones, T. R., Roberts, M., Morgan, J. L., Tapia, J. C., Seung, H. S., Roncal, W. G., Vogelstein, J. T., Burns, R., Sussman, D. L., Priebe, C. E.,…Lichtman, J. W. (2015). Saturated Reconstruction of a Volume of Neocortex. *Cell*, *162*(3), 648-661. https://doi.org/10.1016/j.cell.2015.06.054

Kawamura, N., Osuka, T., Kaneko, R., Kishi, E., Higuchi, R., Yoshimura, Y., Hirabayashi, T., Yagi, T., & Tarusawa, E. (2023). Reciprocal Connections between Parvalbumin-Expressing Cells and Adjacent Pyramidal Cells Are Regulated by Clustered Protocadherin gamma. *eNeuro*, *10*(10). https://doi.org/10.1523/ENEURO.0250-23.2023

Kawata, S., Miyazaki, T., Yamazaki, M., Mikuni, T., Yamasaki, M., Hashimoto, K., Watanabe, M., Sakimura, K., & Kano, M. (2014). Global scaling down of excitatory postsynaptic responses in cerebellar Purkinje cells impairs developmental synapse elimination. *Cell Rep*, *8*(4), 1119-1129. https://doi.org/10.1016/j.celrep.2014.07.014

Keeler, A. B., Schreiner, D., & Weiner, J. A. (2015). Protein Kinase C Phosphorylation of a gamma-Protocadherin C-terminal Lipid Binding Domain Regulates Focal Adhesion Kinase Inhibition and Dendrite Arborization. *J Biol Chem*, *290*(34), 20674-20686. https://doi.org/10.1074/jbc.M115.642306

Kenakin, T. (2005). New concepts in drug discovery: collateral efficacy and permissive antagonism. *Nat Rev Drug Discov*, *4*(11), 919-927. https://doi.org/10.1038/nrd1875

Kiefer, L., Chiosso, A., Langen, J., Buckley, A., Gaudin, S., Rajkumar, S. M., Servito, G. I. F., Cha, E. S., Vijay, A., Yeung, A., Horta, A., Mui, M. H., & Canzio, D. (2023). WAPL functions as a rheostat of Protocadherin isoform diversity that controls neural wiring. *Science*, *380*(6651), eadf8440. https://doi.org/10.1126/science.adf8440

Knudsen, E. I. (2002). Instructed learning in the auditory localization pathway of the barn owl. *Nature*, *417*(6886), 322-328. https://doi.org/10.1038/417322a

Knudsen, E. I., Esterly, S. D., & Knudsen, P. F. (1984). Monaural occlusion alters sound localization during a sensitive period in the barn owl. *Journal of Neuroscience*, *4*(4), 1001-1011.

Ko, J., Fuccillo, M. V., Malenka, R. C., & Sudhof, T. C. (2009). LRRTM2 functions as a neurexin ligand in promoting excitatory synapse formation. *Neuron*, *64*(6), 791-798. https://doi.org/10.1016/j.neuron.2009.12.012

Koch, C., Svoboda, K., Bernard, A., Basso, M. A., Churchland, A. K., Fairhall, A. L., Groblewski, P. A., Lecoq, J. A., Mainen, Z. F., Mathis, M. W., Olsen, S. R., Phillips, J. w., Pouget, A., Saxena, S., Siegle, J. H., & Zador, A. M. (2022). Next-generation brain observatories. *Neuron*, *110*(22), 3661-3666. https://doi.org/https://doi.org/10.1016/j.neuron.2022.09.033

Kolterud, A. s., Alenius, M., Carlsson, L., & Bohm, S. (2004). The Lim homeobox gene Lhx2 is required for olfactory sensory neuron identity. *Development*, *131*(21), 5319-5326. https://doi.org/10.1242/dev.01416

Kong, Q., Yu, M., Zhang, M., Wei, C., Gu, H., Yu, S., Sun, W., Li, N., & Zhou, Y. (2020). Conditional Dnmt3b deletion in hippocampal dCA1 impairs recognition memory. *Mol Brain*, *13*(1), 42. https://doi.org/10.1186/s13041-020-00574-9

Kozareva, V., Martin, C., Osorno, T., Rudolph, S., Guo, C., Vanderburg, C., Nadaf, N., Regev, A., Regehr, W. G., & Macosko, E. (2021). A transcriptomic atlas of mouse cerebellar cortex comprehensively defines cell types. *Nature*, *598*(7879), 214-219. https://doi.org/10.1038/s41586-021-03220-z

Krishnaswamy, A., Yamagata, M., Duan, X., Hong, Y. K., & Sanes, J. R. (2015). Sidekick 2 directs formation of a retinal circuit that detects differential motion. *Nature*, *524*(7566), 466-470. https://doi.org/10.1038/nature14682

Kurihara, H., Hashimoto, K., Kano, M., Takayama, C., Sakimura, K., Mishina, M., Inoue, Y., & Watanabe, M. (1997). Impaired parallel fiber-->Purkinje cell synapse stabilization during cerebellar development of mutant mice lacking the glutamate receptor delta2 subunit. *J Neurosci*, *17*(24), 9613-9623. https://doi.org/10.1523/JNEUROSCI.17-24-09613.1997

Kuwako, K.-i., Nishimoto, Y., Kawase, S., Okano, Hirotaka J., & Okano, H. (2014). Cadherin-7 Regulates Mossy Fiber Connectivity in the Cerebellum. *Cell Reports*, *9*(1), 311-323. https://doi.org/https://doi.org/10.1016/j.celrep.2014.08.063

Le Vay, S., Wiesel, T. N., & Hubel, D. H. (1980). The development of ocular dominance columns in normal and visually deprived monkeys. *Journal of Comparative Neurology*, *191*(1), 1-51. https://doi.org/https://doi.org/10.1002/cne.901910102

Lefebvre, J. L., Kostadinov, D., Chen, W. V., Maniatis, T., & Sanes, J. R. (2012). Protocadherins mediate dendritic self-avoidance in the mammalian nervous system. *Nature*, *488*(7412), 517-521. https://doi.org/10.1038/nature11305

Lefebvre, J. L., Zhang, Y., Meister, M., Wang, X., & Sanes, J. R. (2008). γ-Protocadherins regulate neuronal survival but are dispensable for circuit formation in retina. *Development*, *135*(24), 4141-4151. https://doi.org/10.1242/DEV.027912

Lendvai, B., Stern, E. A., Chen, B., & Svoboda, K. (2000). Experience-dependent plasticity of dendritic spines in the developing rat barrel cortex in vivo. *Nature*, *404*(6780), 876-881. https://doi.org/10.1038/35009107

Lenneberg, E. H. (1967). The Biological Foundations of Language. *Hospital Practice*, *2*(12), 59-67. https://doi.org/10.1080/21548331.1967.11707799

Letellier, M., Bailly, Y., Demais, V., Sherrard, R. M., Mariani, J., & Lohof, A. M. (2007). Reinnervation of late postnatal Purkinje cells by climbing fibers: neosynaptogenesis without transient multi-innervation. *J Neurosci*, *27*(20), 5373-5383. https://doi.org/10.1523/JNEUROSCI.0452-07.2007

Letellier, M., Wehrle, R., Mariani, J., & Lohof, A. M. (2009). Synapse elimination in olivo-cerebellar explants occurs during a critical period and leaves an indelible trace in Purkinje cells. *Proc Natl Acad Sci U S A*, *106*(33), 14102-14107. https://doi.org/10.1073/pnas.0902820106

Linhoff, M. W., Lauren, J., Cassidy, R. M., Dobie, F. A., Takahashi, H., Nygaard, H. B., Airaksinen, M. S., Strittmatter, S. M., & Craig, A. M. (2009). An unbiased expression screen for synaptogenic proteins identifies the LRRTM protein family as synaptic organizers. *Neuron*, *61*(5), 734-749. https://doi.org/10.1016/j.neuron.2009.01.017

Love, M. I., Huber, W., & Anders, S. (2014). Moderated estimation of fold change and dispersion for RNA-seq data with DESeq2. *Genome Biol*, *15*(12), 550. https://doi.org/10.1186/s13059-014-0550-8

Luo, F., Sclip, A., Jiang, M., & Sudhof, T. C. (2020). Neurexins cluster Ca(2+) channels within the presynaptic active zone. *EMBO J*, *39*(7), e103208. https://doi.org/10.15252/embj.2019103208

Luo, L., apos, & Leary, D. D. M. (2005). AXON RETRACTION AND DEGENERATION IN DEVELOPMENT AND DISEASE. *Annual Review of Neuroscience*, *28*(Volume 28, 2005), 127-156. https://doi.org/https://doi.org/10.1146/annurev.neuro.28.061604.135632

Lv, X., Li, S., Li, J., Yu, X. Y., Ge, X., Li, B., Hu, S., Lin, Y., Zhang, S., Yang, J., Zhang, X., Yan, J., Joyner, A. L., Shi, H., Wu, Q., & Shi, S. H. (2022). Patterned cPCDH expression regulates the fine organization of the neocortex. *Nature*, *612*(7940), 503-511. https://doi.org/10.1038/s41586-022-05495-2

Marino, L. (2002). Convergence of complex cognitive abilities in cetaceans and primates. *Brain Behav Evol*, *59*(1-2), 21-32. https://doi.org/10.1159/000063731

Markov, N. T., Ercsey-Ravasz, M., Van Essen, D. C., Knoblauch, K., Toroczkai, Z., & Kennedy, H. (2013). Cortical High-Density Counterstream Architectures. *Science*, *342*(6158), 1238406. https://doi.org/10.1126/science.1238406

Mason, A., & Larkman, A. (1990). Correlations between morphology and electrophysiology of pyramidal neurons in slices of rat visual cortex. II. Electrophysiology. *Journal of Neuroscience*, *10*(5), 1415-1428.

Mason, C. A., & Gregory, E. (1984). Postnatal maturation of cerebellar mossy and climbing fibers: transient expression of dual features on single axons. *J Neurosci*, *4*(7), 1715-1735. https://doi.org/10.1523/JNEUROSCI.04-07-01715.1984

McCall, T., Weil, Z. M., Nacher, J., Bloss, E. B., El Maarouf, A., Rutishauser, U., & McEwen, B. S. (2013). Depletion of polysialic acid from neural cell adhesion molecule (PSA-NCAM) increases CA3 dendritic arborization and increases vulnerability to excitotoxicity. *Experimental Neurology*, *241*, 5-12. https://doi.org/https://doi.org/10.1016/j.expneurol.2012.11.028

McGee, A. W., Yang, Y., Fischer, Q. S., Daw, N. W., & Strittmatter, S. M. (2005). Experience-Driven Plasticity of Visual Cortex Limited by Myelin and Nogo Receptor. *Science*, *309*(5744), 2222-2226. https://doi.org/10.1126/science.1114362

Meltzer, S., Boulanger, K. C., Chirila, A. M., Osei-Asante, E., DeLisle, M., Zhang, Q., Kalish, B. T., Tasnim, A., Huey, E. L., Fuller, L. C., Flaherty, E. K., Maniatis, T., Garrett, A. M., Weiner, J. A., & Ginty, D. D. (2023). gamma-Protocadherins control synapse formation and peripheral branching of touch sensory neurons. *Neuron*, *111*(11), 1776-1794 e1710. https://doi.org/10.1016/j.neuron.2023.03.012

Missler, M., Zhang, W., Rohlmann, A., Kattenstroth, G., Hammer, R. E., Gottmann, K., & Sudhof, T. C. (2003). Alpha-neurexins couple Ca2+ channels to synaptic vesicle exocytosis. *Nature*, *423*(6943), 939-948. https://doi.org/10.1038/nature01755

Miyazaki, T., Fukaya, M., Shimizu, H., & Watanabe, M. (2003). Subtype switching of vesicular glutamate transporters at parallel fibre-Purkinje cell synapses in developing mouse cerebellum. *Eur J Neurosci*, *17*(12), 2563-2572. https://doi.org/10.1046/j.1460-9568.2003.02698.x

Miyazaki, T., Hashimoto, K., Shin, H. S., Kano, M., & Watanabe, M. (2004). P/Q-type Ca2+ channel alpha1A regulates synaptic competition on developing cerebellar Purkinje cells. *J Neurosci*, *24*(7), 1734-1743. https://doi.org/10.1523/JNEUROSCI.4208-03.2004

Moberg, S., & Takahashi, N. (2022). Neocortical layer 5 subclasses: From cellular properties to roles in behavior [Review]. *Frontiers in Synaptic Neuroscience*, *Volume 14 - 2022*. https://doi.org/10.3389/fnsyn.2022.1006773

Molumby, M. J., Anderson, R. M., Newbold, D. J., Koblesky, N. K., Garrett, A. M., Schreiner, D., Radley, J. J., & Weiner, J. A. (2017). gamma-Protocadherins Interact with Neuroligin-1 and Negatively Regulate Dendritic Spine Morphogenesis. *Cell Rep*, *18*(11), 2702-2714. https://doi.org/10.1016/j.celrep.2017.02.060

Monahan, K., Rudnick, N. D., Kehayova, P. D., Pauli, F., Newberry, K. M., Myers, R. M., & Maniatis, T. (2012). Role of CCCTC binding factor (CTCF) and cohesin in the generation of single-cell diversity of protocadherin-alpha gene expression. *Proc Natl Acad Sci U S A*, *109*(23), 9125-9130. https://doi.org/10.1073/pnas.1205074109

Mountoufaris, G., Chen, W. V., Hirabayashi, Y., O'Keeffe, S., Chevee, M., Nwakeze, C. L., Polleux, F., & Maniatis, T. (2017). Multicluster Pcdh diversity is required for mouse olfactory neural circuit assembly. *Science*, *356*(6336), 411-414. https://doi.org/10.1126/science.aai8801

Mudge, Jonathan M., Carbonell-Sala, S., Diekhans, M., Martinez, Jose G., Hunt, T., Jungreis, I., Loveland, Jane E., Arnan, C., Barnes, I., Bennett, R., Berry, A., Bignell, A., Cerdán-Vélez, D., Cochran, K., Cortés, Lucas T., Davidson, C., Donaldson, S., Dursun, C., Fatima, R.,…Frankish, A. (2025). GENCODE 2025: reference gene annotation for human and mouse. *Nucleic Acids Research*, *53*(D1), D966-D975. https://doi.org/10.1093/nar/gkae1078

Nakayama, H., Miyazaki, T., Abe, M., Yamazaki, M., Kawamura, Y., Choo, M., Konno, K., Kawata, S., Uesaka, N., Hashimoto, K., Miyata, M., Sakimura, K., Watanabe, M., & Kano, M. (2024). Direct and indirect pathways for heterosynaptic interaction underlying developmental synapse elimination

in the mouse cerebellum. *Commun Biol*, *7*(1), 806. https://doi.org/10.1038/s42003-024-06447-4

Napper, R. M. A., & Harvey, R. J. (1988). Number of parallel fiber synapses on an individual Purkinje cell in the cerebellum of the rat. *Journal of Comparative Neurology*, *274*(2), 168-177. https://doi.org/https://doi.org/10.1002/cne.902740204

Nelson, T. E., King, J. S., & Bishop, G. A. (1997). Distribution of tyrosine hydroxylase-immunoreactive afferents to the cerebellum differs between species. *Journal of Comparative Neurology*, *379*(3), 443-454. https://doi.org/https://doi.org/10.1002/(SICI)1096-9861(19970317)379:3<443::AID-CNE9>3.0.CO;2-3

Nern, A., Pfeiffer, B. D., & Rubin, G. M. (2015). Optimized tools for multicolor stochastic labeling reveal diverse stereotyped cell arrangements in the fly visual system. *Proceedings of the National Academy of Sciences*, *112*(22), E2967-E2976. https://doi.org/10.1073/pnas.1506763112

Nguyen-Minh, V. T., Tran-Anh, K., Luo, Y., & Sugihara, I. (2019). Electrophysiological Excitability and Parallel Fiber Synaptic Properties of Zebrin-Positive and -Negative Purkinje Cells in Lobule VIII of the Mouse Cerebellar Slice [Original Research]. *Frontiers in Cellular Neuroscience*, *Volume 12 - 2018*. https://doi.org/10.3389/fncel.2018.00513

Okuno, Y., Sakoori, K., Matsuyama, K., Yamasaki, M., Watanabe, M., Hashimoto, K., Watanabe, T., & Kano, M. (2023). PTPdelta is a presynaptic organizer for the formation and maintenance of climbing fiber to Purkinje cell synapses in the developing cerebellum. *Front Mol Neurosci*, *16*, 1206245. https://doi.org/10.3389/fnmol.2023.1206245

Özel, M. N., Simon, F., Jafari, S., Holguera, I., Chen, Y. C., Benhra, N., El-Danaf, R. N., Kapuralin, K., Malin, J. A., Konstantinides, N., & Desplan, C. (2020). Neuronal diversity and convergence in a visual system developmental atlas. *Nature 2020 589:7840*, *589*(7840), 88-95. https://doi.org/10.1038/s41586-020-2879-3

Pantano, L. (2023). *DEGreport: Report of DEG analysis*. In https://bioconductor.org/packages/DEGreport

Patz, C., Brachtendorf, S., & Eilers, J. (2018). The transgenic mouse line Igsf9-eGFP allows targeted stimulation of inferior olive efferents. *J Neurosci Methods*, *296*, 84-92. https://doi.org/10.1016/j.jneumeth.2017.12.024

Paul, M. A., Sigoillot, S. M., Marti, L., Urra Quiroz, F. J., Delagrange, M., Cheung, H. W., Martinelli, D. C., Oriol, E., Hakim, V., Mailly, P., & Selimi, F. (2024). Stepwise molecular specification of excitatory synapse diversity onto cerebellar Purkinje cells. *Nat Neurosci*. https://doi.org/10.1038/s41593-024-01826-w

Pelvig, D. P., Pakkenberg, H., Stark, A. K., & Pakkenberg, B. (2008). Neocortical glial cell numbers in human brains. *Neurobiology of Aging*, *29*(11), 1754-1762. https://doi.org/https://doi.org/10.1016/j.neurobiolaging.2007.04.013

Peng, J., Sheng, A. L., Xiao, Q., Shen, L., Ju, X. C., Zhang, M., He, S. T., Wu, C., & Luo, Z. G. (2019). Single-cell transcriptomes reveal molecular specializations of neuronal cell types in the developing cerebellum. *J Mol Cell Biol*, *11*(8), 636-648. https://doi.org/10.1093/jmcb/mjy089

Peters, A., & Feldman, M. L. (1976). The projection of the lateral geniculate nucleus to area 17 of the rat cerebral cortex. I. General description. *J Neurocytol*, *5*(1), 63-84. https://doi.org/10.1007/BF01176183

Phillips, G. R., Huang, J. K., Wang, Y., Tanaka, H., Shapiro, L., Zhang, W., Shan, W. S., Arndt, K., Frank, M., Gordon, R. E., Gawinowicz, M. A., Zhao, Y., & Colman, D. R. (2001). The presynaptic particle web: ultrastructure, composition, dissolution, and reconstitution. *Neuron*, *32*(1), 63-77. https://doi.org/10.1016/s0896-6273(01)00450-0

Picelli, S., Faridani, O. R., Bjorklund, A. K., Winberg, G., Sagasser, S., & Sandberg, R. (2014). Full-length RNA-seq from single cells using Smart-seq2. *Nat Protoc*, *9*(1), 171-181. https://doi.org/10.1038/nprot.2014.006

Putignano, E., Lonetti, G., Cancedda, L., Ratto, G., Costa, M., Maffei, L., & Pizzorusso, T. (2007). Developmental Downregulation of Histone Posttranslational Modifications Regulates Visual Cortical Plasticity. *Neuron*, *53*(5), 747-759. https://doi.org/https://doi.org/10.1016/j.neuron.2007.02.007

Qiu, P. (2020). Embracing the dropouts in single-cell RNA-seq analysis. *Nature Communications*, *11*(1), 1169. https://doi.org/10.1038/s41467-020-14976-9

Quy, P. N., Fujita, H., Sakamoto, Y., Na, J., & Sugihara, I. (2011). Projection patterns of single mossy fiber axons originating from the dorsal column nuclei mapped on the aldolase C compartments in the rat cerebellar cortex. *Journal of Comparative Neurology*, *519*(5), 874-899. https://doi.org/https://doi.org/10.1002/cne.22555

Rai, Y., Watanabe, T., Matsuyama, K., Sakimura, K., Uesaka, N., & Kano, M. (2021). Phospholipase C beta3 is Required for Climbing Fiber Synapse Elimination in Aldolase C-positive Compartments of the Developing Mouse Cerebellum. *Neuroscience*, *462*, 36-43. https://doi.org/10.1016/j.neuroscience.2020.04.035

Redfern, P. A. (1970). Neuromuscular transmission in new-born rats. *The Journal of Physiology*, *209*(3), 701-709. https://doi.org/https://doi.org/10.1113/jphysiol.1970.sp009187

Reeber, S. L., White, J. J., George-Jones, N. A., & Sillitoe, R. V. (2012). Architecture and development of olivocerebellar circuit topography. *Front Neural Circuits*, *6*, 115. https://doi.org/10.3389/fncir.2012.00115

Rees, C. L., Moradi, K., & Ascoli, G. A. (2017). Weighing the Evidence in Peters' Rule: Does Neuronal Morphology Predict Connectivity? *Trends Neurosci*, *40*(2), 63-71. https://doi.org/10.1016/j.tins.2016.11.007

Reiss, K., Maretzky, T., Haas, I. G., Schulte, M., Ludwig, A., Frank, M., & Saftig, P. (2006). Regulated ADAM10-dependent ectodomain shedding of gamma-protocadherin C3 modulates cell-cell adhesion. *J Biol Chem*, *281*(31), 21735-21744. https://doi.org/10.1074/jbc.M602663200

Reissner, C., Runkel, F., & Missler, M. (2013). Neurexins. *Genome Biol*, *14*(9), 213. https://doi.org/10.1186/gb-2013-14-9-213

Remesal, L., Roger-Baynat, I., Chirivella, L., Maicas, M., Brocal-Ruiz, R., Pérez-Villalba, A., Cucarella, C., Casado, M., & Flames, N. (2020). PBX1 acts as terminal selector for olfactory bulb dopaminergic neurons. *Development*, *147*(8), dev186841. https://doi.org/10.1242/dev.186841

Roth, G., & Dicke, U. (2005). Evolution of the brain and intelligence. *Trends Cogn Sci*, *9*(5), 250-257. https://doi.org/10.1016/j.tics.2005.03.005

Rubinstein, R., Thu, C. A., Goodman, K. M., Wolcott, H. N., Bahna, F., Mannepalli, S., Ahlsen, G., Chevee, M., Halim, A., Clausen, H., Maniatis, T., Shapiro, L., & Honig, B. (2015). Molecular logic of neuronal self-recognition through protocadherin domain interactions. *Cell*, *163*(3), 629-642. https://doi.org/10.1016/j.cell.2015.09.026

Sando, R., Bushong, E., Zhu, Y., Huang, M., Considine, C., Phan, S., Ju, S., Uytiepo, M., Ellisman, M., & Maximov, A. (2017). Assembly of Excitatory Synapses in the Absence of Glutamatergic Neurotransmission. *Neuron*, *94*(2), 312-321.e313. https://doi.org/10.1016/j.neuron.2017.03.047

Sanes, J. R., & Yamagata, M. (2009). Many paths to synaptic specificity. *Annu Rev Cell Dev Biol*, *25*, 161-195. https://doi.org/10.1146/annurev.cellbio.24.110707.175402

Sanes, J. R., & Zipursky, S. L. (2020). Synaptic Specificity, Recognition Molecules, and Assembly of Neural Circuits. *Cell*, *181*(6), 1434-1435. https://doi.org/10.1016/j.cell.2020.05.046

Scheiffele, P., Fan, J., Choih, J., Fetter, R., & Serafini, T. (2000). Neuroligin expressed in nonneuronal cells triggers presynaptic development in contacting axons. *Cell*, *101*(6), 657-669. https://doi.org/10.1016/s0092-8674(00)80877-6

Schreiner, D., Nguyen, T. M., Russo, G., Heber, S., Patrignani, A., Ahrne, E., & Scheiffele, P. (2014). Targeted combinatorial alternative splicing generates brain region-specific repertoires of neurexins. *Neuron*, *84*(2), 386-398. https://doi.org/10.1016/j.neuron.2014.09.011

Schreiner, D., & Weiner, J. A. (2010). Combinatorial homophilic interaction between γ-protocadherin multimers greatly expands the molecular diversity of cell adhesion. *Proceedings of the National Academy of Sciences of the United States of America*, *107*(33), 14893-14898. https://doi.org/10.1073/PNAS.1004526107/SUPPL_FILE/PNAS.201004526SI.PDF

Shannon, C. E. (1997). The mathematical theory of communication. 1963. *MD Comput*, *14*(4), 306-317. https://www.ncbi.nlm.nih.gov/pubmed/9230594

Shen, K., & Scheiffele, P. (2010). Genetics and cell biology of building specific synaptic connectivity. *Annu Rev Neurosci*, *33*, 473-507. https://doi.org/10.1146/annurev.neuro.051508.135302

Sigler, A., Oh, W. C., Imig, C., Altas, B., Kawabe, H., Cooper, B. H., Kwon, H.-B., Rhee, J.-S., & Brose, N. (2017). Formation and Maintenance of Functional Spines in the Absence of Presynaptic Glutamate Release. *Neuron*, *94*(2), 304-311.e304. https://doi.org/10.1016/j.neuron.2017.03.029

Sperry, R. W. (1963). Chemoaffinity in the orderly growth of nerve fiber patterns and connections. *Proceedings of the National Academy of Sciences of the United States of*, *50*(4), 703-710. https://doi.org/10.1073/pnas.50.4.703

Steffen, D. M., Ferri, S. L., Marcucci, C. G., Blocklinger, K. L., Molumby, M. J., Abel, T., & Weiner, J. A. (2021). The gamma-Protocadherins Interact Physically and Functionally with Neuroligin-2 to Negatively Regulate Inhibitory Synapse Density and Are Required for Normal Social Interaction. *Mol Neurobiol*, *58*(6), 2574-2589. https://doi.org/10.1007/s12035-020-02263-z

Steffen, D. M., Hanes, C. M., Mah, K. M., Ramos, P. V., Bosch, P. J., Hinz, D. C., Radley, J. J., Burgess, R. W., Garrett, A. M., & Weiner, J. A. (2023). A Unique Role for Protocadherin γC3 in Promoting Dendrite Arborization through an Axin1-Dependent Mechanism. *Journal of Neuroscience*, *43*(6), 918-935. https://doi.org/10.1523/JNEUROSCI.0729-22.2022

Stoodley, C. J., D'Mello, A. M., Ellegood, J., Jakkamsetti, V., Liu, P., Nebel, M. B., Gibson, J. M., Kelly, E., Meng, F., Cano, C. A., Pascual, J. M., Mostofsky, S. H., Lerch, J. P., & Tsai, P. T. (2017). Altered cerebellar connectivity in autism and cerebellar-mediated rescue of autism-related behaviors in mice. *Nature Neuroscience*, *20*(12), 1744-1751. https://doi.org/10.1038/s41593-017-0004-1

Stuart, D. G., & Brownstone, R. M. (2011). The beginning of intracellular recording in spinal neurons: Facts, reflections, and speculations. *Brain Research*, *1409*, 62-92. https://doi.org/https://doi.org/10.1016/j.brainres.2011.06.007

Sugihara, I. (2005). Microzonal projection and climbing fiber remodeling in single olivocerebellar axons of newborn rats at postnatal days 4-7. *J Comp Neurol*, *487*(1), 93-106. https://doi.org/10.1002/cne.20531

Sugihara, I., & Shinoda, Y. (2004). Molecular, topographic, and functional organization of the cerebellar cortex: a study with combined aldolase C and olivocerebellar labeling. *J Neurosci*, *24*(40), 8771-8785. https://doi.org/10.1523/JNEUROSCI.1961-04.2004

Sugihara, I., Wu, H. S., & Shinoda, Y. (2001). The entire trajectories of single olivocerebellar axons in the cerebellar cortex and their contribution to Cerebellar compartmentalization. *J Neurosci*, *21*(19), 7715-7723. https://doi.org/10.1523/JNEUROSCI.21-19-07715.2001

Sytnyk, V., Leshchyns'ka, I., & Schachner, M. (2017). Neural Cell Adhesion Molecules of the Immunoglobulin Superfamily Regulate Synapse Formation, Maintenance, and Function. *Trends Neurosci*, *40*(5), 295-308. https://doi.org/10.1016/j.tins.2017.03.003

Takesian, A. E., & Hensch, T. K. (2013). Balancing plasticity/stability across brain development. *Prog Brain Res*, *207*, 3-34. https://doi.org/10.1016/B978-0-444-63327-9.00001-1

Tarusawa, E., Sanbo, M., Okayama, A., Miyashita, T., Kitsukawa, T., Hirayama, T., Hirabayashi, T., Hasegawa, S., Kaneko, R., Toyoda, S., Kobayashi, T., Kato-Itoh, M., Nakauchi, H., Hirabayashi, M., Yagi, T., & Yoshimura, Y. (2016). Establishment of high reciprocal connectivity between clonal cortical neurons is regulated by the Dnmt3b DNA methyltransferase and clustered protocadherins. *BMC Biol*, *14*(1), 103. https://doi.org/10.1186/s12915-016-0326-6

Tasic, B., Nabholz, C. E., Baldwin, K. K., Kim, Y., Rueckert, E. H., Ribich, S. A., Cramer, P., Wu, Q., Axel, R., & Maniatis, T. (2002). Promoter choice determines splice site selection in protocadherin alpha and gamma pre-mRNA splicing. *Molecular cell*, *10*(1), 21-33. https://doi.org/10.1016/s1097-2765(02)00578-6

Toyoda, S., Kawaguchi, M., Kobayashi, T., Tarusawa, E., Toyama, T., Okano, M., Oda, M., Nakauchi, H., Yoshimura, Y., Sanbo, M., Hirabayashi, M., Hirayama, T., Hirabayashi, T., & Yagi, T. (2014). Developmental epigenetic modification regulates stochastic expression of clustered protocadherin genes, generating single neuron diversity. *Neuron*, *82*(1), 94-108. https://doi.org/10.1016/j.neuron.2014.02.005

Treutlein, B., Gokce, O., Quake, S. R., & Sudhof, T. C. (2014). Cartography of neurexin alternative splicing mapped by single-molecule long-read mRNA sequencing. *Proc Natl Acad Sci U S A*, *111*(13), E1291-1299. https://doi.org/10.1073/pnas.1403244111

Turney, S. G., & Lichtman, J. W. (2012). Reversing the Outcome of Synapse Elimination at Developing Neuromuscular Junctions In Vivo: Evidence for Synaptic Competition and Its Mechanism. *PLOS Biology*, *10*(6), e1001352-e1001352. https://doi.org/10.1371/JOURNAL.PBIO.1001352

Tyssowski, K. M., DeStefino, N. R., Cho, J.-H., Dunn, C. J., Poston, R. G., Carty, C. E., Jones, R. D., Chang, S. M., Romeo, P., Wurzelmann, M. K., Ward, J. M., Andermann, M. L., Saha, R. N., Dudek, S. M., & Gray, J. M. (2018). Different Neuronal Activity Patterns Induce Different Gene Expression Programs. *Neuron*, *98*(3), 530-546.e511. https://doi.org/10.1016/j.neuron.2018.04.001

Uemura, T., Lee, S. J., Yasumura, M., Takeuchi, T., Yoshida, T., Ra, M., Taguchi, R., Sakimura, K., & Mishina, M. (2010). Trans-synaptic interaction of GluRdelta2 and Neurexin through Cbln1 mediates synapse formation in the cerebellum. *Cell*, *141*(6), 1068-1079. https://doi.org/10.1016/j.cell.2010.04.035

Uesaka, N., Uchigashima, M., Mikuni, T., Nakazawa, T., Nakao, H., Hirai, H., Aiba, A., Watanabe, M., & Kano, M. (2014). Retrograde semaphorin signaling regulates synapse elimination in the developing mouse brain. *Science*, *344*(6187), 1020-1023. https://doi.org/10.1126/science.1252514

Van Essen, D. C., Glasser, M. F., Dierker, D. L., & Harwell, J. (2012). Cortical parcellations of the macaque monkey analyzed on surface-based atlases. *Cereb Cortex*, *22*(10), 2227-2240. https://doi.org/10.1093/cercor/bhr290

Verhage, M., Maia, A. S., Plomp, J. J., Brussaard, A. B., Heeroma, J. H., Vermeer, H., Toonen, R. F., Hammer, R. E., van den Berg, T. K., Missler, M., Geuze, H. J., & Sudhof, T. C. (2000). Synaptic assembly of the brain in the absence of neurotransmitter secretion. *Science*, *287*(5454), 864-869. https://doi.org/10.1126/science.287.5454.864

Waddington, C. H. (1942). CANALIZATION OF DEVELOPMENT AND THE INHERITANCE OF ACQUIRED CHARACTERS. *Nature*, *150*(3811), 563-565. https://doi.org/10.1038/150563a0

Walsh, M. K., & Lichtman, J. W. (2003). In vivo time-lapse imaging of synaptic takeover associated with naturally occurring synapse elimination. *Neuron*, *37*(1), 67-73. https://doi.org/10.1016/S0896-6273(02)01142-X

Wang, X., Su, H., & Bradley, A. (2002). Molecular mechanisms governing Pcdh-γ gene expression: Evidence for a multiple promoter and cis-alternative

splicing model. *Genes and Development*, *16*(15), 1890-1905. https://doi.org/10.1101/gad.1004802

Wang, X., Weiner, J. A., Levi, S., Craig, A. M., Bradley, A., & Sanes, J. R. (2002). Gamma protocadherins are required for survival of spinal interneurons. *Neuron*, *36*(5), 843-854. https://doi.org/10.1016/s0896-6273(02)01090-5

Watanabe, T., & Kano, M. (2024). Molecular and cellular mechanisms of developmental synapse elimination in the cerebellum: Involvement of autism spectrum disorder-related genes. *Proc Jpn Acad Ser B Phys Biol Sci*, *100*(9), 508-523. https://doi.org/10.2183/pjab.100.034

Weiner, J. A., Wang, X., Tapia, J. C., & Sanes, J. R. (2005). Gamma protocadherins are required for synaptic development in the spinal cord. *Proc Natl Acad Sci U S A*, *102*(1), 8-14. https://doi.org/10.1073/pnas.0407931101

Williams, R. W., & Herrup, K. (1988). The control of neuron number. *Annu Rev Neurosci*, *11*, 423-453. https://doi.org/10.1146/annurev.ne.11.030188.002231

Wiseglass, G., Boni, N., Smorodinsky-Atias, K., & Rubinstein, R. (2024). Clustered protocadherin *cis* -interactions are required for combinatorial cell–cell recognition underlying neuronal self-avoidance. *Proceedings of the National Academy of Sciences*, *121*(29). https://doi.org/10.1073/pnas.2319829121

Woodbury, J., & Patton, H. D. (1952a). Electrical activity of single spinal cord elements. Cold Spring Harbor Symposia on Quantitative Biology,

Woodbury, J., & Patton, H. D. (1952b). Properties of spinal cord elements studied with intracellular ultramicroelectrodes. Federation Proceedings,

Wu, H. S., Sugihara, I., & Shinoda, Y. (1999). Projection patterns of single mossy fibers originating from the lateral reticular nucleus in the rat cerebellar cortex and nuclei. *Journal of Comparative Neurology*, *411*(1), 97-118. https://doi.org/https://doi.org/10.1002/(SICI)1096-9861(19990816)411:1<97::AID-CNE8>3.0.CO;2-O

Wu, Q., & Jia, Z. (2021). Wiring the Brain by Clustered Protocadherin Neural Codes. *Neurosci Bull*, *37*(1), 117-131. https://doi.org/10.1007/s12264-020-00578-4

Wu, Q., & Maniatis, T. (1999). A striking organization of a large family of human neural cadherin-like cell adhesion genes. *Cell*, *97*(6), 779-790. https://doi.org/10.1016/s0092-8674(00)80789-8

Wu, Q., & Maniatis, T. (2000). Large exons encoding multiple ectodomains are a characteristic feature of protocadherin genes. *Proc Natl Acad Sci U S A*, *97*(7), 3124-3129. https://doi.org/10.1073/pnas.97.7.3124

Wu, Q., Zhang, T., Cheng, J. F., Kim, Y., Grimwood, J., Schmutz, J., Dickson, M., Noonan, J. P., Zhang, M. Q., Myers, R. M., & Maniatis, T. (2001). Comparative DNA sequence analysis of mouse and human protocadherin gene clusters. *Genome Res*, *11*(3), 389-404. https://doi.org/10.1101/gr.167301

Xie, Z., Bailey, A., Kuleshov, M. V., Clarke, D. J. B., Evangelista, J. E., Jenkins, S. L., Lachmann, A., Wojciechowicz, M. L., Kropiwnicki, E., Jagodnik, K. M., Jeon, M., & Ma'ayan, A. (2021). Gene Set Knowledge Discovery with Enrichr. *Curr Protoc*, *1*(3), e90. https://doi.org/10.1002/cpz1.90

Yagi, T. (2012). Molecular codes for neuronal individuality and cell assembly in the brain. *Front Mol Neurosci*, *5*, 45. https://doi.org/10.3389/fnmol.2012.00045

Yamagata, M., & Sanes, J. R. (2012). Expanding the Ig Superfamily Code for Laminar Specificity in Retina: Expression and Role of Contactins. *The Journal of Neuroscience*, *32*(41), 14402. https://doi.org/10.1523/JNEUROSCI.3193-12.2012

Yan, W., Peng, Y.-R., van Zyl, T., Regev, A., Shekhar, K., Juric, D., & Sanes, J. R. (2020). Cell Atlas of The Human Fovea and Peripheral Retina. *Scientific Reports*, *10*(1), 9802. https://doi.org/10.1038/s41598-020-66092-9

Zhang, B., Chen, Lulu Y., Liu, X., Maxeiner, S., Lee, S.-J., Gokce, O., & Südhof, Thomas C. (2015). Neuroligins Sculpt Cerebellar Purkinje-Cell Circuits by Differential Control of Distinct Classes of Synapses. *Neuron*, *87*(4), 781-796. https://doi.org/10.1016/j.neuron.2015.07.020

Zhang, P., Lu, H., Peixoto, R. T., Pines, M. K., Ge, Y., Oku, S., Siddiqui, T. J., Xie, Y., Wu, W., Archer-Hartmann, S., Yoshida, K., Tanaka, K. F., Aricescu, A. R., Azadi, P., Gordon, M. D., Sabatini, B. L., Wong, R. O. L., & Craig, A. M. (2018). Heparan Sulfate Organizes Neuronal Synapses through Neurexin Partnerships. *Cell*, *174*(6), 1450-1464 e1423. https://doi.org/10.1016/j.cell.2018.07.002

Zhang, Z., Chen, F., Zhang, Z., Guo, L., Feng, T., Fang, Z., Xin, L., Yu, Y., Hu, H., Liu, Y., & He, Y. (2025). Structural insights into the in situ assembly of clustered protocadherin gammaB4. *Nat Commun*, *16*(1), 1682. https://doi.org/10.1038/s41467-025-56948-x

Zhou, H., Lin, Z., Voges, K., Ju, C., Gao, Z., Bosman, L. W. J., Ruigrok, T. J. H., Hoebeek, F. E., De Zeeuw, C. I., & Schonewille, M. (2014). Cerebellar modules operate at different frequencies. *eLife*, *3*, e02536. https://doi.org/10.7554/eLife.02536

Zhu, Y.-j., Deng, C.-y., Fan, L., Wang, Y.-Q., Zhou, H., & Xu, H.-t. (2024). Combinatorial expression of γ-protocadherins regulates synaptic

connectivity in the mouse neocortex. *eLife*, *12*. https://doi.org/10.7554/ELIFE.89532

Zhu, Y., Uytiepo, M., Bushong, E., Haberl, M., Beutter, E., Scheiwe, F., Zhang, W., Chang, L., Luu, D., Chui, B., Ellisman, M., & Maximov, A. (2021). Nanoscale 3D EM reconstructions reveal intrinsic mechanisms of structural diversity of chemical synapses. *Cell Reports*, *35*(1). https://doi.org/10.1016/j.celrep.2021.108953